WASM: Minerals, Energy and Chemical Engineering

Department of Chemical Engineering

Graphene Based Membranes and Their Application in Gas Separation

Fatemeh Abolhasan Nezhad

This thesis is presented for the degree of

Master of Philosophy

of

Curtin University

March 2020

Declaration

To the best of my knowledge and belief this thesis contains no material previously published by any other person except where due acknowledgment has been made.

This thesis contains no material which has been accepted for the award of any other degree or diploma in any university.

Signature: Fatemeh A-NEZHAD

Date: 10/03/2020

Abstract

Membrane separation technology is one of the most cost-effective methods for gas separation which can be a promising replacement for these conventional gas separation methods with high energy consumption such as cryogenic distillation.

Among different materials used in membrane fabrication, polymeric membranes are the most utilised material group; however, their performance is limited by Robeson upper bound which is a trade-off between the gas selectivity and permeability. This problem has been addressed in another group of membranes called molecular sieving membranes (MSMs). In these types of membranes typically made from zeolite, silica, or metal organic frameworks (MoFs), it is possible to have both excellent gas permeability and super-high selectivity which is a phenomenal advantage for effective gas separation. However, there are two disadvantages in these MSMs which are hindering their further development in large scale. The first disadvantage is the high preparation cost of these membranes which makes it not feasible for large scale production. The second issue associated with these typical MSMs is the formation of non-selective structural defects during the high temperature growth process which leads to poor gas separation performance.

Recently, a new family of two-dimensional (2D) layered materials with a typical example of graphene has been reported and utilised for fabricating MSMs at room temperature. These graphene membranes possess a laminar structure with van der Waals force and hydrogen bonds to bind these nano-sheet layers. Graphene nanosheets themselves are impermeable to all gases even the smallest gas molecules such as He and H_2. Therefore, different stacking methods have been used to assemble the graphene layers and their interlayer spacing is used as the main pathway for gas separation. One of the most famous derivatives in graphene family is called graphene oxide (GO), which is the oxidised form of graphene and thus has different functional groups on the surface and the edges of GO flakes. The impulse force between the functional groups of two adjacent GO layers leads to bigger interlayer spacing in GO membranes compared with pure graphene membranes where the interlayer spacing is

very narrow. This phenomenon makes graphene oxide an ideal choice for high-permeance gas separation membrane. However, in such a group of graphene membranes, non-selective defects are easily formed during the GO assembling process which can deteriorate the membrane performance. Therefore, to avoid this, a certain thickness of GO layers should be assembled to ensure high selectivity.

The aim of this project was to develop a type of molecular sieving graphene-based membrane with high gas permeability as well as excellent selectivity using a facile fabrication method. In this work, the graphene (not GO) flake with thickness of 7 nm was used as the building block to form the graphene membrane so that we benefit from the high mechanical strength of graphene nanosheets which is a vital factor in achieving highly-stable membranes with excellent gas separation performance. For fabricating the membranes, a facile way using hydraulic pressure is introduced. To further improve the performance of the membranes, zeolite was employed as an adsorptive material, making the pure graphene membranes to an asymmetric layered membrane. Owing to the uniform system of pores with molecule size dimensions, zeolite membranes are usually fabricated for high molecular sieving separation performance with thermal and chemical stability making it a good choice for long-term applications. Therefore, this attribute was utilised to further enhance the performance of our graphene membranes by adding a mixture of graphene/zeolite to the initial graphene membranes as a porous support layer.

The resulting membranes exhibited excellent gas separation performance. Experimental results demonstrate that the pressed graphene membranes in thickness of around 0.75 mm displayed excellent molecular sieving properties with He/CO_2 selectivity up to 65 and He permeance $2.02*10^{-8}$ [mol m^{-2} s^{-1} Pa^{-1}].

Publication

The following paper is published in **Journal of Membrane Science** on Jan 2020:

'Experimental and theoretical exploration of gas permeation mechanism through 2D graphene (not graphene oxide) membranes'

Fatemeh A. Nezhad, Ning Han, Zhangfeng Shen, Yun Jin, Yangang Wang, Naitao Yang, Shaomin Liu

https://doi.org/10.1016/j.memsci.2020.117883

Acknowledgements

First, I would like to express my sincere gratitude to my supervisor, Professor Shaomin Liu for his patience, knowledge and continues support throughout my master studies. His guidance always helped me through my research and writing this thesis.

I would also like to thank Dr Hussein Abid for his unfailing support and expertise during my lab experiments.

I am also grateful to my research group members who were always ready to help me in various occasions and Mrs. Roshanak Doroushi and Mr. Xiao Hua for their kind assistance in laboratory equipment and instructions.

I also gratefully acknowledge the contribution of an Australian Government Research Training Program Scholarship in supporting this research.

Last but not least, I would like to thank my husband, Mehdi, for his endless and loving support throughout this time and always motivating me to believe in myself and stay positive. Also, I am deeply grateful to my parents and my brothers who didn't let our thousands-of-miles distance to be an obstacle for being always there for me whenever I needed them. I simply couldn't have done this without them. Thank you.

Table of Contents

List of Figures

List of Tables

Nomenclatures

A_m	Membrane active surface area (m^2)
α	Separation factor
BET	Brunauer-Emmett-Teller
C_i	Concentration of component i in the mixture
D	Diffusion coeficient
E_d	Activation energy (kJ/mol)
F	Volumetric permeation flow rate (ml/min)
FIB-SEM	Focused Ion Beam Scanning Electron Microscopy
GC	Gas Chromatography
GO	Graphene oxide
K_n	Knudsen number
L	Membrane thickness (mm)
M	Molecular weight (g mol^{-1})
p_i	Gas permeance of component *i* through the membrane (mol m^{-2} s^{-1} Pa^{-1})
P	Pressure (bar)
R	Gas constant, 8.3145 (J K^{-1} mol^{-1})
rGO	Reduced graphene oxide
RPM	Round per minute
S	Ideal selectivity

SEM	Scanning Electron Microscopy
T	Temperature (K)
TCD	Thermal Conductivity Detector
wt	Weight (g)
XRD	X-ray powder diffraction

Chapter 1 Introduction

Separation, concentration or purification of chemical compounds present in a mixture, is a critical stage in many areas such as chemical, petroleum refining, desalination, material processing, food and pharmaceutical industries. This stage plays an important role in energy/cost-saving, raw material utilisation efficiency and waste reduction since separation process is normally the most expensive stage (1, 2). For chemical production, the cost of the separation stage is up to 85% of the total energy cost; thus, a cost-effective separation or purification method is always required to improve the economics and achieve the environmental friendliness.

There are several methods for this important separation process including adsorption, desorption, distillation, crystallization, precipitation, ion exchange, membrane operation. Membrane separation, as a more recently emerged technology in this area, has attracted a lot of attention and evolved from an analytical tool used in biomedical and chemical laboratories to a significant part of different industries (3). Membrane separation processes, can be widely used in different applications leading to considerable technical and commercial improvements compared to conventional separation methods via cryogenic distillation and adsorption (4).

Membrane technology is one the easiest ways that can be used in gas separation. This method can be utilised in several chemical industries such as hydrogen recovery (5), CO_2 capture (6, 7), separation of hydrocarbons (8) , and air purification (9).

In membrane separation, because usually no phase, chemical, thermal, or biological change of the components is required, separation could be performed with much less energy consumption which is a huge advantage over the conventional methods such as thermal distillation and adsorption (1). Moreover, this method enables the process to be carried out in a smaller operating unit with high process flexibility as well as much less challenging procedures for device installation, maintenance, and safety concerns (10), all of which are making membrane separation an attractive option for various industries with fast-growing interest (4).

Recently, two dimensional (2D) layered graphene-based membranes have attracted a lot of attention in separation applications both in gas or liquid state. One of the problems in most of the graphene-based membranes is that they have be fabricated using graphene oxide (GO) which is a very expensive derivative of graphene and makes it an issue for large-scale production. Therefore, we used graphene nanosheets as the starting material to assemble membranes, making them more cost-effective and economical in large-scale production.

Several researches have been carried out for improving the separation performance of graphene-based membranes using different methods such as adding other materials (e.g. polymers) to the membrane structure or using robust supports to be able to use thin and highly selective graphene layers (11, 12) for higher permeability.

This dissertation focuses on fabrication of novel graphene-based membranes prepared using facile and cost-effective methods with considerably small amount of energy consumption and high separation performance.

The following chapters are included in this dissertation:

Chapter 1 summarizes the importance of membrane separation and the starting point of this thesis which is the necessity of introducing a facile and effective way in graphene membrane fabrication with high separation performance.

Chapter 2 provides a summary and background in membrane separation and factors affecting molecular transport through the membranes. There is also an extensive review on graphene-based membranes and their applications in gas and water purification. Also, the history of zeolite membranes in separation technologies are presented.

Chapter 3 explains the experimental section of the thesis including the equipment, equations, and the calculations applied in the next chapters.

Chapter 4 proposes a facile way for fabricating graphene membranes using pure graphene layers rather than graphene oxide and discusses the effect of graphene properties on the membrane performance**.**

Chapter 5 presents a method for improving the separation performance of the graphene membranes and investigates the effect of the added zeolite materials on the membrane performance. Mixed gas permeation test, the effect of temperature on membrane performance, and molecular transport modelling are also investigated in this chapter.

Chapter 6 provides a comprehensive conclusion referring to all of the previous chapters and summarizes the important parts of the project. Also, this chapter proposes some recommendations for future works in this area.

References

1. Council NR. Separation Technologies for the Industries of the Future. Washington, DC: The National Academies Press; 1998. 128 p.
2. Ohwoka A, Ogbuke I, Gobina E. Performance of pure and mixed gas transport in reconfigured hybrid inorganic membranes Pt. 1. Membrane Technology. 2012;2012(6):7-12.
3. Lonsdale HK. The growth of membrane technology. J Membrane Sci. 1982;10(2):81-181.
4. Cui ZF, Jiang Y, Field RW. Chapter 1 - Fundamentals of Pressure-Driven Membrane Separation Processes. In: Cui ZF, Muralidhara HS, editors. Membrane Technology. Oxford: Butterworth-Heinemann; 2010. p. 1-18.
5. Ockwig NW, Nenoff TM. Membranes for Hydrogen Separation. Chemical Reviews. 2007;107(10):4078-110.
6. Scholes CA, Smith KH, Kentish SE, Stevens GW. CO2 capture from pre-combustion processes—Strategies for membrane gas separation. International Journal of Greenhouse Gas Control. 2010;4(5):739-55.
7. Zhang Y, Sunarso J, Liu S, Wang R. Current status and development of membranes for CO2/CH4 separation: A review. International Journal of Greenhouse Gas Control. 2013;12:84-107.
8. Faiz R, Li K. Olefin/paraffin separation using membrane based facilitated transport/chemical absorption techniques. Chemical Engineering Science. 2012;73:261-84.
9. Murali RS, Sankarshana T, Sridhar S. Air Separation by Polymer-based Membrane Technology. Separation & Purification Reviews. 2013;42(2):130-86.
10. Tabe-Mohammadi A. A Review of the Applications of Membrane Separation Technology in Natural Gas Treatment. Separation Science and Technology. 1999;34(10):2095-111.
11. Berean KJ, Ou JZ, Nour M, Field MR, Alsaif M, Wang YC, et al. Enhanced Gas Permeation through Graphene Nanocomposites. J Phys Chem C. 2015;119(24):13700-12.
12. Zhu JC, Meng XX, Zhao JP, Jin Y, Yang NT, Zhang SG, et al. Facile hydrogen/nitrogen separation through graphene oxide membranes supported on YSZ ceramic hollow fibers. J Membrane Sci. 2017;535:143-50.

Chapter 2 Literature Review

2.1 Membrane principles

The term "membrane" is used to describe two different matters: biological membranes (as a part of some organs) and synthetic membranes (which is referred in thesis) (4). Providing a precise definition of the membrane covering all its aspects in different applications is quite difficult. In most general terms, membrane refers a thin barrier separating two phases which moderates the passage of the chemical species through the membranes by restricting the passage of a certain group while letting the other ones pass through it (12). There are different terms in the membrane processes that are being used throughout the literature survey including permeant, filtrate, retentate, permeability, and permselectivity.

Permeant is the component which can pass through or into the membrane. Filtrate is considered as the components which have been able to pass through the membrane from the feed side to the other side (permeate side) and retentate is the rejected species which are either remained on the feed side or vented into the air.

In general, the performance of the membrane can be characterised by two factors: productivity and permselectivity. Productivity, is described by the flux of the permeation called the *permeate flux or permeability* which is the amount of mass, transported through the membrane (13). Permeability is conversely proportional to the membrane thickness and is one of the properties of the materials making the membrane. However, there is another term called permeance which is defined as the ratio of permeability (P) to the membrane thickness (L) and therefore is independent of the thickness of the membrane. Permeance is considered as one the membrane properties.

Permselectivity referred as the *ideal selectivity* in gas separation field, reflects the membrane ability in separating components and can be calculated by the ratio of the permeation flux of each two components (4). The membrane selectivity is given by:

$$S_{A,B} = \frac{p_A}{p_B} \tag{2.1}$$

Where $S_{A,B}$ is the membrane selectivity, and p_A and p_B are the permeation rate of components A and B, respectively.

2.1.1 Driving force in membrane processes

Based on the principles of mass transport, for the molecules to be able to pass through a membrane, it needs a driving force under which the species can permeate from the feed to the permeate side. Such driving force can be energy gradient or a difference in the electrochemical potential across the membrane.

Generally, there are three types of driving forces which are used in different membrane processes: pressure, concentration, and electrical potential (14). Pressure-driven processes such as microfiltration and ultrafiltration where the difference in the hydrostatic pressure of the feed side and the permeate side makes the molecules flow through the membrane (15).

Concentration gradient driven processes are the ones in which the chemical potential on different sides of the interphase (membrane) are different. In this type of mass transport, which is also called “diffusion”, the molecules transport mechanism happens by dissolution and diffusion of these molecules through the membrane. Reverse osmosis and dialysis could be examples of this type of driving force.

The last form of driving force for the membrane separation mechanism is an electrical potential gradient such as electrodialysis. In this type of transport, the components need to be carrying electrical charges (such as ions) to be able to permeate through the membrane. This form of molecule transport is also referred to as “migration”. In all three ways of driving forces for molecular transport, the molecules always flow from the higher potential towards the lower potential side as illustrated in Figure 2.1 (4).

The permeation flux through the membrane can be calculated using the following equation:

$$\mathrm{J} = -P\frac{\mathrm{dX}}{\mathrm{dz}} \tag{2.2}$$

Where J is the permeation flux of the permeants, *P* is the phenomenological coefficient which is related to the membrane permeability, and $\frac{dX}{dZ}$ is the driving force with dx being as pressure, concentration or electrical potential across the membrane with the thickness of dz.

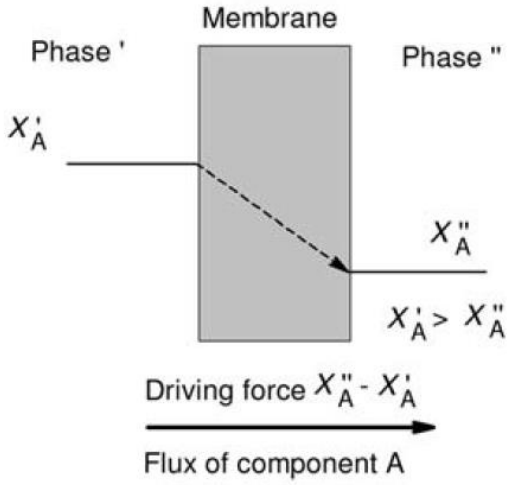

Figure 2.1 Schematic of driving force effect on the component permeation (4)

It is also worth mentioning that the negative sign in the equation (2.1) demonstrates the direction of the permeation flow which is usually in the reverse direction of the energy gradient.

Depending on the type of driving force dominant in the membrane process, the equation (2.1) and the phenomenological coefficient are different. The main driving forces present in many of the membrane separation processes and their corresponding flux equations are summarized below (14):

Darcy's law (pressure gradient):

$$J_v = -\mathrm{L_p}\frac{\mathrm{dp}}{\mathrm{dz}} \qquad (2.3)$$

Fick's law (concentration gradient):

$$J_n = -\mathrm{D}\frac{\mathrm{dc}}{\mathrm{dz}} \tag{2.4}$$

Ohm's law (electrical potential gradient):

$$J_e = -\kappa\frac{\mathrm{d}\varphi}{\mathrm{dz}} \tag{2.5}$$

2.1.2 Membrane structure

There are different categories of the membranes based on their structure such as asymmetric and symmetric, porous and dense. Symmetric and asymmetric (or anisotropic) are the more general terms in describing the membrane structure. A membrane is described as symmetric when the membranes share the similar structure and transport properties through the membrane cross section and the thickness. However, in asymmetric membranes, the structure changes through the membrane cross section and it usually consists of one "skin" layer supported by a highly porous support layer. The skin layer is the actual selective layer to control the permeation flux and selectivity while the porous layer provides the mechanical support to increase the membrane stability but with minimal transport resistance. Therefore, in asymmetric membrane, the thickness of the skin layer significantly determines the flux (13).

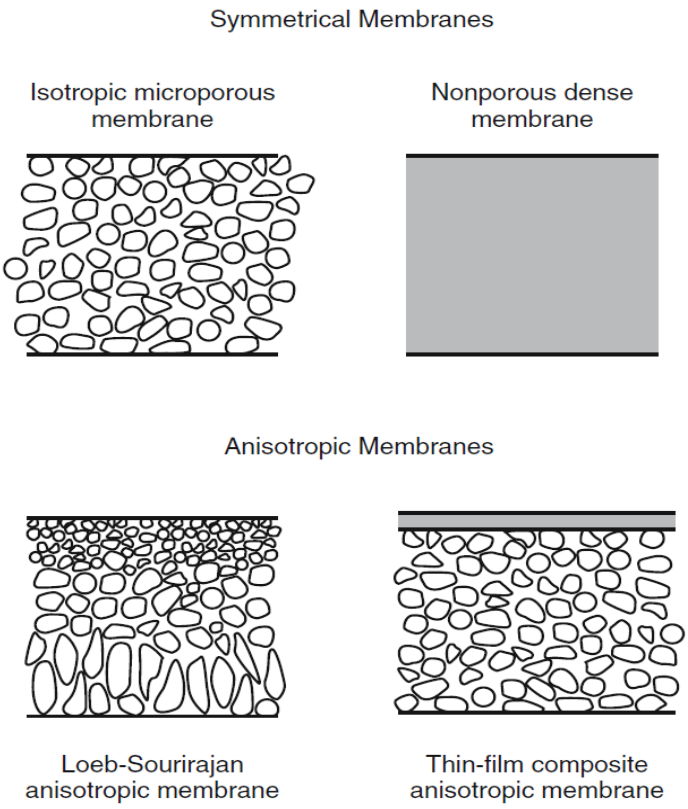

Figure 2.2 Schematic of Symmetric and Asymmetric membrane structure (3)

2.1.2.1 Nonporous, dense membranes

In this category, the membrane is usually a dense film with no pores in the skin layer for the molecule passage. Therefore, the driving force will push the permeants to diffuse through the membrane material which means despite the porous structure of the substrate, the molecular size does not affect the species permeation and even molecules with similar kinetic sizes may not have the same penetration rate. The reason is that in this group of membranes, the separation is based on the difference in diffusivity and solubility of the molecules in the membrane matrix. This mechanism of transport is called solution-diffusion model usually resulting in low permeabilities, which is used in separation processes such as pervaporation and reverse osmosis where the purpose is to separate two components with similar sizes but different natures (4).

The transport mechanism in dense membranes is solution-diffusion model (for polymer and metal membranes) in which the permeating species are first dissolved in the membrane material from the feed side and then diffuse through the medium to the permeate side which has lower concentrations of the permeants. In this model, where diffusion is the basis of the molecular permeation, the difference in the solubilities and diffusion rates of various permeants in the membrane material leads to separation as the main objective of the membrane process.

Fick's law is used to describe the transport mechanism in these membranes where concentration gradient is considered as the driving force. This concentration gradient which is because of a difference in composition, temperature or pressure of the fluids on the two sides makes the components to pass through the membrane from the high concentration side to the lower concentration side. Fick's law of diffusion equation is described as following:

$$J_i = -\mathrm{D_i}\frac{\mathrm{dc_i}}{\mathrm{dz}} \tag{2.4}$$

Where J_i is the permeation flux of component *i*, D_i is the diffusion coefficient and is a measure of the molecules mobility and $\frac{\mathrm{dc_i}}{\mathrm{dz}}$ is the concentration gradient of component i through the membrane.

2.1.2.2 Porous membranes

Porous structure is one of the simplest forms of the membranes and can be considered in the symmetric or asymmetric category depending on the pore size distribution through the membrane cross section. This form is similar to the conventional filter structure only with a difference in the size range of the pores. Porous membranes consist of pore in the size range of 1 nm-10 µm which much is extremely smaller than the conventional filter pore sizes. In this structure, in the presence of driving force, the molecule exclusion occurs by a sieving mechanism with the membrane pore and the molecule size as the determining factors. This method is based on the size and/or molecular weight of the species which means the species with the molecular kinetic diameter bigger than the biggest pore in the membrane are completely rejected while

the ones in the range of the pore size are partly rejected and the molecules smaller than the small pores can easily permeate through the membrane.

The permeation mechanism in this method is generally called pore-flow model. In this model, where pressure-driven convective flow is the basis of the molecular permeation across the porous medium, the separation occurs because some of the molecules are filtered through the pores from the others in the feed side due to the difference in their kinetic sizes or molecular weights (3). Considering pressure as the driving force, Darcy's law can be used to describe this model. The basic equation for Darcy's law is as follows:

$$J_i = -\mathrm{K'c_i}\frac{\mathrm{dp}}{\mathrm{dz}} \tag{2.3}$$

Where J_i is the permeation flux of component i, K' is coefficient depending on the nature of the medium, c_i is the concentration of component i in the medium and $\frac{dp}{dz}$ is the pressure gradient across the membrane thickness (3).

It is also worth mentioning that the permeation flux of the components in mediums with pore-flow transport model is generally higher than those in dense membranes with solution-diffusion model.

There are different types of porous structures defined for membranes. Therefore, the separation mechanisms of these porous-structured membranes are not exactly the same and they greatly depend on the pore size range of the membranes and the size of the molecules present in the feed mixture. The specific transport mechanisms based on the pore size will be discussed in more detail in the next sections.

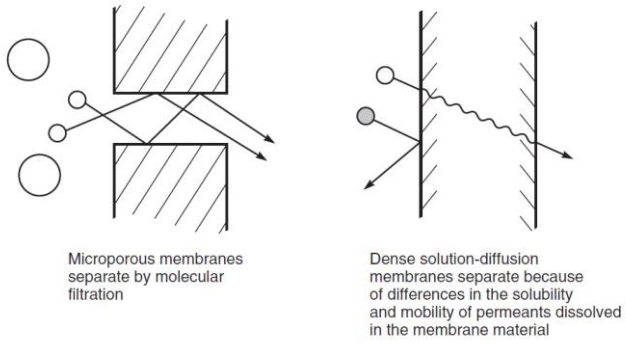

Figure 2.3 Molecular transport through porous and dense membranes (1)

2.1.3 Gas transport mechanism in membrane processes

As mentioned above, the transport mechanism for the membrane separation processes, vastly depend on the microstructure of the membranes. As illustrated in figure 2.4, there are various types of separation mechanisms defined and each of them demonstrates a different kind of method in separating the chemical species. Viscous flow, Knudsen diffusion, surface diffusion, molecular sieving, solution diffusion are only some of the mechanisms used for defining the transport behaviour(16). Based on the pore size and the molecules kinetic diameter, usually there are multiple transport mechanism present in each system; however, it is possible to distinguish the dominant transport mechanism for the membrane process.

When gases permeate through a porous medium, there are two general types of collision considered. One is the molecular collision between the gas molecules together and second, is the collision between the gas molecules and the membrane pore walls. The intensity and frequency of these molecular interactions depends on various factors such as temperature, pressure, membrane pore size, and molecule kinetic diameter (17).

To be able to determine the dominant transport mechanism in the gas permeation system, a dimensionless number called Knudsen number (K_n) is very useful. Knudsen number is defined as below:

$$K_n = \frac{\lambda}{\mathrm{d_p}} \tag{2.6}$$

Where λ is the mean free path of the gas and d_p is the representative physical length scale which in this case is the pore size diameter (18).

The mean free path of the gas λ is defined as the distance needed to be travelled by the gas molecules for a molecular collision to happen and it can be calculated using the following equation (17):

$$\lambda = \frac{k_B T}{\sqrt{2} p \pi d_g^2} \tag{2.7}$$

Where P is the gas pressure, d_g is the effective diameter of gas molecule, k_B is the Boltzmann constant (1.3807×10^{-23} J/K), and T is the gas temperature (K).

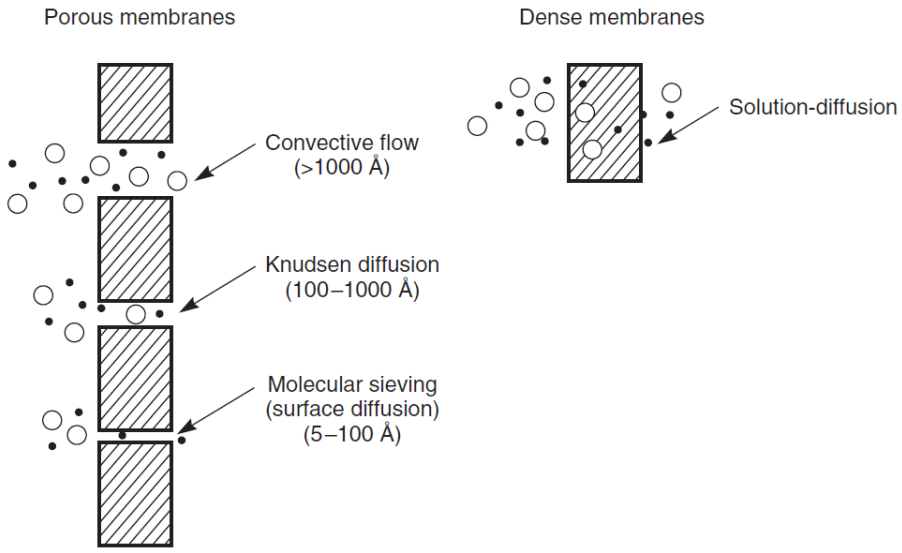

Figure 2.4 "Mechanism for permeation of gas through porous and dense gas separation membranes "(2)

As illustrated on figure 2.4, the transport mechanism of the membrane separation process can be distinguished by considering the Knudsen number range. For example, if the Kn is much greater than 10 (Kn>>10), means that the pore size is much smaller than the mean free path of the gas molecules which makes them to have collision with the pore walls in a much more frequency than they have collision with other molecules. In this case, the molecular diffusion has negligible contribution on the permeation,

which does not lead to high permeation rate because of the considerably small pore size (17).

In the next subsections, three of the most important gas transport mechanisms in pore flow model as well as the solution diffusion model and their corresponding Knudsen number will be discussed.

2.1.3.1 Convective flow

Convective flow also referred to as viscous flow or advection is a transport mechanism in porous membranes with pressure gradient as the driving force. This mechanism governs the transport behaviour when the pore size of the media in which the permeation is happening, is extremely bigger than the mean free path of the gas molecules. Therefore, the gas molecule-molecule interaction is much more predominant than the collision between the gas molecules and the pore walls which causes continues flow in the porous membrane.

The Knudsen number in this model is in the range of $Kn<0.001$ and due to the big media pore size (>1000 Å), the permeation flux is high with usually poor separation performance for the membranes (19).

Darcy's law is the equation as mentioned before (equation 2.7) usually used for viscous flow. This equation which uses the pressure gradient as the driving force is applicable for the low velocity flows which means away from the pore walls. Darcy's equation is the analogous to Fourier's law in heat conduction, Ohm law in the field of electrical networks, or Fick's law in diffusion which will be discussed later (20).

2.1.3.2 Knudsen diffusion

Knudsen flow or free-molecule diffusion is one of the forms of convective flow but with some differences. The main difference between these two models is that the pore size (100-1000 Å) in Knudsen diffusion is smaller than the pores in viscous flow. In fact, in this case, the pore size is almost the same range or smaller than the mean free

path of the gas molecules which makes them to have more wall collision rather than molecule-molecule interaction.

The Knudsen number range for this model is larger than 10 indicating the very smaller pore sizes compared to the gas mean free path (21). In this transport mechanism, the separation performance of the membrane is much better than the convective flow described above because the walls actually have an influence on the gas permeation flux.

The molecular flux of gas *i* in a Knudsen regime follow the general diffusion equation:

$$J_{iK} = -\mathrm{D_{iK}}\frac{\mathrm{dc_i}}{\mathrm{dz}} \tag{2.8}$$

Where J_{iK} is the Knudsen molar permeation flux of component i (mol/m^2.s), D_{iK} is the Knudsen diffusivity and dc_i/dz is the concentration gradient of component i through the membrane.

In case of gas permeation, the concentration gradient is embodied directly in the pressure gradient, therefore, the pressure gradient leads to concentration or gas partial pressure gradient as the driving force.

Considering the ideal gas equation (n=P/RT), the Knudsen diffusivity for gas i can be estimated using the following equation (22):

$$D_{iK} = \frac{\mathrm{d_p}}{3}\sqrt{\frac{8\mathrm{RT}}{\pi\,\mathrm{M_i}}} \tag{2.9}$$

Where d_p is the pore diameter, R is the ideal gas constant, T is the system temperature, and M_i is the molecular weight of component i.

Therefore, in Knudsen diffusion, the higher the molecular weight, the smaller the permeation rate of the gas component will be.

In a binary gas system, the ideal selectivity for the Knudsen regime which is also referred to as the Knudsen selectivity, can be calculated as below:

$$\alpha_{ab} = \frac{J_a}{\mathrm{J_b}} = \sqrt{\frac{\mathrm{M_b}}{\mathrm{M_a}}} \qquad (2.10)$$

Where α_{ab} is the Knudsen selectivity, J_a and J_b are the permeation flux of gas a and b, and M_a and M_b are the macular weights of gas a and b respectively.

2.1.3.3 Molecular sieving

Molecular sieving is a process that takes over the Knudsen flow and molecule-pore wall interaction mainly dominates the flow. For the membrane to be able to separate the gas molecules by molecular sieving mechanism, the pore size of the porous media needs to be much smaller than the pore size in Knudsen diffusion (5-100 Å). In fact, the pore size should approach the diameter of the gas molecules attempting to pass through the membrane so that the species which are smaller than the pore size, can pass through the membrane while the bigger ones are excluded (23). In this type of separation regime, since the pore size is really small and in the range of molecular size, very high separation factor of the membrane would be achieved. However, due to low porosity, the permeation rates of the permeants are usually much smaller than the above mentioned mechanisms which lead to a trade-off between the gas flow rate and the selectivity. Therefore, to fabricate the best performing membrane with both a reasonable permeation flow rate and a good selectivity, there should be a balance between the membrane pore size and porosity (24).

The Knudsen number in the molecular sieving mechanism is much higher than the range for the Knudsen flow.

To be able to indicate the sieving mechanism in membrane separation performance, there is common way. First, the theoretical Knudsen selectivity for two components of the gas mixture can be calculated using equation 2.12. Then the ideal selectivity of the two components is calculated for the real experiments using the equation 2.1. By comparing the two calculated selectivities, it is possible to predict the transport mechanism in the membrane separation. If the ideal selectivity of the system is bigger

than the Knudsen selectivity, then it can be derived that molecular sieving is dominating the gas molecules transport mechanism (16).

2.1.3.4 Solution diffusion

Once the pore size of the membrane decreases to 1 Å range or smaller, then the membrane is considered as dense and molecular transport occurs by solution-diffusion (25). This mechanism consists of three steps for gas separation. The first stage is the dissolution or absorption of the permeants into the membrane material. Therefore, the solubility of the molecules into the membrane plays an important role in the final performance. Henry's law is used for describing this important factor and it states that at a constant temperature, the amount of gas dissolved in a unit volume of a medium, is proportional to the partial pressure of the gas in the medium. Henry's law equation is as follow:

$$C_i = P_i K_{Hi} \tag{2.11}$$

Where C_i is the solubility of gas i in the material, P_i is the component i partial pressure (often in units of atm), K_{Hi} is the Henry's law constant (often in units of M/atm).

The second important stage which affects the membrane performance with solution diffusion separation mechanism is the diffusion of the previously dissolved molecules through the membrane and how fast this diffusion can actually happen. Fick's first law of diffusion (equation 2.6) is the dominant model for this stage which estimates the diffusion rate of gas i through the unit area of membrane under steady-state conditions:

$$J_i = -\mathrm{D_i}\frac{\mathrm{dc_i}}{\mathrm{dz}} \tag{2.4}$$

As mentioned before, D_i is the diffusion coefficient of component i and dc_i/dz is the concertation gradient f gas i through the membrane (23).

And finally, after gas diffusion, the last step of this mechanism is called desorption where the gas molecules are desorbed to the permeate side of the membrane.

Both the solution stage and the diffusion stage determine the membrane performance and affect the final gas flow rate through the membrane. In mixed systems, the selectivity of the membrane is affected by the difference of the gas molecules in solubility speed as well as diffusion rate which makes one gas to pass more easily than the other resulting in effective separation (4).

2.2 Membrane materials

Synthetic membranes can be fabricated using a wide range of materials. Depending on the material used in the structure, membranes are categorized into two general groups: organic and inorganic. Organic membranes are made from organic materials such as polymers and other organics while inorganics are made of inorganic materials such as ceramic, carbon, and zeolite. Currently, polymeric membranes are the most popular membranes due to their low synthetic cost; however, their selectivity is low and they are not stable at high temperature, pressure and chemically aggressive environments (26). Besides, their "upper bound" limitation which is a trade-off between the gas selectivity and permeability has been always an obstacle for achieving excellent separation performance (27, 28). On the other hand, inorganic materials such as zeolite, silica, and metal organic frameworks (MoF) have been recently in great interest for membrane fabrication because of their high selectivities and robustness in harsh conditions and high chemical/mechanical stability. However, these membranes are difficult to be scaled up for large applications due to their complex and costly synthesis procedures and the presence of unavoidable defects. Recently, graphene-based materials have emerged as a novel group of inorganics to be used for the next generation of molecular sieving membranes. Graphene has high mechanical strength (29), high chemical and thermal stability and low-cost production (30). Some of the graphene derivatives like graphene oxide (GO), have exhibited a great potential for molecular sieving applications in the field of nanofiltration with high stability in aqueous solutions (6, 30-32). All of these features make graphene a more favourable choice in comparison to the other microporous materials.

2.2.1 What is graphene?

Isolated from graphite since its discovery in 2004 (33), graphene is a flat monolayer of sp^2 hybridized carbon atoms arranged in two-dimensional honeycomb lattice structure (11). This monolayer is the basic shape for all the other dimensions of carbon-based allotropes such as fullerene (0D), carbon nanotubes (1D), diamond (3D), and graphite (3D). Due to only one carbon atom thickness (0.345 nm thick), graphene is known as the thinnest material on earth and interestingly, but even so, it exhibits extraordinary mechanical and chemical stability which makes it known as one of the strongest materials on earth too (34). One of the other interesting properties of graphene is that even with one atom thickness, it is visible with naked eye and carries a high optical absorptivity of 2.3%. It is also electrically conductive 1,000,000 times more than copper and has thermal conductivity more than other forms of carbon (diamond and graphite) (33, 35).

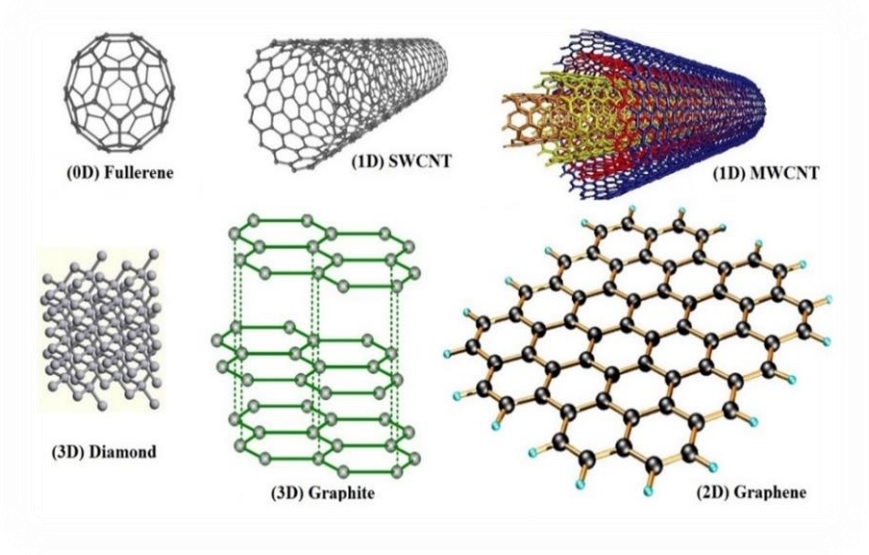

Figure 2.5 Different allotropes of graphite (5)

One of the most interesting properties of graphene is its impermeability to even the smallest atoms like helium. The reason for this surprising attribute considering its only one atom thickness, is the electrical field developed in the carbon lattice structure preventing the passage of any species. As illustrated in figure 2.6, graphene π orbitals shape a very dense cloud which blocks the space in the aromatic ring and leaves a 0.064

nm geometric pore which is smaller than even the smallest molecules such as hydrogen (0.314 nm) or helium (0.28 nm) even with 5 atm pressure difference through the layer (11, 36, 37).

Because of all these exceptional properties in addition to the cost-effective production, graphene and graphene derivatives (such as graphene oxide and graphene-based composites) have drawn considerable attention in different fields such as chemistry, material science, physics, membrane fabrication, electronics, sensors and energy storage applications (6, 30) . Recently, graphene-based membranes have been widely studied in gas separation and water purification areas because of the super physical, mechanical and separation properties of this layered material which will be discussed in the next sections.

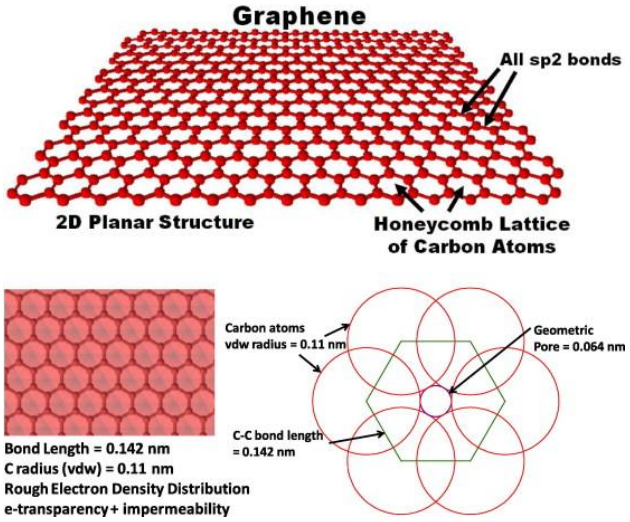

Figure 2.6 "Graphene lattice structure: sp2 hybridized carbon atoms arranged in a 2D honeycomb lattice. (Bottom) the molecular structure with rough electronic density distribution: while graphene is relatively transparent to electrons, it is practically impermeable to all molecules at room temperature. Geometric pore (0.064 nm) is also small enough not to allow molecules to pass through." (11)

2.3 Graphene based membranes

Graphene is being studied in various scientific areas and some derivatives of graphene have been produced and utilised in different applications. There are a range of structures used in graphene-based membranes depending on the materials used in the membrane. Each of these structures exhibits a certain separation performance and application which lies on their physical and mechanical properties. In this section, graphene and its

production and modification methods will be discussed and then two important graphene derivatives such as graphene oxide and graphene-based composites will be clarified.

2.3.1 Porous graphene layer (PG)

In general, graphene can be produced using different methods which can be categorized in 5 major groups:

1. Mechanical exfoliation from bulk graphite
2. Chemical vapour deposition (CVD)
3. Crystal growth
4. Longitudinal cutting of carbon nanotubes
5. Reduction of graphene oxide

Mechanical exfoliation can be done by Scotch tape method or using sonication. Scotch tape method and CVD are the production method used for high quality graphene while sonication and reduction of graphene derivatives are utilised for large-scale graphene production.

Two of graphene outstanding features, made the scientists to find a way to use graphene monolayers in membrane separation. The first one, was the one atom thickness monolayers of graphene. Since the permeation rate is inversely proportional to the membrane thickness, one atom thickness of graphene layer was an exceptional feature resulting in high flow rate. The second feature is great mechanical strength of the layers under high pressure differences as high as 6 atm which could lead to excellent membrane mechanical stability.

To be able to use impermeable graphene as membranes, the monolayers needed to be perforated. This means introducing artificial pores with nanoscale size on the layer surface to enhance the membrane permeability and selectivity. The resulting graphene is called porous graphene (PG), holy graphene (hG) or graphene nanomesh (38). There are a number of possibilities for perforating graphene layers which have been studied in other literatures. Polymerization reaction on the graphene surface and chemical etching (39-41), electron beam irradiation (42, 43), ion bombardment (44), oxygen

plasma etching (45, 46), MnO_2 etching of graphene sheets (47), nitrogen assisted etching (48, 49), and ultraviolent- induced oxidative etching (50-52) are some of the reported ways for introducing structural vacancies on graphene sheets to produce porous graphene. These porous graphene membranes can be used in molecular sieving with high permeation rate for different applications. However, introducing defect-free and uniform pores on graphene sheets surface to ensure high separation performance and high stability of the membrane is usually an expensive process which makes it a technical challenge for large-scale production and industrial applications. However, there is one method which is more cost effective and is viable for practical applications which is reduction of graphene oxide (GO) using thermal treatment to produce porous reduced graphene oxide (rGO) (53). GO and rGO are both derivatives of graphene which will be discussed later.

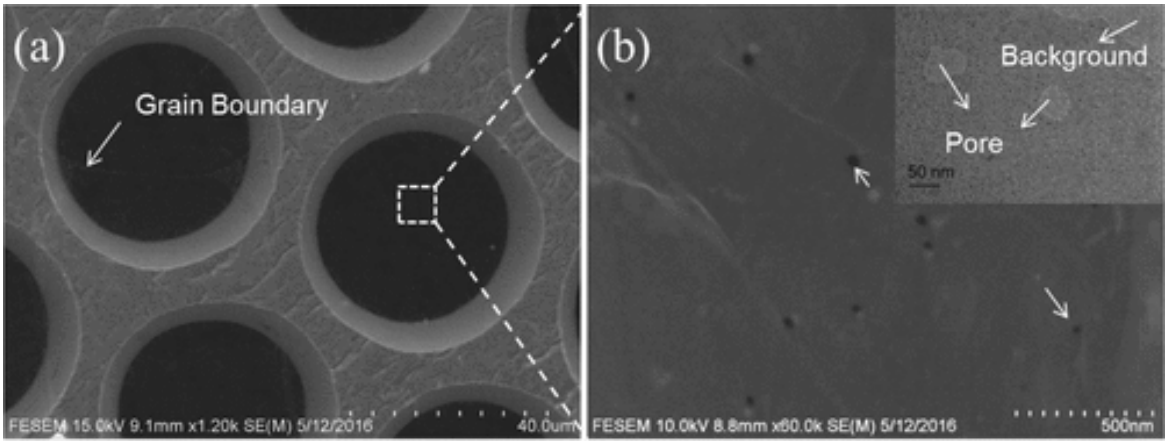

Figure 2.7 (a) SEM image of porous graphene on a TEM grid. (b) Enlarged view of the marked area in (a). The inset shows a TEM of the sample. (7)

2.3.2 Assembled graphene laminates

Since graphene is an impermeable single layer of carbon atoms, a number of ways have been used to assemble these monolayers together and fabricate layered-structured membranes which can be used for effective molecular separation. An important factor in these membranes affecting the membrane separation performance, is a term called the interlayer spacing (d-spacing). This term states the distance between adjacent layers

and can be measured by x-ray powder diffraction (XRD) and it mainly depends on the type of the layers in use (54) and the method of assembling the monolayers which can be vacuum filtration, spin coating, dip coating, spray coating or a layer-by-layer self-assembly approach (55, 56) . There are two types of graphene based derivatives which are used as graphene-based layers in assembled layered structures:

2.3.2.1 Graphene oxide (GO)

Graphene oxide (GO) is the chemically modified graphene which possess oxygen-containing groups such as hydroxyl, carboxyl, and epoxy on the basal plane and edges Very soon after graphene discovery, GO has become one of the most favourable derivatives of graphene and has drawn considerable interest in various applications such as water filtration, gas separation, transparent conductive films, fuel cells and supercapacitors (57, 58) because of its easier large-scale production as well as unique properties that are different from graphene. Graphene oxide is also a layer-structured material with a bigger interlayer spacing (d-spacing) compared to graphene. The functional groups develop an electrostatic repulsion between the adjacent layers leading to an interlayer spacing (d-spacing) of around 6-12 Å which is much bigger than the 3 Å interlayer distance in graphene (59).

Based on *Geim et al.* pioneering report about the submicrometer-thick laminated graphene oxide, this graphene derivative is known as completely impermeable to gases including Helium, but it is highly permeable for water vapour (60). The presence of polar groups as well as C/O atomic ratio of around 2.0 make GO hydrophilic and dispersible in water which has been one of its most useful properties especially in membrane water purification and desalination (61). The hydrophilic groups in GO easily accommodate water molecules to be graphene oxide layers and on the other hand, the hydrophobic non-oxidized regions (also referred to as non-polar or graphene sites) provide low-friction 2D capillaries resulting in ultra-fast and unimpeded permeation of water through GO-based membranes (62, 63).

One of the other interesting benefits of functional groups on GO sheets is that they can be used for adjustment of the interlayer spacing. For example in humid state, depending on the number of the H_2O molecules present between the layers, the d-spacing can grow

which is called GO swelling (54). This means that while the interlayer distance in dry state is less than 6Å while in wet GO this distance could increase up to even 6-7 nm (9). However, using another technique called cross-linking, the over swelling of graphene oxide layers can be hindered to maintain the ideal d-spacing for the application. In this technique, a group multivalent cationic metal contaminants are crosslinked to the GO sheets and functional groups, which affects the resultant modified graphene oxide in several ways such as enhanced mechanical stability and better performance in aqueous solutions (64, 65). In another research, *Li et al*. used pressure for adjusting the graphene oxide interlayer spacing in humid state. They called this external pressure regulation. These membranes show high KCl, NaCl, and $CaCl_2$ rejection of around 97% as well as excellent water permeation rate of 25 $Lm^{-2}h^{-1}$ at only 2 bar feed pressure (54).

Therefore, using of graphene oxide in membrane structure which provides adaptive and controllable interlayer distance, makes the size exclusion range of the membranes adjustable depending on the application. This is an exceptional attribute for high separation performance especially in water purification which does not exist for porous graphene-based membranes.

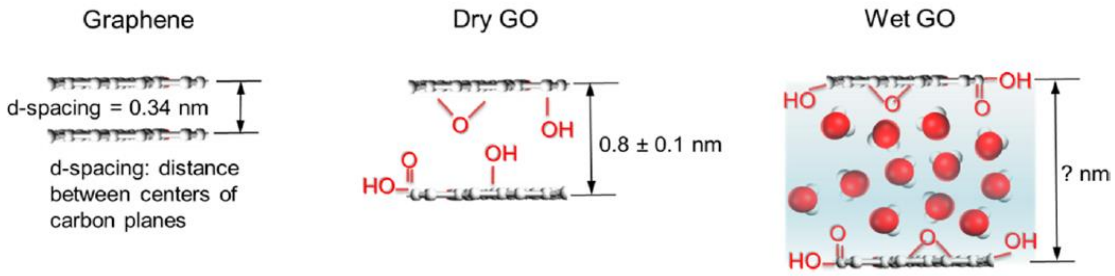

Figure 2.8 Schematic illustration of d-spacing of graphene, dry GO, and GO soaked in water (9).

In general, GO is synthesised by exfoliation of graphite oxide which is the oxidized form of graphite. The methods of synthesis are basically different ways of graphite oxidization. To date, several oxidation methods have been introduced for producing graphite oxide and in each of these procedures, the preparation time and temperature

are different which hugely affect the resultant GO nature and oxidation degree (carbon/oxygen ratio in GO structure). In 1859, Brodie developed the first method for oxidizing graphite. Since then, several other ways have been introduced and Hummer's method (66) is the most famous procedure used by researches due to its ease and short time of attainment. Recently, modified or improved Hummer's methods (67) have been developed making the Hummer's synthesis procedure (68) more efficient and less time consuming. However, in all of these preparation methods, there are a number of serious problems such as danger of explosion because of using very strong oxidants as well as environmental pollution. To address these issues, Ren et al. reported an eco-friendly method of water electrolytic oxidation of graphite which not only results in fast and high yield fabrication but also is safer and imposes less negative impact on the environment (69).

2.3.2.2 Reduced graphene oxide (rGO)

Reduced graphene oxide or rGO is a form of graphene oxide but with lower amount of oxygen groups on its layers. rGO has excellent electrical properties close to graphene but is much higher than graphene oxide. GO is reduced to rGO either for mass production of graphene or to improve the electron mobility, and conductivity of the material which is critical in various applications such as energy storage devices and electronics (70). In rGO, the interlayer spacing is smaller than in GO because the amount of oxygen-containing groups has been reduced and therefore, the layer-layer repulsion is not that severe. In addition, rGO is more stable in aqueous solutions which makes it an ideal material for membrane separation applications in such environments (61). The properties of reduced GO highly depends on the method of fabrication such as reduction time, intensity of materials and/or other reducing factors. These factors can determine the level of GO reduction leading to partially reduced or highly reduced graphene oxide with significant number of defects and holes on the surface.

Graphene oxide can be reduced in three main ways: 1) Photo reduction, where the GO suspension is placed under a UVA radiation, 2) Chemical reduction using chemical reducing agents (e.g. hydrazine), and 3) Thermal reduction where the GO powder is heated in the furnace at high temperatures (71, 72). Recent studies have shown that GO also can be reduced to rGO by bacterial degradation and sunlight exposure (73).

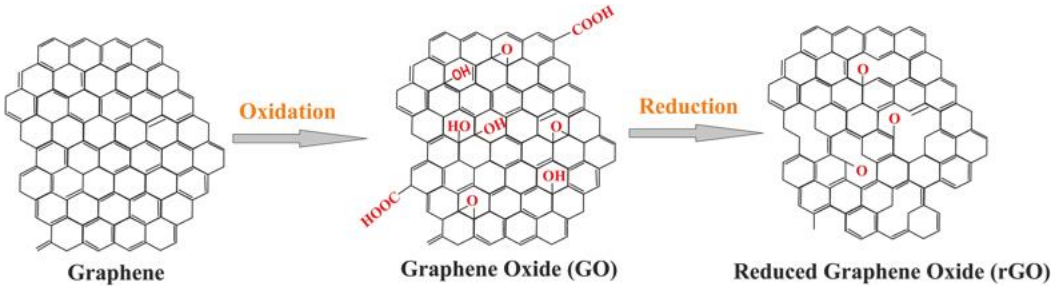

Figure 2.9 Schematic of graphene oxide and reduced graphene oxide sheets (10).

2.3.3 Graphene-based composites

Graphene-based composites are fabricated by integration of GO or rGO with another functional material such as polymers. Due to the polarity of these two materials, they can be well mixed together and make covalent or noncovalent bonds. The inorganic-polymer composites are also referred to as Mixed Matrix Membranes (MMMs) and they can be widely used in different separation applications such as water purification and gas separation (74, 75). In figure 2.10, the structure of mixed matrix membranes is illustrated.

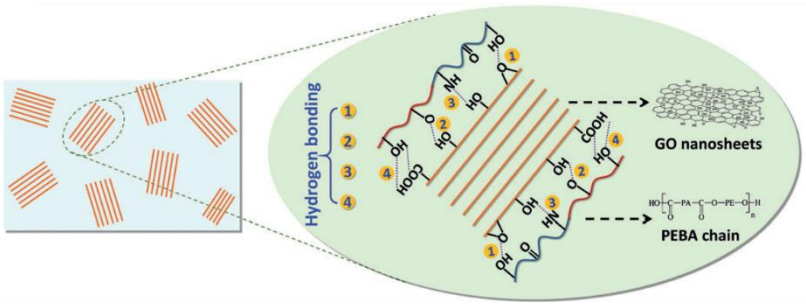

Figure 2.10 Schematic representation of the assembly of GO Nano sheets in polymeric environment (8)

2.3.4 Graphene-based membranes modules

Graphene based membranes can be developed in two ways: free-standing (75, 76) or supported by a porous substrate (75, 77-81). Free-standing membranes without a robust support are fragile and do not possess high mechanical stability which is huge drawback especially in practical applications (75, 82). Therefore, in most cases, supported graphene membranes have been frequently utilised and different configurations of supports such as planar or hollow fiber have been developed to increase the mechanical strength and stability of the membranes (78-81, 83, 84). Among diverse types of supports, porous hollow fiber substrates are favourable structures because of their high area/volume ratio, low transport resistance and low synthesis cost (77-81, 85).

Interestingly, in most of the synthesized membranes with hollow fiber support, the selective layer has been deposited outside the substrate (77, 78, 80, 81). Graphene can be fabricated effectively on the hollow fiber support via different methods such as dip-coating (77) and vacuum suction method (80, 81). However, in many of these membranes, when the operation pressure or the interfacial stress surpasses a specific value, graphene layer peels off from the support which is a serious issue for membrane integrity (77, 80, 81). This problem can be mainly caused by the weak interfacial adhesion between the membrane and the support (77, 81). For resolving this issue, some researchers attempted to increase the bonding strength between the support and the active layer (e.g. via silane grafting (77, 86)).

Besides, some researches are carried out to prepare the selective layer inside the hollow fiber support (87-90). In these cases the membrane layer is better protected from the possible damages that may be caused physically or mechanically during the operation (88, 90) which is a benefit for large-scale industrial modules (87, 89-91).

By embedding the graphene selective layer as the inner part of the hollow fiber, the graphene layer won't peel off so quickly from the substrate at high pressures (92). This problem is a real challenge in the other similar membranes in which graphene is synthesized on the outside surface of the hollow fiber substrates (93).

2.4 Graphene-based membranes applications in gas separation and water purification

Graphene-based membranes have been used extensively in a wide range of separation applications both in water and gas separations. Excellent separation performance of these membranes as well as high chemical and mechanical stability in harsh environments are the most critical features exhibited by graphene-based membranes.

Recently, porous graphene membranes drilled via an oxygen plasma etching process have been proposed for efficient desalination and water treatment. The drilled membranes, exhibit almost 100% salt rejection rate and very fast water transport (46). In another report, a porous graphene molecular sieving membrane, perforated with ultraviolent-induced oxidative etching, displays size-selective separation of CO_2 from Ar and CH_4 (51).

Due to great potential of GO-based membranes in water purification, they have been widely investigated. One of the good examples of such applications was reported by *Huang et al.* on the separation of aqueous organic solution mixture using pervaporation process. They coated a layer of graphene oxide on a ceramic hollow fiber support by vacuum-assisted suction method. The resultant membrane was tested for water and dimethyl carbonate separation and result showed a final water weight percentage of 92% with excellent water permeation flux (80).

For better membrane separation performance in aqueous solutions, modified graphene oxide membranes have been widely prepared and reported. *Yeh et al.* suggested a method for preparing the graphene oxide membranes supported on porous anodic aluminium oxide (AAO) filter discs. In this design, the GO flakes were cross-linked with Al^{3+} released from the filter discs during vacuum filtration process resulting in high quality GO membrane with high stability in water-based environments (64).

Another type of modified graphene oxide membrane in water purification is reduced graphene oxide (rGO). As proposed by *Thebo et al.* rGO membranes reduced by theanine amino acid and tannic acid reducing agents exhibited good separation efficiency of rhodamine B and methylene blue rejection of around 100% as well as 1000 L m^{-2} h^{-1} bar^{-1} of water permeance. This performance is described as 10-1000 times better than most of the previously reported commercial membranes (61).

GO-based membranes have been used not only in water purification applications but also in other liquid filtration processes. One good example of these works is the ceramic hollow fiber supported graphene oxide membrane fabricated by *Aba et al.* for organic solvents nanofiltartion applications with a molecular weight cut off lower than 300 Da as well as a high acetone and methanol permeation rates. These membranes assembled by facile vacuum filtration method showed high stability in wet environments; however, the selective GO layer was shrunk and peeled off from the support. Therefore, it was suggested to keep the membranes in wet conditions to maintain their high stability (81).

Based on the research by *Nair et al.* GO sheets are impermeable to gases even as small as helium (63). However, *Li et al.* discovered that using the defects within GO flakes, high performance for gas separation is possible for graphene oxide membranes**.** They suggested a facile way of filtration process to prepare GO membrane with extraordinary mixture separation selectivities of 3400 and 900 for H_2/CO_2 and H_2/N_2 gas mixtures respectively. They proved that hydrogen permeation through the graphene oxide membranes occurred mainly through selective structural defects created during the membrane fabrication (94).

At the same time, *Kim et al.* also reported GO membranes with CO_2-philic permeation. By using different stacking methods, the prepared GO membranes in several layers with thickness in a few nanometres gas permeation with high selectivity through these membranes is possible. They future advised that the selectivity of the membrane can be increased by controlling the gas flow channels and introducing extra porosity on GO sheets (95).

GO-based composites have also been used in gas separation applications. *Shen et al*. proposed a preparation method via which the membrane shows excellent selectivity for CO_2/N_2 with a CO_2 permeability of 100 Barrer as well as extraordinary operational stability, expanding the possibility for practical applications. The reported GO layers assembled in PEBA polymeric environment exhibited strong interactions between GO and the polymeric chains developing molecular sieving channels for gas separation (75).

2.5 Separation mechanism in graphene-based membranes

Depending on the application, there are different types of separation mechanisms and factors affecting the molecular transport in graphene-based membranes which are briefly discussed below.

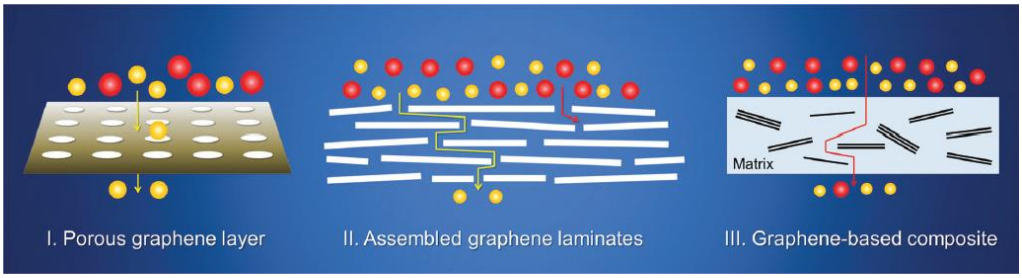

Figure 2.11 Three types of transport mechanism in graphene-based membranes (6)

2.5.1 Channels from interlayer space

As discussed earlier, graphene and its derivatives have planar layered structures in which the distance between each two parallel adjacent layers is called d-spacing (Figure 2.11 (I)). The interlayer space is one of the major pathways for transporting molecules through the membrane.

In liquid separation and especially water filtration, the interlayer spacing is the major transport channel via which water easily passes through the membrane while other unwanted molecules are blocked. As mentioned in section 3.2.2.2, graphene oxide layers include hydrophilic oxygen-containing groups in their structure which absorb water into the 2D channels and develop a capillary-like driving force. *Geim et al.* used Hagen-Poiseuille's law to describe the water flow regime between the interlayer spacing. They assumed the water flow behaviour as classic liquid and ΔP = 1 bar to be able to use this model (63, 96):

$$J = \frac{\mathrm{d}^4 . \Delta P}{12\ \mathrm{L}^2 . \eta . h} \qquad (2.12)$$

Where d is the interlayer spacing, L is the lateral size of graphene sheets, η is the water viscosity and h is the membrane thickness.

However, they observed that the water permeation rate was actually 4-6 orders of magnitude higher than the theoretical prediction from equation 2.12.

They explained that the real reason of the super-high water permeation flux is the pristine graphene regions (non-polar sites) with slip flow theory (97). Therefore, the hydrophobic non-polar parts on GO sheets provide friction less carbon walls for water transport which is ideal for fast transport and high permeation rate.

2.5.2 Pores or defects

In addition to the interlayer channels between graphene sheets, drilled pores or structural defects also can contribute the membrane transport mechanism. When these pores and defects are claimed to be the major molecular pathways for gas separation (94) convective flow, Knudsen diffusion, or molecular sieving can dominate the system, depending on the size of the pore and/or defects which is discussed in section 2.3 comprehensively.

In some cases, the microstructural defects or drilled pores provide diffusion shortcuts for the species transport. It means the molecules are able to pass through the space between the layers much quicker due to the presence of defects or pores on the graphene sheets. This phenomenon is equivalent to reduce the membrane effective thickness, thus leading to higher permeation rates ultimately (6, 81) (figure 2.12).

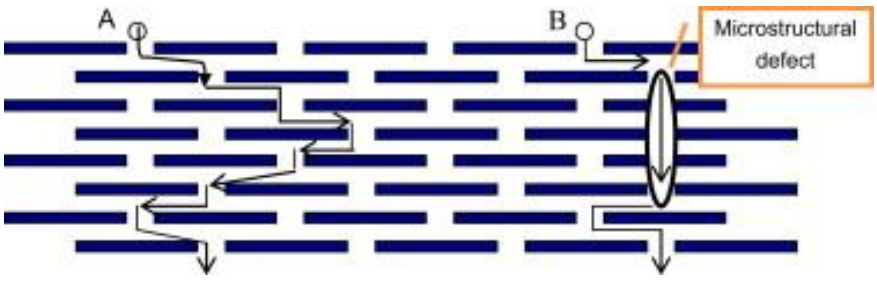

Figure 2.12 Schematic of diffusion shortcut provided by the microstructural defects (85)

2.5.3 Functional groups

The presence of polar functional groups on the basal planes and edges of graphene derivative (e.g., GO and rGO) layers will play another critical role in molecular transport through graphene-based membranes. These oxygen-containing groups are able to interact with chemical species which may facilitate the transport of some molecules through the membrane. For example, based on the research by *Liang et al.* on water sorption measurements for some GO membranes, it indicates that the water selective graphene oxide membrane has a higher water sorption value compared to the organic compounds which transports through the membrane in a much slower rate (98).

The adsorption property of the graphene polar groups can also be used for CO_2 separation from gas mixtures. This adsorption is due to the interactions between the polar C-O bonds of carbon dioxide with –OH and –COOH groups on graphene sheets. *Li et al.* measured the adsorption of different gases by graphene oxide illustrating high adsorption of CO_2. They reported that the membrane performance for CO_2 separation based on adsorption difference is widely dependent on many factors like temperature, which can be either facilitating or prohibitive factor for permeation of the adsorbed molecules (94, 95).

Practically, molecular transport mechanism through graphene based membranes may be a synergetic performance of all the above mentioned mechanisms and the dominant regime is determined using the experimental measurements.

2.6 Graphene membranes financial aspects

Owing to high dispersibility of graphene oxide in aqueous solutions, which makes it ideal for the preparation of supported membranes, it is the most favourite starting membrane material among these graphene derivatives. However, compared to graphene, GO is a very expensive material which is a drawback for large-scale production of the membrane for industrial applications.

On the other hand, 2D graphene nanosheet is a more affordable option also with a layered structure like GO which can lead to good separation performance if a suitable method of fabrication is employed.

Table 2.1 summarizes the price of some types of graphene oxide and graphene powders derived from a range of suppliers websites:

Material	Supplier	Price (AUD)/g
GO	Sigma-Aldrich	$475
	Graphene-supermarket.com	$300
	Graphenea.com	$97
Graphene	Sigma-Aldrich (this work)	$1.1
	Graphene-supermarket.com	$4.95
	Alibaba.com	$10

Table 2.1 Graphene and graphene oxide prices in current market in June 2019

As is illustrated in table 2.1, there is a significant difference between the unit prices of graphene and graphene oxide powder. This difference can lead to a huge change in capital costs of the membranes large-scale production which is a very important fact to consider. Therefore, in this project, graphene nanosheets will be attempted to prepare the membrane directly.

2.7 Scope of research

Exploration of novel molecular sieving membranes with improved performance and reduced synthesis cost is always a hot topic with one typical example of recently emerged 2D graphene oxides (GO) membranes. These graphene oxide (GO) nanoflakes with thickness less than 10 nm have been applied as the building block to assemble these 2D membranes. Most of these multi-layered GO nanosheets themselves have inherent interlayer channels. *Schulz et al.* have reported a method of graphite disc membranes for steam reforming of ethanol (99). However, the proposed fabrication method needed a lot of energy consumption for membrane fabrication under extremely

high pressures. Here, graphene nanoplatelets are used instead which is much easier to be formed to membrane discs under a pressure almost 50 times smaller than the reported pressure in previous literature. To clarify the molecular sieving property stemmed from the interspace of the building block itself or between two neighbouring blocks, in this work, commercial graphene flakes (GF) with average thickness of 7 nm were applied to form GF membranes under the hydraulic pressure. In this project, different flake sizes and surface areas of graphene nanoplatelets are used (5, 15, and 25 μm flake size) for fabricating the membranes to study the effect of graphene properties on the membrane performance. GF membrane in the overall thickness of 0.75 mm made from 25-μm-sized flakes displayed good molecular sieving property and the measured helium permeance of $2.02*10^{-8}$ $mol.s^{-1}.m^{-2}.Pa^{-1}$ with selectivity of 65 (He/CO_2) and 22 (He/N_2) and separation factor more than 10 from gas mixture separation. Such results clearly demonstrate that molecular sieving properties are sourced from the tortuous interspace between the building blocks as the individual GFs are gas impermeable.

Moreover, in order to further improve the membrane performance for CO_2 separation, zeolite (13X and 4A) is introduced to the membrane structure in the support layer as well which helped in improving the separation performance of the above membranes significantly.

References

1. Membrane Transport Theory. Membrane Technology and Applications.
2. Gas Separation. Membrane Technology and Applications.
3. Overview of Membrane Science and Technology. Membrane Technology and Applications.
4. Membrane Separation Processes, 1. Principles. Ullmann's Encyclopedia of Industrial Chemistry.
5. Atta NF, Galal A, El-Ads EH. Graphene — A Platform for Sensor and Biosensor Applications. Biosensors - Micro and Nanoscale Applications2015.
6. Liu G, Jin W, Xu N. Graphene-based membranes. Chem Soc Rev. 2015;44(15):5016-30.
7. Wei G, Quan X, Chen S, Yu H. Superpermeable Atomic-Thin Graphene Membranes with High Selectivity. ACS Nano. 2017;11(2):1920-6.
8. Shen J, Liu G, Huang K, Jin W, Lee K-R, Xu N. Membranes with Fast and Selective Gas-Transport Channels of Laminar Graphene Oxide for Efficient CO2 Capture. Angewandte Chemie. 2015;127(2):588-92.
9. Zheng S, Tu Q, Urban JJ, Li S, Mi B. Swelling of Graphene Oxide Membranes in Aqueous Solution: Characterization of Interlayer Spacing and Insight into Water Transport Mechanisms. ACS Nano. 2017;11(6):6440-50.
10. Priyadarsini S, Mohanty S, Mukherjee S, Basu S, Mishra M. Graphene and graphene oxide as nanomaterials for medicine and biology application. Journal of Nanostructure in Chemistry. 2018;8(2):123-37.
11. Berry V. Impermeability of graphene and its applications. Carbon. 2013;62:1-10.
12. Strathmann H. Membrane separation processes. J Membrane Sci. 1981;9(1):121-89.
13. Cui ZF, Jiang Y, Field RW. Chapter 1 - Fundamentals of Pressure-Driven Membrane Separation Processes. In: Cui ZF, Muralidhara HS, editors. Membrane Technology. Oxford: Butterworth-Heinemann; 2010. p. 1-18.
14. Li X, Li J. Fluxes and Driving Forces in Membrane Separation Processes. In: Drioli E, Giorno L, editors. Encyclopedia of Membranes. Berlin, Heidelberg: Springer Berlin Heidelberg; 2015. p. 1-3.
15. Greenhouse H, Lowry R, Romenesko B. 3 - The Flow of Gases. In: Greenhouse H, Lowry R, Romenesko B, editors. Hermeticity of Electronic Packages (Second Edition). Oxford: William Andrew Publishing; 2012. p. 37-61.
16. Orakwe I, Nwogu N, Gobina E, editors. Characterization of an Alumina Membrane Using Single Gas Permeation2016; Singapore: Springer Singapore.
17. He W, Lv W, Dickerson JH. Gas Diffusion Mechanisms and Models. Gas Transport in Solid Oxide Fuel Cells. Cham: Springer International Publishing; 2014. p. 9-17.
18. Colin S. Chapter 2 - Single-Phase Gas Flow in Microchannels. In: Kandlikar SG, Garimella S, Li D, Colin S, King MR, editors. Heat Transfer and Fluid Flow in Minichannels and Microchannels (Second Edition). Oxford: Butterworth-Heinemann; 2014. p. 11-102.
19. Ho C, Webb S. Gas Transport in Porous Media2006.
20. Whitaker S. Flow in porous media I: A theoretical derivation of Darcy's law. Transport in Porous Media. 1986;1(1):3-25.
21. Aydin O, Avci M, editors. Convective Heat Transfer Correlations in Some Common Micro-Geometries2010; Dordrecht: Springer Netherlands.
22. Cunningham RE, Williams RJJ. Diffusion in gases and porous media. New York: Plenum Press; 1980. xxiii, 275 p. p.

23. Rackley SA. 8 - Membrane separation systems. In: Rackley SA, editor. Carbon Capture and Storage (Second Edition). Boston: Butterworth-Heinemann; 2017. p. 187-225.
24. Pandey P, Chauhan RS. Membranes for gas separation. Progress in Polymer Science. 2001;26(6):853-93.
25. Rackley SA. 8.1 Physical and Chemical Fundamentals. Carbon Capture and Storage: Elsevier. p. 1-36.
26. Ladewig B, Al-Shaeli MNZ. Fundamentals of Membrane Processes. Fundamentals of Membrane Bioreactors: Materials, Systems and Membrane Fouling. Singapore: Springer Singapore; 2017. p. 13-37.
27. Robeson LM. The upper bound revisited. J Membrane Sci. 2008;320(1):390-400.
28. Seo Y, Hong SU, Lee B-S. Overcoming the "Upper Bound" in Polymeric Gas-Separation Membranes. Angewandte Chemie International Edition. 2003;42(10):1145-9.
29. Lee C, Wei XD, Kysar JW, Hone J. Measurement of the elastic properties and intrinsic strength of monolayer graphene. Science. 2008;321(5887):385-8.
30. Geim AK. Graphene: Status and Prospects. Science. 2009;324(5934):1530-4.
31. Celebi K, Buchheim J, Wyss RM, Droudian A, Gasser P, Shorubalko I, et al. Ultimate Permeation Across Atomically Thin Porous Graphene. Science. 2014;344(6181):289-92.
32. Chang Y, Shen Y, Kong D, Ning J, Xiao Z, Liang J, et al. Fabrication of the reduced preoxidized graphene-based nanofiltration membranes with tunable porosity and good performance. Rsc Adv. 2017;7(5):2544-9.
33. Novoselov KS, Geim AK, Morozov SV, Jiang D, Zhang Y, Dubonos SV, et al. Electric Field Effect in Atomically Thin Carbon Films. Science. 2004;306(5696):666-9.
34. Geim AK, Novoselov KS. The rise of graphene. Nature Materials. 2007;6:183.
35. Tassin P, Koschny T, Kafesaki M, Soukoulis CM. A comparison of graphene, superconductors and metals as conductors for metamaterials and plasmonics. Nature Photonics. 2012;6:259.
36. Bunch JS, Verbridge SS, Alden JS, van der Zande AM, Parpia JM, Craighead HG, et al. Impermeable Atomic Membranes from Graphene Sheets. Nano Lett. 2008;8(8):2458-62.
37. Sreeprasad TS, Berry V. How Do the Electrical Properties of Graphene Change with its Functionalization? Small. 2013;9(3):341-50.
38. Lin Y, Liao Y, Chen Z, Connell JW. Holey graphene: a unique structural derivative of graphene. Materials Research Letters. 2017;5(4):209-34.
39. Bieri M, Treier M, Cai J, Aït-Mansour K, Ruffieux P, Gröning O, et al. Porous graphenes: two-dimensional polymer synthesis with atomic precision. Chemical Communications. 2009(45):6919-21.
40. Bieri M, Nguyen M-T, Gröning O, Cai J, Treier M, Aït-Mansour K, et al. Two-Dimensional Polymer Formation on Surfaces: Insight into the Roles of Precursor Mobility and Reactivity. Journal of the American Chemical Society. 2010;132(46):16669-76.
41. Schneider GF, Kowalczyk SW, Calado VE, Pandraud G, Zandbergen HW, Vandersypen LMK, et al. DNA Translocation through Graphene Nanopores. Nano Lett. 2010;10(8):3163-7.
42. Girit ÇÖ, Meyer JC, Erni R, Rossell MD, Kisielowski C, Yang L, et al. Graphene at the Edge: Stability and Dynamics. Science. 2009;323(5922):1705-8.
43. Yuan W, Chen J, Shi G. Nanoporous graphene materials. Materials Today. 2014;17(2):77-85.
44. Bai J, Zhong X, Jiang S, Huang Y, Duan X. Graphene nanomesh. Nature nanotechnology. 2010;5(3):190-4.
45. Sint K, Wang B, Král P. Selective Ion Passage through Functionalized Graphene Nanopores. Journal of the American Chemical Society. 2008;130(49):16448-9.
46. Surwade SP, Smirnov SN, Vlassiouk IV, Unocic RR, Veith GM, Dai S, et al. Water desalination using nanoporous single-layer graphene. Nature Nanotechnology. 2015;10:459.

47. Fan Z. Easy synthesis of porous graphene nanosheets and their use in supercapacitors. Carbon. 2012;v. 50(no. 4):pp. 1699-703-2012 v.50 no.4.
48. Fox D, Gallagher A, Zhou D, Boese M, N. Coleman J, Zhang H. Nitrogen assisted etching of graphene layers in a scanning electron microscope2011. 243117- p.
49. Lin Z, Waller GH, Liu Y, Liu M, Wong C-p. Simple preparation of nanoporous few-layer nitrogen-doped graphene for use as an efficient electrocatalyst for oxygen reduction and oxygen evolution reactions. Carbon. 2013;53:130-6.
50. Liu L, Ryu S, Tomasik MR, Stolyarova E, Jung N, Hybertsen MS, et al. Graphene Oxidation: Thickness-Dependent Etching and Strong Chemical Doping. Nano Lett. 2008;8(7):1965-70.
51. Koenig SP, Wang L, Pellegrino J, Bunch JS. Selective molecular sieving through porous graphene. Nature Nanotechnology. 2012;7:728.
52. Chang H, Bard AJ. Scanning tunneling microscopy studies of carbon-oxygen reactions on highly oriented pyrolytic graphite. Journal of the American Chemical Society. 1991;113(15):5588-96.
53. Tabish TA, Memon FA, Gomez DE, Horsell DW, Zhang S. A facile synthesis of porous graphene for efficient water and wastewater treatment. Scientific Reports. 2018;8(1):1817.
54. Li W, Wu W, Li Z. Controlling Interlayer Spacing of Graphene Oxide Membranes by External Pressure Regulation. ACS Nano. 2018;12(9):9309-17.
55. Huang H, Ying Y, Peng X. Graphene oxide nanosheet: an emerging star material for novel separation membranes. J Mater Chem A. 2014;2(34):13772-82.
56. Dikin DA, Stankovich S, Zimney EJ, Piner RD, Dommett GHB, Evmenenko G, et al. Preparation and characterization of graphene oxide paper. Nature. 2007;448:457.
57. Zheng Q, Li Z, Yang J, Kim J-K. Graphene oxide-based transparent conductive films. Progress in Materials Science. 2014;64:200-47.
58. Upadhyay RK, Naicker S, Barman A, Roy SS, Thundat T, Waghmare PR. Fabrication of free-standing graphene oxide films using a facile approach toluene swollen paraffin peeling and green reduction of these films into highly conductive reduced graphene oxide films. Chemical Engineering Journal. 2018;354:149-61.
59. Hung W-S, Lin T-J, Chiao Y-H, Sengupta A, Hsiao Y-C, Wickramasinghe SR, et al. Graphene-induced tuning of the d-spacing of graphene oxide composite nanofiltration membranes for frictionless capillary action-induced enhancement of water permeability. J Mater Chem A. 2018;6(40):19445-54.
60. Wei N, Peng X, Xu Z. Understanding Water Permeation in Graphene Oxide Membranes. Acs Appl Mater Inter. 2014;6(8):5877-83.
61. Thebo KH, Qian X, Zhang Q, Chen L, Cheng H-M, Ren W. Highly stable graphene-oxide-based membranes with superior permeability. Nat Commun. 2018;9(1):1486.
62. Mural PKS, Jain S, Kumar S, Madras G, Bose S. Unimpeded permeation of water through biocidal graphene oxide sheets anchored on to 3D porous polyolefinic membranes. Nanoscale. 2016;8(15):8048-57.
63. Nair RR, Wu HA, Jayaram PN, Grigorieva IV, Geim AK. Unimpeded Permeation of Water Through Helium-Leak-Tight Graphene-Based Membranes. Science. 2012;335(6067):442-4.
64. Yeh C-N, Raidongia K, Shao J, Yang Q-H, Huang J. On the origin of the stability of graphene oxide membranes in water. Nature Chemistry. 2015;7:166.
65. Park S, Lee K-S, Bozoklu G, Cai W, Nguyen ST, Ruoff RS. Graphene Oxide Papers Modified by Divalent Ions—Enhancing Mechanical Properties via Chemical Cross-Linking. ACS Nano. 2008;2(3):572-8.
66. Hummers WS, Offeman RE. Preparation of Graphitic Oxide. Journal of the American Chemical Society. 1958;80(6):1339-.

67. Zaaba NI, Foo KL, Hashim U, Tan SJ, Liu W-W, Voon CH. Synthesis of Graphene Oxide using Modified Hummers Method: Solvent Influence. Procedia Engineering. 2017;184:469-77.
68. Yu H, Zhang B, Bulin C, Li R, Xing R. High-efficient Synthesis of Graphene Oxide Based on Improved Hummers Method. Scientific Reports. 2016;6:36143.
69. Pei S, Wei Q, Huang K, Cheng H-M, Ren W. Green synthesis of graphene oxide by seconds timescale water electrolytic oxidation. Nat Commun. 2018;9(1):145.
70. Chowdhury I, Mansukhani ND, Guiney LM, Hersam MC, Bouchard D. Aggregation and Stability of Reduced Graphene Oxide: Complex Roles of Divalent Cations, pH, and Natural Organic Matter. Environmental Science & Technology. 2015;49(18):10886-93.
71. Komeily Nia Z, Chen J-Y, Tang B, Yuan B, Wang X-G, Li J-L. Optimizing the free radical content of graphene oxide by controlling its reduction. Carbon. 2017;116:703-12.
72. De Silva KKH, Huang HH, Joshi RK, Yoshimura M. Chemical reduction of graphene oxide using green reductants. Carbon. 2017;119:190-9.
73. Salas EC, Sun Z, Lüttge A, Tour JM. Reduction of Graphene Oxide via Bacterial Respiration. ACS Nano. 2010;4(8):4852-6.
74. Zahri K, Wong KC, Goh PS, Ismail AF. Graphene oxide/polysulfone hollow fiber mixed matrix membranes for gas separation. Rsc Adv. 2016;6(92):89130-9.
75. Shen J, Liu GP, Huang K, Jin WQ, Lee KR, Xu NP. Membranes with Fast and Selective Gas-Transport Channels of Laminar Graphene Oxide for Efficient CO2 Capture. Angew Chem-Int Edit. 2015;54(2):578-82.
76. Liu F, Seo TS. A Controllable Self-Assembly Method for Large-Scale Synthesis of Graphene Sponges and Free-Standing Graphene Films. Adv Funct Mater. 2010;20(12):1930-6.
77. Lou YY, Liu GP, Liu SN, Shen J, Jin WQ. A facile way to prepare ceramic-supported graphene oxide composite membrane via silane-graft modification. Appl Surf Sci. 2014;307:631-7.
78. Zhu JC, Meng XX, Zhao JP, Jin Y, Yang NT, Zhang SG, et al. Facile hydrogen/nitrogen separation through graphene oxide membranes supported on YSZ ceramic hollow fibers. J Membrane Sci. 2017;535:143-50.
79. Li H, Song ZN, Zhang XJ, Huang Y, Li SG, Mao YT, et al. Ultrathin, Molecular-Sieving Graphene Oxide Membranes for Selective Hydrogen Separation. Science. 2013;342(6154):95-8.
80. Huang K, Liu GP, Lou YY, Dong ZY, Shen J, Jin WQ. A Graphene Oxide Membrane with Highly Selective Molecular Separation of Aqueous Organic Solution. Angew Chem-Int Edit. 2014;53(27):6929-32.
81. Aba NFD, Chong JY, Wang B, Mattevi C, Li K. Graphene oxide membranes on ceramic hollow fibers - Microstructural stability and nanofiltration performance. J Membrane Sci. 2015;484:87-94.
82. Mi BX. Graphene Oxide Membranes for Ionic and Molecular Sieving. Science. 2014;343(6172):740-2.
83. Wang HH, Feldhoff A, Caro J, Schiestel T, Werth S. Oxygen Selective Ceramic Hollow Fiber Membranes for Partial Oxidation of Methane. Aiche J. 2009;55(10):2657-64.
84. Tan XY, Li K. Oxygen production using dense ceramic hollow fiber membrane modules with different operating modes. Aiche J. 2007;53(4):838-45.
85. Shi Z, Zhang Y, Cai C, Zhang C, Gu X. Preparation and characterization of α-Al2O3 hollow fiber membranes with four-channel configuration. Ceramics International. 2015;41(1):1333-9.
86. Ma J, Zhang MH, Wu H, Yin X, Chen J, Jiang ZY. Mussel-inspired fabrication of structurally stable chitosan/polyacrylonitrile composite membrane for pervaporation dehydration. J Membrane Sci. 2010;348(1-2):150-9.

87. Richter H, Voigt I, Fischer G, Puhlfurss P. Preparation of zeolite membranes on the inner surface of ceramic tubes and capillaries. Sep Purif Technol. 2003;32(1-3):133-8.
88. Pera-Titus M, Llorens J, Cunill F, Mallada R, Santamaria J. Preparation of zeolite NaA membranes on the inner side of tubular supports by means of a controlled seeding technique. Catal Today. 2005;104(2-4):281-7.
89. Pera-Titus M, Bausach M, Llorens J, Cunill F. Preparation of inner-side tubular zeolite NaA membranes in a continuous flow system. Sep Purif Technol. 2008;59(2):141-50.
90. Huang K, Dong ZY, Li QQ, Jin WQ. Growth of a ZIF-8 membrane on the inner-surface of a ceramic hollow fiber via cycling precursors. Chemical Communications. 2013;49(87):10326-8.
91. Aguado S, Gascón J, Jansen JC, Kapteijn F. Continuous synthesis of NaA zeolite membranes. Microporous and Mesoporous Materials. 2009;120(1):170-6.
92. Zhou F, Tien HN, Xu WL, Chen J-T, Liu Q, Hicks E, et al. Ultrathin graphene oxide-based hollow fiber membranes with brush-like CO2-philic agent for highly efficient CO2 capture. Nat Commun. 2017;8(1):2107.
93. Dikin DA, Stankovich S, Zimney EJ, Piner RD, Dommett GHB, Evmenenko G, et al. Preparation and characterization of graphene oxide paper. Nature. 2007;448(7152):457-60.
94. Li H, Song Z, Zhang X, Huang Y, Li S, Mao Y, et al. Ultrathin, Molecular-Sieving Graphene Oxide Membranes for Selective Hydrogen Separation. Science. 2013;342(6154):95-8.
95. Kim HW, Yoon HW, Yoon S-M, Yoo BM, Ahn BK, Cho YH, et al. Selective Gas Transport Through Few-Layered Graphene and Graphene Oxide Membranes. Science. 2013;342(6154):91-5.
96. Majumder M, Chopra N, Hinds BJ. Mass Transport through Carbon Nanotube Membranes in Three Different Regimes: Ionic Diffusion and Gas and Liquid Flow. ACS Nano. 2011;5(5):3867-77.
97. Han Y, Xu Z, Gao C. Ultrathin Graphene Nanofiltration Membrane for Water Purification. Adv Funct Mater. 2013;23(29):3693-700.
98. Liang B, Zhan W, Qi G, Lin S, Nan Q, Liu Y, et al. High performance graphene oxide/polyacrylonitrile composite pervaporation membranes for desalination applications. J Mater Chem A. 2015;3(9):5140-7.
99. Schulz A, Steinbach F, Caro J. Pressed graphite crystals as gas separation membrane for steam reforming of ethanol. J Membrane Sci. 2014;469:284-91.

Chapter 3 Methodology

3.1 Materials

The two main materials used for the membrane fabrication were graphene nanoplatelets and zeolite powder.

Graphene nanoplatelets were purchased from Sigma-Aldrich, manufactured by XGnP®. Graphene nanoplatelets are nanoparticles consisting of short stacks of graphene sheets which have platelet shape. The type of graphene was Grade M which has an average thickness of approximately 6-8 nanometres with a typical surface area of 120-150 m^2/g. Three flake sizes of this grade of graphene nanoplatelets were purchased with 5, 15, and 25 µm diameter.

Two types of zeolite powder were used in membrane fabrication. The first type is zeolite molecular sieves powder 13X with particle size of 2 µm and the second type is zeolite molecular sieves type 4A with pore diameter of 4Å. Bothe these types are manufactured by Fluka Analytical and supplied by Sigma-Aldrich.

For the gas permeation tests, helium (99.99% purity), nitrogen (99.98% purity) and carbon dioxide (99.98 % purity) supplied by BOC and Coregas Pty.Ltd were used.

3.2 Membrane preparation

3.2.1 Pressing Device

Figure 3.1 illustrates the stainless-steel pressing die which is used for shaping the initial powders into disc-shaped membranes. There are four main parts in this pressing die as demonstrated in Figure 3.2. These parts are such as 1) Top Pressing Rod, 2) Pressing Die Sleeve, 3) Support Plate, and 4) Bottom Pressing Rod. All these parts are removable and cleaned before and after pressing using ethanol. After cleaning the parts, the weighed powder was poured inside the Pressing Die Sleeve and then, the Top Pressing Rod was carefully placed on top of the powder.

Figure 3.1 Stainless-Steel pressing die

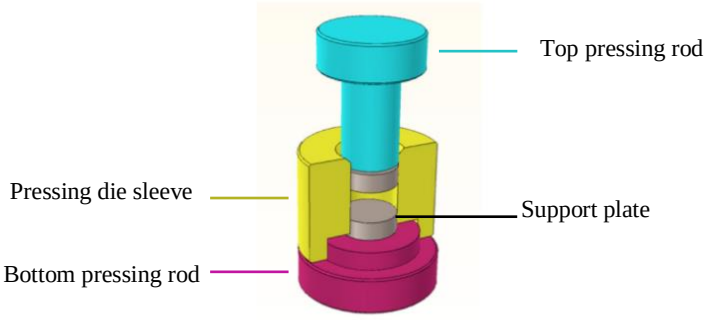

Figure 3.2 Schematic illustration of pressing die parts

Once the pressing die was filled with powder and the Top Pressing Rod was in place, the powder was pressed using the pressing machine. As illustrated in Figure 3.3, the lab-scale powder pressing machine consists of two pressing plates where the pressing die is placed in between. There is a handle to increase the pressure and a pressure gauge to show the pressing pressure. The highest pressure which could be used for pressing was 20 MPa (Mega Pascal).

Figure 3.3 Lab scale pressing machine

3.2.2 Pure membrane preparation

Pure graphene flakes were weighed and poured inside the pressing die sleeve and it was pressed to form disc-shaped pure membranes.

3.2.3 Layered asymmetric membrane preparation

For the layered membranes, first a certain amount of graphene/zeolite mixture was weighed and poured inside the pressing die sleeve and then the pure graphene was poured subsequently. Afterwards, the second layer was pressed simultaneously with the first layer to form the layered membranes.

The mixed layer of the membrane consisting of graphene flakes and zeolite powder needed was mixed using one of the following methods: 1) Hand grinding, and 2) Ball milling.

3.2.4 Hand grinding

In hand-mixing the powders, first graphene and zeolite powder were weighed depending on the required zeolite weight percentage and then they were poured inside the Mortar and grinded with hand smoothly until a uniform mixture is formed.

Figure 3.4 Lab scale Mortar and Pestle used for hand grinding the powder mixture

3.2.5 Ball milling

In the second method of mixing the two powders, using ball milling equipment. In this method, first the weighed powders were poured inside the mill jar containing 12 mm ceramic mill balls (Figure 3.5) with the ball milling ratio of 10:1 (balls: materials). Then ethanol was added to the powders to facilitate the milling procedure. The mill jar was located inside the ball milling equipment which was Pulverisette 6 (Planetary Mono Mill) on 100rpm speed with 4 repeats (each repeat was 10 min duration). Once the milling was completed the mixture/ethanol solution was dried in the oven at 40℃ to obtain the graphene/zeolite dry mixture.

Figure 3.5 Mill jar and ceramic ball mills

Figure 3.6 Ball milling machine

3.3 Single gas permeation test

Single gas permeation test was performed for helium, carbon dioxide and nitrogen at 1 bar pressure difference. The setup used for this part of the experiments was designed using different stainless-steel tubes and fittings supplied by Swagelok Australia. As illustrated in Figure 3.7, the membrane was first sealed with ceramabond on one end of a ½ inch stainless steel tube. Then the ½ inch tube was inserted inside a 1 inch stainless steel membrane cell which was connected to a pressure gauge. To be able to secure the ½ inch tube inside the 1 inch tube with the membrane attached to it, nylon ferrules set was used for this tube due to its capability in being removed and reattached to the tube, while for all the other fittings stainless steel nuts and ferrules were utilised which is fixed on the tubes and cannot be removed later. The membrane cell included a vent close to the end of the membrane cell to make sure that it is full with pure test gas and not air or any other residual gases from the previous tests. The other end of the ½ inch tube (the permeate side of

the membrane) was connected to a digital ADM flowmeter (Agilent Technologies) and the permeated flow (ml/min) was measured.

Feed gas was sent to the membrane cell using a gas flow controller (GFC) with a flow rate of around 20ml/min and the feed pressure was kept constant at 2 bar and permeate pressure at 1 bar.

This setup was used for both pure and asymmetric layered composite membranes to evaluate their single gas permeation performance. The measurable gas flow rate using the ADM flow meter was V>0.01 ml/min. Where V is volumetric flow rate of the permeated gas (ml/min).

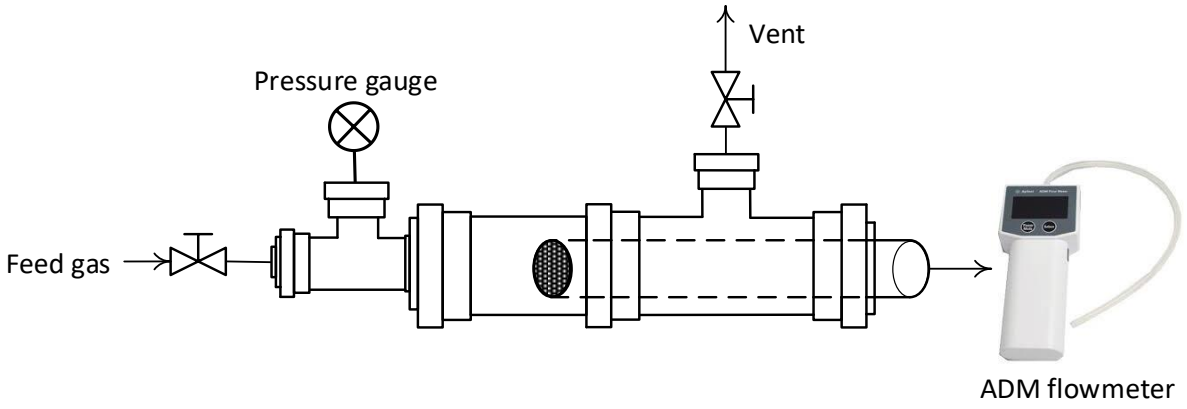

Figure 3.7 Schematic of single gas permeation setup

The gas permeation rate can be calculated using the general permeance p formula which can be defined as:

(3.1)

$$p = \frac{\mathrm{n}}{\mathrm{A_m}.\Delta P.t}$$

Where p is the membrane permeance (mol m^{-2} s^{-1} Pa^{-1}); n is the number of moles permeated through the membrane (mol) during the test time; A_m is the membrane active surface area (m^2); ΔP is the pressure difference across the membrane (Pa) and t is the permeation test time (s).

In this project, the permeance p of the membrane was calculated as follows:

$$p = \frac{(7.44 * 10^{-7}).\mathrm{V}}{\mathrm{A_m}.\Delta P} \tag{3.2}$$

Where p is the membrane permeance (mol m^{-2} s^{-1} Pa^{-1}); V is the permeated flow measured by the ADM flowmeter (ml/min); A_m is the membrane active surface area (m^2) and ΔP is the pressure difference across the membrane (Pa). The factor used for the above equation is calculated using the following assumptions:

1. The gas is ideal
2. The temperature is constant at ambient

The permselectivity (or ideal selectivity) S of the membrane was calculated by the ratio of the single gas permeances:

$$S = \frac{p_{He}}{p_{CO2}} \tag{3.3}$$

Where p_{He} and p_{CO2} are the He and CO_2 single permeance respectively.

3.4 Mixed gas permeation test

The above-mentioned gas permeation test was applied in most of the cases. However, there was a drawback in some experiments with small CO_2 permeation rates. The problem in this method was that the amount of permeated carbon dioxide through the membrane was actually less than the lower limit of the ADM flowmeter range which was 0.01 ml/min. Therefore, to be able to measure carbon dioxide, two parts were added to the permeation setup (Figure 3.8) for the membranes with very small permeation rates of carbon dioxide.

As illustrated in Figure 3.8, in this setup, a 1/8-inch stainless steel tube connected to a bore-through tee was inserted inside the permeate side of the membrane cell to send the sweep gas (10 ml/min) to the permeate side. Therefore, the carbon dioxide permeated through the membrane was carried towards the outlet of the membrane cell where a Gas Chromatograph (Agilent 7890A) was installed to measure the mixture ratio of the gas. The sweep gas chosen for this experiment was nitrogen with the flow

rate of 10 ml/min which was controlled with a gas flow controller (Aalborg GFC stainless steel compression fitting, 0-100 ml/min N_2).

The volumetric permeation flowrate F of carbon dioxide was calculated as follows:

$$F = C_{CO2}.F_{out} \tag{3.4}$$

Where F is the carbon dioxide permeation flow $(\mathrm{ml/min})$; C_{CO2} is the volumetric concentration of CO_2 in the mixture measured by the GC and F_{out} is the flow rate of the N_2+CO_2 mixture measured by the ADM flowmeter $(\mathrm{ml/min})$. The gas permeance $(\mathrm{mol\ m^{-2}\ s^{-1}\ Pa^{-1}})$ can be calculated by substituting F in equation 3.2.

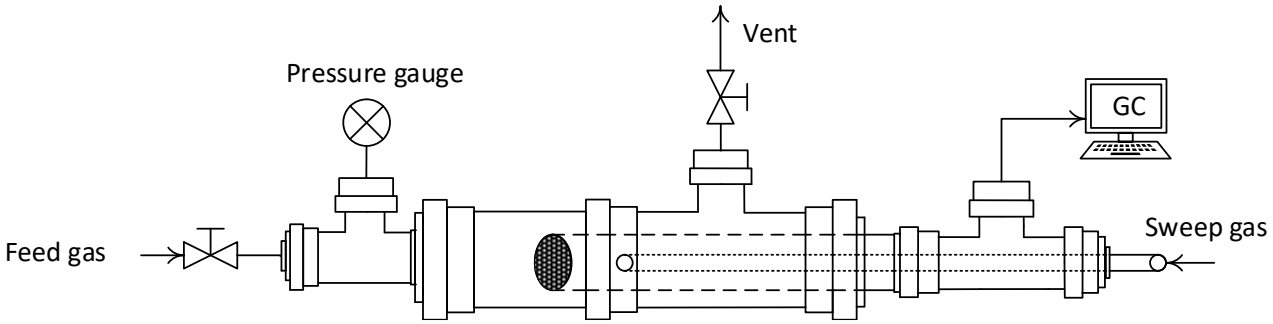

Figure 3.8 Schematic of single gas permeation setup for CO_2

In another experiment, the separation performance of the membrane for the gas mixture was tested. In this case, the same setup was used for the mixed gas permeation tests (Figure 3.9). Only in this setup, He and CO_2 were inserted inside a mixing chamber with the same volume flow rates so that the mixture concentration is 50%-50% of the two gases. The 50%-50% mixture of helium and carbon dioxide with the flow rate of 10 ml/min was sent to the membrane at constant pressure of 2 bar and the permeated gas was swept to the outlet of the setup which was connected to the GC to analyse. Nitrogen was also used as the sweep gas with the flow rate of around 5-10 ml/min.

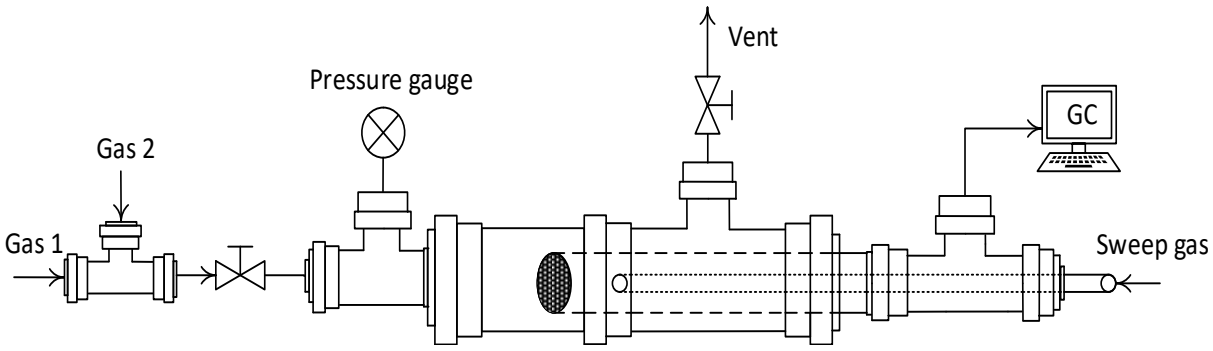

Figure 3.9 Schematic of mixed gas permeation setup

The separation factor α was calculated by:

$$\alpha = \frac{y_{He}}{y_{CO2}} / \frac{x_{He}}{x_{CO2}} \tag{3.5}$$

Where α is the He/CO_2 separation factor in the mixture and y and x is the volumetric fraction of the gas in permeate and feed side respectively.

The flow rates of He and CO_2 can be calculated using the same method in equation 4.4.

3.4.1 Gas Chromatography

The gas chromatograph (GC) used analysing the composition of the permeate gas was Agilent 7890A with the column of FS CAP CARBOXEN 1010 PLOT 30M x0.53MM NON-HAZ installed on the GC and a Thermal Conductivity Detector (TCD).

Before running the permeation tests calibration of the GC with CO_2 and N_2 was performed. To do this, the two gases were mixed with different volume ratios and sent to the GC. The gases volume flow rates were controlled using the Aalborg gas flow controllers and they were altered from 0 – 100% in the gas mixture. After the calibration was completed, a calibration curve was obtained as illustrated in Figure 3.10:

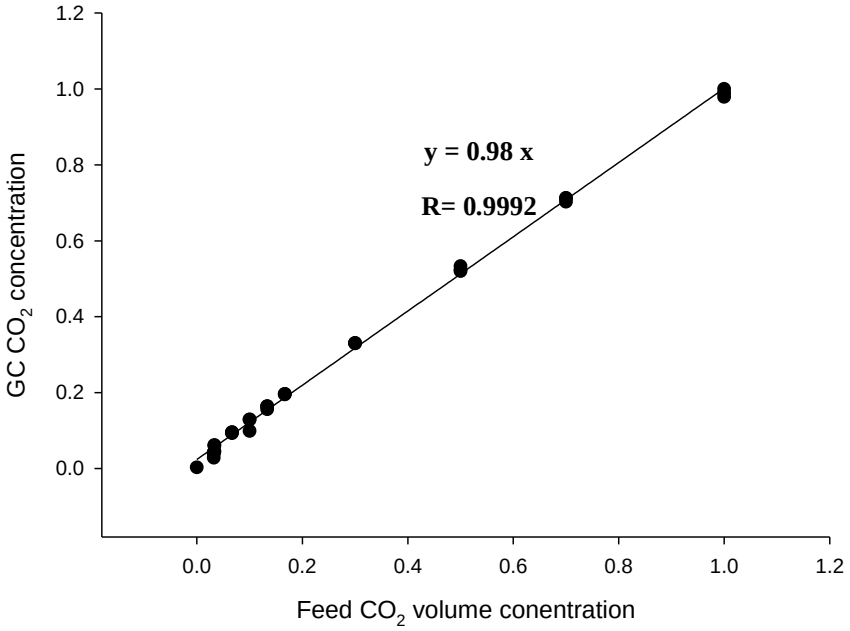

Figure 3.10 GC calibration curve for CO_2 and N_2 mixture

Using the above calibration curve, a precise concentration of the gases in the mixture was calculated. It is worth mentioning that the GC gas concentration can be calculated using the ratios of either the height or the area of the gases detected in the gas chromatograph. For example:

$$C_{CO2} = \frac{A_{CO2}}{(A_{CO2} + A_{N2})} \tag{3.6}$$

Where C_{CO2} is the concentration of carbon dioxide measured by the GC, A_{CO2} and A_{N2} can be the area or the height of each gas on the chromatography curve.

Another way of calibrating the GC is sending various gas concentrations to the GC and allocate each area to its corresponding known concentration. The resulting plot will have the same linear shape as Figure 3.10. The only difference in this type of calibration is that there is no need to calculate the GC concentration using equation 3.6. This type of calibration was mainly used in binary gas permeation experiments.

3.5 Gas permeation test at higher temperatures

As illustrated in Figure 3.11, the experimental setup used for permeation tests at higher temperatures was quite different with the previously used one for lower temperature measurement. In this setup, the membrane cell was covered with a flexible heather and insulated to insure a stable heating system. A digital thermometer with a metal sensor was inserted inside the membrane chamber to measure the precise temperature in the permeation cell. The volume flow rate of the permeated gases was measured using the ADM flowmeter in ml/min unit.

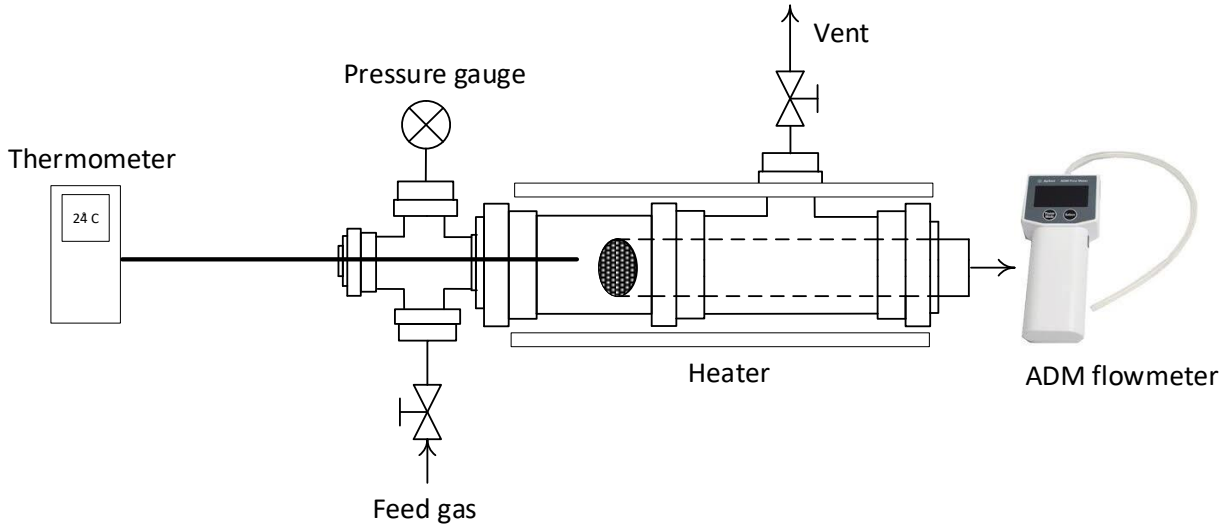

Figure 3.11 Schematic of gas permeation setup at higher temperatures

3.6 Characterization

Different methods were utilised for characterisation of the powders and the membranes which will be discussed in the following:

3.6.1 SEM

Scanning Electron Microscopy (SEM) and FIB-SEM (Focused Ion Beam Scanning Electron Microscopy) analysis was performed using two devices. Neon (SEM) was

used for normal imaging with no etching of the surface and LYRA3 TESCAN (FIB-SEM) was utilised to take images of the cross section of the membranes with Ion Beam etching technique. The excitation voltage used for both devices was 5kV.

3.6.2 XRD

The crystalline structure of graphene membranes was characterized by X-ray diffraction. The X-ray powder diffraction (XRD) measurements were carried out on a Bruker D8 Advance diffractometer (AXS, Germany) with a copper Kα radiation source (@40 kV & 40 mA) and a LynxEye detector. The XRD measurements of the membranes were performed between 7.5° and 90° (2θ), step size of 0.015°, time per step of 0.7 s, and a total scan time of 1 hr.

3.6.3 BET

BET surface area measurements of the three graphene nanoplatelets powders were carried out using TriStar II Plus surface area and porosity analyser (Micrometrics). The tests were performed using nitrogen gas at 77 K bath temperature (liquid nitrogen).

3.6.4 Adsorption test

Adsorption test for CO_2 and N_2 gases on graphene membranes were carried out using the same equipment as above. The test absolute pressure range was 2-120 kPa and the bath temperature was kept at 0 ^oC (ice bath).

Chapter 4 Graphene Disc Membranes and Their Application in Gas Separation

4.1 Introduction

Gas separation and purification is an important stage in many industries such as natural gas processing, CO_2 capture from syngas, flue gas and biogas (1, 2), nitrogen and hydrogen separation (3). Therefore, introducing an efficient and cost-effective separation method like membrane separation has played a crucial role in reducing the capital costs of the industries in these fields. Compared to the other conventional methods of gas separation in chemical industry, membrane separation leads to less energy consumption and operation costs, making it much easier to scale up in real world.

Nowadays, various types of membranes using different materials such as polymers, ceramic, zeolite, graphene and MOF are being fabricated and employed in large scale separation applications (4). Graphene is a recently emerged material which has attracted a lot of attention because of its fascinating properties, making it an ideal option for membrane preparation especially in harsh conditions (5, 6).

Graphene-based membranes have been widely used in gas separation applications. *Li et al*. introduced a facile way for fabricating graphene-based membrane for gas separation with excellent separation of H_2/CO_2 and H_2/N_2 gas mixtures (7). At the same time, *Kim et al.* also reported graphene-based membranes with CO_2-philic permeation which exhibited high selectivity as well (8).

However, in most of the prepared graphene-based membranes, the material used in the membrane structure was graphene oxide which is a very expensive derivative of graphene. This could be a critical issue in large-scale production of the membrane for using in real-world applications. Therefore, we have used graphene nanoplatelets in membrane fabrication which is much less expensive and makes an ideal first material for industrial scale-up.

Here, we report a facile way in fabricating graphene disc membranes with excellent mechanical and chemical stability which can be used in a wide range in gas molecular sieving applications.

4.2 Experimental Section

4.2.1 Materials and Chemicals

Commercially available graphene nanoplatelets were purchased from Sigma-Aldrich and manufactured by XGnP®. Different types of graphene were used. Grade M with flake sizes of 5 µm, 15 µm and 25 µm (surface area 120-150 m^2 g^{-1}) and 6-8 nm thickness of the layers.

4.2.2 Membrane Preparation

Pure graphene membrane discs were prepared by pressing the material using a lab scale pressing device as explained in chapter 3. First a certain amount of powder (0.04-0.2 g) were weighed and poured inside the pressing module. Then it was pressed for 2 minutes under different pressures (4-20 MPa). The obtained disc membrane had the thickness of 0.5-0.75 mm and 13 mm diameter.

For all the membranes, it was crucial to make sure that the surface of the membrane is smooth and crack-free since even smallest defects on the surface could affect the final performance and stability of the membrane in the future.

4.2.3 Characterization

The morphology of graphene membrane cross-section and surface was characterized using SEM (Scanning Electron Microscopy) and FIB-SEM (Focused Ion Beam Scanning Electron Microscopy). Figures 4.1 and 4.2 show the SEM images of the surface and cross section of the graphene membrane respectively. As it can be

observed in Figure 4.1, the surface of the graphene membrane possess a uniform structure of the graphene flakes and there are no structural defects on the surface which indicates that the membrane have been fabricated successfully. In addition, Figure 4.2 demonstrates the layered structure of the graphene membrane cross section which is the result of assembling the graphene flakes during the fabrication procedure. In this figure, during the sample preparation for the SEM imaging, the membrane has been broken by hand resulting in less uniform interlayer spacing between the graphene flakes. Focused Ion Beam SEM (FIB-SEM) which uses Ion beam to etch the membrane cross section gives a more accurate image of the membrane cross section (Figure 4.8).

4.2.4 Membrane performance evaluation

4.2.4.1 Gas permeation test

Single and mixed gas permeation tests were carried out using three gases such as helium, carbon dioxide and nitrogen. The setups used for each experiment as well as the methods of calculations have been discussed in detail in chapter 3.

4.3 Results and discussion

4.3.1 Graphene membrane preparation

In graphene membrane preparation stage, different factors could affect the membrane structure and therefore membrane performance for the future applications. These factors such as, graphene flake size and weight used in membrane, and pressing pressure and time were investigated through a wide range of experiments to realize what the most optimum preparation conditions are to prepare a membrane with the best separation performance and stability which will be discussed extensively.

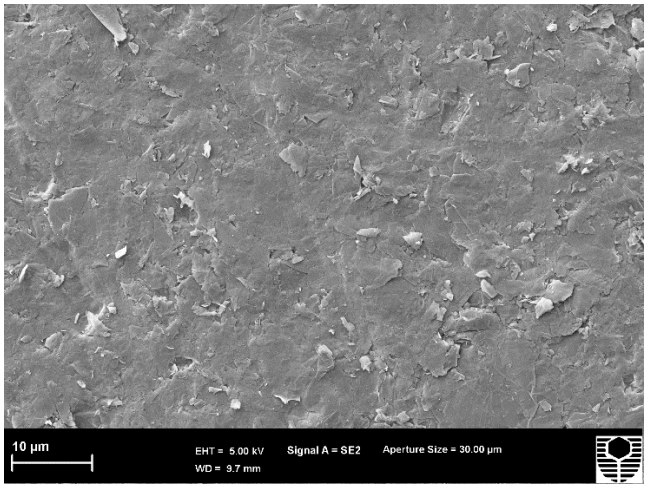

Figure 4.1 SEM image of the surface of the graphene membrane made of 5 µm graphene flakes, pressed under 8 MPa pressure for 2 minutes.

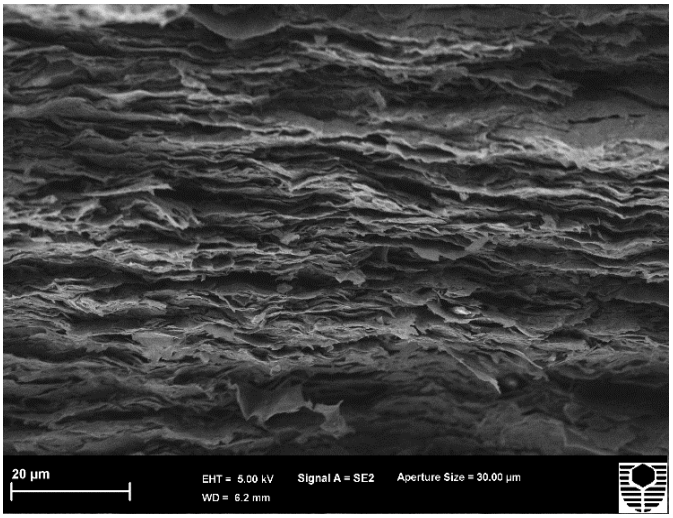

Figure 4.2 SEM image of the cross section of the graphene membrane made of 5 µm graphene flakes, pressed under 8 MPa pressure for 2 minutes.

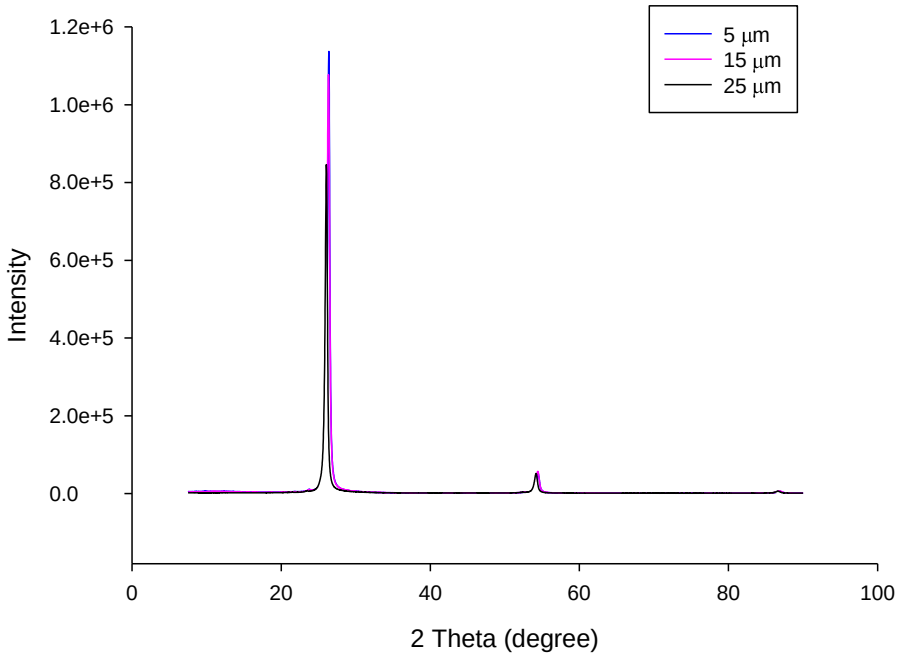

Figure 4.3 XRD patterns for the graphene membranes pressed under 8 MPa pressure for 2 minutes.

4.3.2 Membrane pressing time

One of the factors that was studied in membrane preparation was the membrane pressing time. This aspect of fabrication process could really impact the stability and ultimate membrane performance.

To find the effect of this factor, the membranes were pressed in different time durations from 1 to 10 minutes. It was observed that by increasing the pressing time minutes, the gas permeation rate decreases which could be because of the decrease in the membrane porosity. However, after 3 minutes of pressing, there is a dramatic reduction in selectivity which indicated microstructural defects in the membrane. Therefore, the membranes were pressed for less than 2 minutes to ensure no structural defects and high separation performance. Figure 4.4 illustrates the separation performance of the graphene members pressed for various durations.

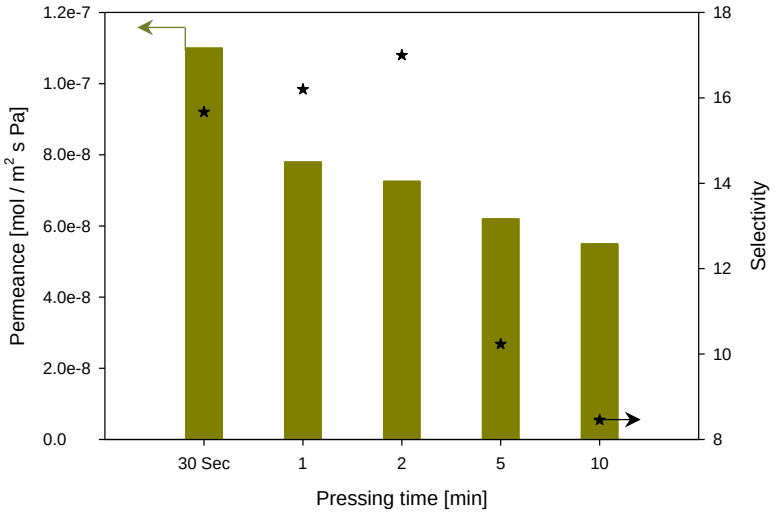

Figure 4.4 Effect of pressing time on the membrane performance at room temperature. The membrane thickness is 0.55 mm fabricated using 0.11 g of 5 µm graphene flakes, pressed under 8 MPa pressure.

4.3.3 Membrane pressing pressure

To find out the most suitable pressure under which graphene flakes was pressed, a series of pressing pressures were tested. The range of pressure used was 4-20 MPa. As shown in Figure 4.5, as the pressure increases, there is almost a trade-off between helium permeance and He/CO_2 selectivity. Membranes pressed under 4 and 6 MPa showed very high permeability but, they did not have an efficient separation of carbon dioxide from helium. However, when the pressure was increased to more than 20 MPa, there was an improvement in the membranes selectivity but with a considerable permeance rate reduction. This trend can be explained by the porosity of the graphene membrane. As the pressure increases the porosity for gas penetration decreases and thus the permeation of gases is affected directly.

The selectivity of the membrane pressed under 8 MPa was the highest even though the permeation was not on its lowest value. This could be due to possible defects on the surface of the membrane as a result of high pressure used for membrane preparation which leads to more CO_2 permeation and selectivity reduction.

Therefore, the most optimum pressure was considered 8 MPa resulted in graphene membrane with the highest selectivity and a reasonable permeance. This pressure is

much smaller than the pressures used in other literature when pressing graphite into discs(9). This could be simply because of the difference in texture softness of graphite and graphene nanoplatelets powder which makes graphite to need much higher pressure to be shaped into disc with the same thickness. Since graphene is exfoliated form of graphite and its layers have already been separated, it needs much less force to press the layers into disc shaped membranes with the same properties.

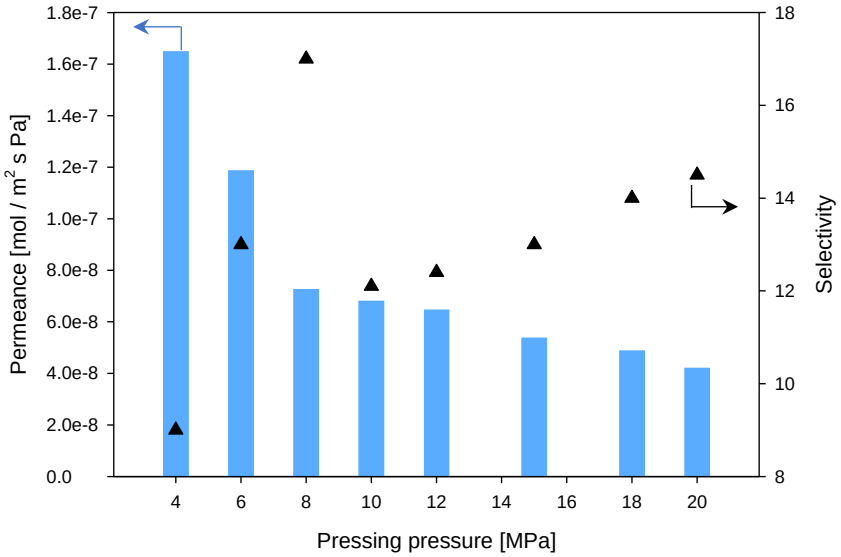

Figure 4.5 The effect of pressing pressure on performance at room temperature. The membrane is thickness is 0.55 mm using 0.11 g of 5 µm graphene flakes, pressed for 2 minutes.

4.3.4 Graphene flake size

As mentioned in part 4.2, three flake sizes of graphene were used for preparing the membranes (25 µm, 15 µm and 5 µm). To investigate the effect of flake size on membrane performance, three different membranes were prepared using pure graphene of a certain flake size. The other conditions of membrane preparations were kept constant.

As illustrated in Figure 4.6, the highest He/CO_2 permselectivity is for 25 µm membrane. This could be expected since the bigger flakes can make less space in the membrane structure between He and CO_2 kinetic diameter and therefore less carbon dioxide gas can pass through the membrane easily. Besides, as illustrated in Figure 4.7, bigger graphene flakes provide a more tortious pathway for the gas molecules

which makes it harder to pass to the permeate side. While in smaller flakes the stacking of the graphene layers will be more porous and less tortious which leads to bigger space and more gas passage. All these factors reduces selectivity of the membranes with smaller particle sizes.

In addition, the permeation rates of the membranes are also affected by the graphene flake size. The smaller graphene flakes form more porous membranes resulting in more space for the gas molecules to pass through the membrane which makes it easier for them to permeate (Figure 4.7). However, there is an exception for 15 µm graphene membrane in our results as illustrated in Figure 4.6. In this membrane, the He permeance has been unexpectedly lower than the range between 5 µm and 25 µm graphene membrane, even though the He/CO_2 selectivity was in a reasonable range. The low helium permeation rate for 15 µm graphene can be explained by other factors affecting the membrane structure which could be porosity, adsorption, surface area etc. To verify this speculation BET test and FIB SEM were performed to observe the mentioned properties of different membranes made of different graphene flake sizes.

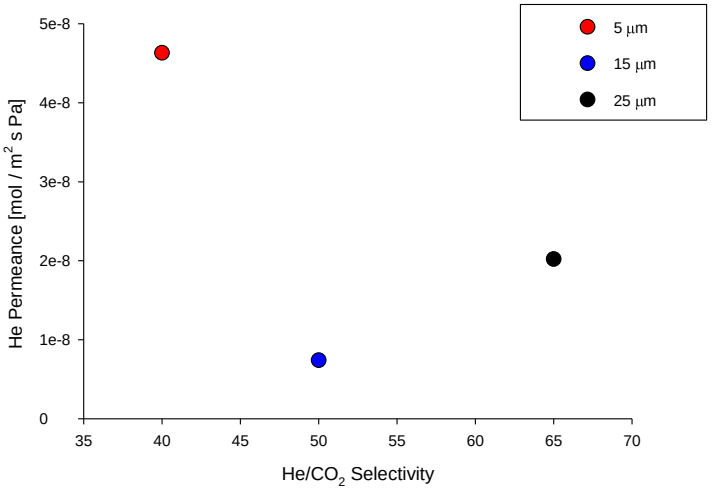

Figure 4.6 The effect of graphene flake size on membrane performance at room temperature. The membranes are made of 0.15 g graphene, pressed under 8 MPa pressure for 2 minutes.

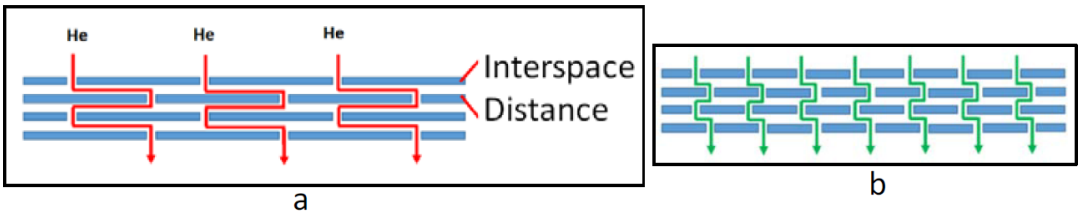

Figure 4.7 The effect of graphene flake size on membrane porosity.

4.3.4.1 FIB SEM

Figure 4.8 shows the FIB SEM (Focused Ion Beam Scanning Electron Microscopy) images of the cross section of three membranes fabricated using graphene powder with different flake sizes. The membranes were etched using ion milling method inside the equipment. As illustrated in these pictures, the porosity of the membrane made of 15 µm graphene is considerably lower than the other two membranes, which results in lower permeation rate for the gases.

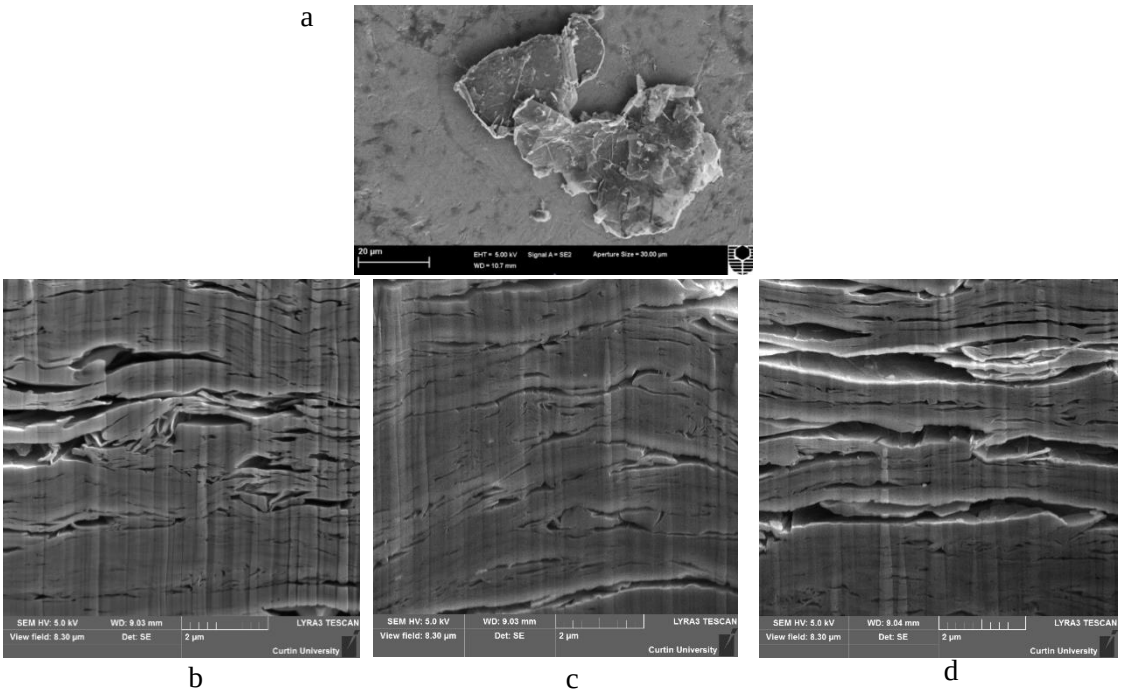

Figure 4.8 Graphene flake and graphene membrane. a) SEM image of 25 µm graphene flakes before pressing FIB-SEM image of the cross section of three membranes fabricated from: b) 5 µm, c) 15 µm, and d) 25 µm under 8 MPa pressure for 2 minutes.

4.3.4.2 BET measurements

To investigate the reason of low porosity of the membrane made with 15 µm graphene, BET measurements were carried out for the powders using Tristar-Plus BET surface area equipment and Nitrogen gas at 77 K.

BET measurements on both membranes and powders showed a considerable difference between the pore size (porosity) of the 5 µm and 25 µm membranes with the 15 µm one. It was observed that the porosity of 15 µm is much smaller than the other two membranes which could be the reason of low gas permeation rates. The reason of the very small porosity of the 15 µm membranes can be the smaller surface area (bigger powder particle size) of the initial graphene nanoplatelets that the 5 µm and 25 µm graphene flakes which showed almost the same values as illustrated in table 4.1.

Graphene flake size [µm]	Powder BET surface area [m^2/g]	Membrane porosity
5	104	0.078
15	91	0.061
25	101	0.075

Table 4.1 The results of BET test on three different graphene flakes sizes and membranes. The membranes are fabricated under 8 MPa pressure for 2 minutes.

Therefore, 5 µm and 25 µm graphene was chosen to be used in membrane fabrication due to their considerably high permselectivity and reasonable He permeance.

4.3.5 Membrane thickness

Membrane thickness was mainly controlled with the amount of graphene used for membrane fabrication. It was essential to find the most applicable weight range of

graphene which resulted in a membrane with good separation performance. Therefore, different amounts of graphene was weighed and pressed under the same conditions, then the thickness associated with each membrane was measured using a Vernier scale as described in table 4.2. Single gas permeation test was performed to analyse the effect of membrane thickness on its performance and the results are summarized in Figure 4.9. As expected, gas permeance decreased by increasing membrane thickness because of higher resistance and therefore less gas molecules are able to pass through the membrane. The selectivity also increased in thicker membranes. The thickest membrane was made of 0.15 g of 25 or 5 µm graphene and the thickness was measured 0.75 mm. The reason for selectivity rise by increasing the membrane thickness is associated to the adsorption capacity of graphene nanosheets for CO_2 which will be discussed in detail later. However, higher membrane thicknesses sacrifice the high gas permeation rate which is not favourable in real-world applications.

Graphene flake size (µm)	Membrane weight (g)	Thickness (mm)
5	0.11	0.55
	0.15	0.75
15	0.11	0.46
	0.15	0.63
25	0.11	0.55
	0.15	0.75

Table 4.2 Thickness of different membranes made of different graphene types. All the membranes were pressed under 8 MPa pressure for 2 minutes.

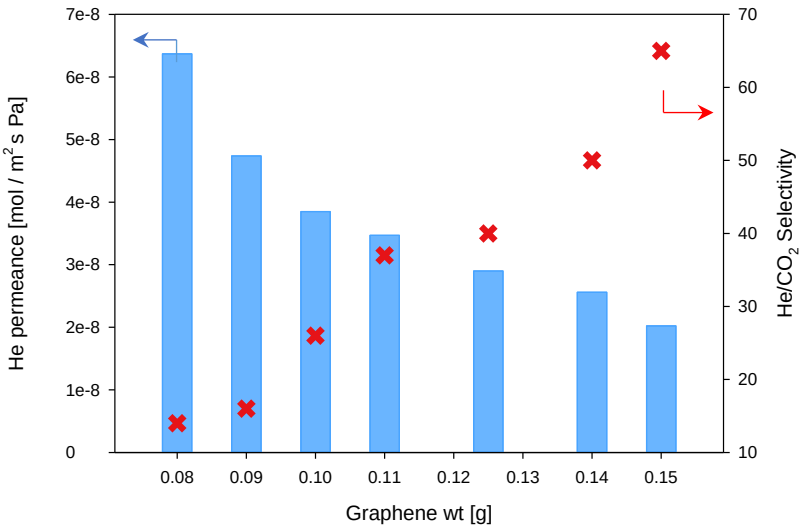

Figure 4.9 The effect of membrane weight (thickness) on its performance at room temperature. The membrane is from 25 µm graphene pressed under 8 MPa pressure for 2 minutes.

4.3.6 Adsorption test

CO_2 and N_2 adsorption tests were carried out on graphene flakes and as expected, the results show a considerable difference in the adsorption capacity of the membrane for the two gases. As illustrated in Figure 4.10, CO_2 is adsorbed much stronger than N_2 on graphene particles. This higher capacity of adsorption for CO_2 results in lower permeation rate for this gas compared to nitrogen even though it is smaller in kinetic diameter.

In addition, high capacity of CO_2 adsorption on the membranes results in selectivity improvement by increasing the membrane thickness. It means that by increasing the membrane thickness, the amount of graphene utilised in membrane is higher, leading to more available sites for carbon dioxide adsorption and smaller permeance. Moreover, since the adsorption quantity of CO_2 is higher than N_2 and He (as inert gases), therefore, the drop in permeation rate of CO_2 is higher than He and N_2 which results in He/CO_2 selectivity increment.

The reason of high CO_2 adsorption on graphene could be due to the natural functional groups present on the edges of the graphene flakes (as reported by the supplier). These functional groups like ethers or hydroxyls can react with carbon dioxide as a polar molecule and prevent it from permeating freely through the membrane. Since there is no such reaction between the polar groups on the graphene edges and the inert gases like N_2 or He, therefore these gases permeation is not affected. This phenomenon facilitates the molecular sieving performance of the membrane, leading to high selectivity and excellent separation performance.

High values of CO_2 adsorption on graphene plates have been also reported in other literature indicating the high capacity of this material in this type of separation which is even higher than zeolite in some cases depending on the graphene structure and preparation method (10, 11).

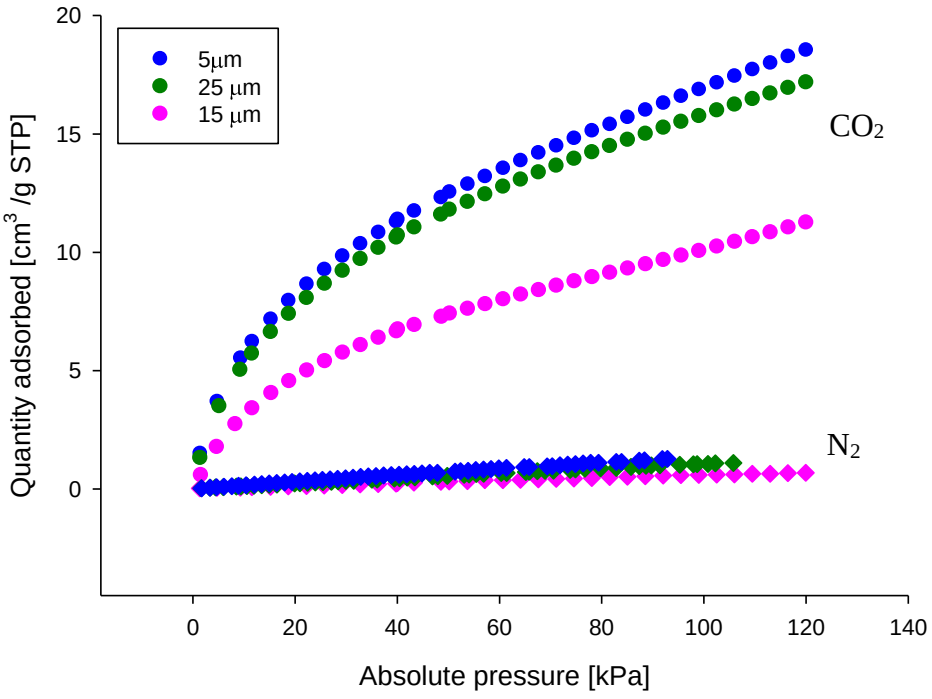

Figure 4.10 Adsorption isotherm of CO_2 and N_2 on different graphene particle sizes at 0℃

4.4 Gas separation mechanism

To identify the mass transport mechanism of the gases through the membrane, single gas permeation test was carried out at 1bar pressure difference for 5 µm and 25 µm membranes. To explore the excellent gas sieving property of the fabricated membranes, three gases (He, CO_2, and N_2) were used in single gas permeation tests.

Figure 4.11 illustrates the permeation rates of the test gases in different membrane thicknesses and graphene type as a function on their kinetic diameter. As mentioned earlier, it is observed that the permeation rate of N_2 is higher than CO_2 despite its bigger kinetic diameter and the reason is the higher adsorption quantity of carbon dioxide.

The excellent molecular sieving mechanism of the graphene membranes is clearly illustrated in Figure 4.12. The black line shows the He/CO_2 Knudsen selectivity which is calculated using the two gases molecular weights as mentioned in chapter 2 (Eq.

2.12) and is constant for all the membranes. The real experimental selectivity of the all 4 membranes is much higher than the ideal Knudsen selectivity indicating high molecular sieving of the membranes in gas transport mechanism.

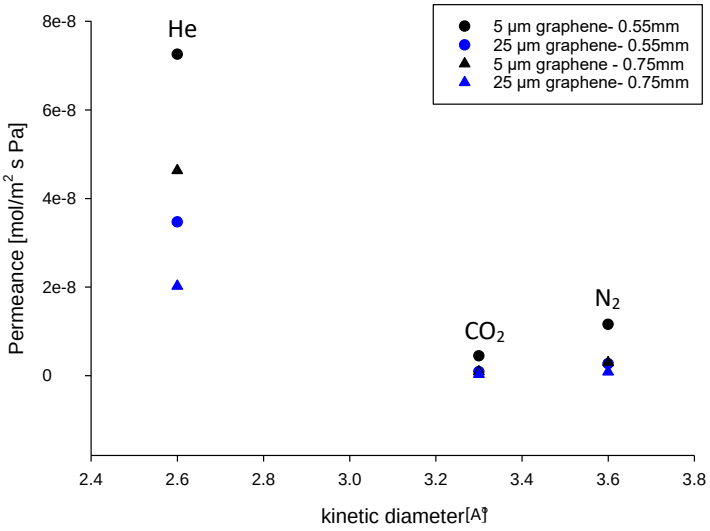

Figure 4.11 Single gas permeance of probe gases at room temperature as a function of gas kinetic diameter. The membranes were fabricated under 8 MPa for 2 minutes.

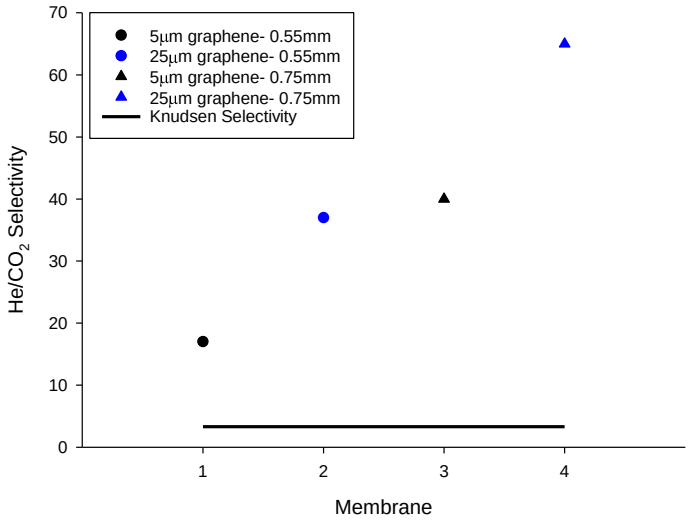

Figure 4.12 Theoretical Knudsen Selectivity and Experimental selectivity of four different pure membranes. The membranes were fabricated under 8 MPa for 2 minutes.

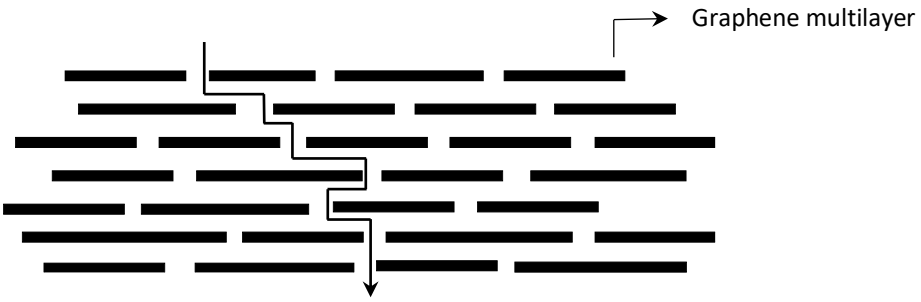

Figure 4.13 Schematic of the gas molecules permeation path through the assembled layered graphene membrane.

The XRD patterns (Figure 4.3) of the fabricated membranes show that all three membranes exhibit graphite crystalline structure after pressing, which could be expected as the graphene nanoplatelets had been pressed on each other forming graphene multilayers or graphite in the membrane. However, even though their crystalline structure seems almost similar, the gas separation performance of the membranes are different from each other. This indicates that the properties of the initial graphene nanosheets used in the membrane fabrication such as particle size, surface area, flake size etc. play an important role in the membrane performance and strongly affect the separation efficiency.

As illustrated in Figure 4.13, the spacing between the graphene multilayers is the main pathway for the gas molecules permeating through the membranes. This spacing which can be altered with various factors such as pressing pressure and graphene nanoplatelets type, acts as molecular sieving pores that prevent bigger molecules (CO_2) from passing through them while let the smaller ones (He) to permeate to the other side of the membrane leading to size-dependant separation.

In addition, as mentioned before, adsorption is another factor in these membranes affecting the gas permeation and membrane separation performance. Therefore, the final molecular sieving mechanism of the graphene membranes can be considered as the collaborative effect of size exclusion and adsorption leading to excellent gas separation performance.

4.5 Conclusion

In this chapter, different types of pressed graphene membranes fabricated using a facile method were reported. These membranes were used for gas separation applications and they showed excellent gas separation performance and molecular sieving mechanism.

Also, the effect of various factors such as graphene flake size, pressing pressure and time and membrane thickness affecting the membranes separation performance was studied. It was observed that the 25 µm membrane has the highest He/CO2 selectivity and the 5 µm possess the highest He permeation rate.

The adsorption capacities, as well as BET measurements of the membranes, were also carried out and they exhibited a big difference in the surface area and porosity of 15µm graphene membrane with the other two, resulting in a significantly smaller helium permeation rate for that membrane.

References

1. Scholes CA, Smith KH, Kentish SE, Stevens GW. CO2 capture from pre-combustion processes—Strategies for membrane gas separation. International Journal of Greenhouse Gas Control. 2010;4(5):739-55.
2. Zhang Y, Sunarso J, Liu S, Wang R. Current status and development of membranes for CO2/CH4 separation: A review. International Journal of Greenhouse Gas Control. 2013;12:84-107.
3. Scholes CA, Stevens GW, Kentish SE. Membrane gas separation applications in natural gas processing. Fuel. 2012;96:15-28.
4. Karkhanechi H, Salmani S, Asghari M. A Review on Gas Separation Applications of Supported Ionic Liquid Membranes. ChemBioEng Reviews. 2015;2(4):290-302.
5. Geim AK. Graphene: Status and Prospects. Science. 2009;324(5934):1530-4.
6. Membrane Gas-Separation: Applications. Membrane Operations.
7. Li H, Song ZN, Zhang XJ, Huang Y, Li SG, Mao YT, et al. Ultrathin, Molecular-Sieving Graphene Oxide Membranes for Selective Hydrogen Separation. Science. 2013;342(6154):95-8.
8. Kim HW, Yoon HW, Yoon S-M, Yoo BM, Ahn BK, Cho YH, et al. Selective Gas Transport Through Few-Layered Graphene and Graphene Oxide Membranes. Science. 2013;342(6154):91-5.
9. Schulz A, Steinbach F, Caro J. Pressed graphite crystals as gas separation membrane for steam reforming of ethanol. J Membrane Sci. 2014;469:284-91.
10. Takeuchi K, Yamamoto S, Hamamoto Y, Shiozawa Y, Tashima K, Fukidome H, et al. Adsorption of CO2 on Graphene: A Combined TPD, XPS, and vdW-DF Study. The Journal of Physical Chemistry C. 2017;121(5):2807-14.
11. Mishra AK, Ramaprabhu S. Carbon dioxide adsorption in graphene sheets. AIP Advances. 2011;1(3):032152.

Chapter 5 Zeolite and Layered Graphene Composite Membranes for Gas Separation

5.1 Introduction

One of the most important factors affecting the membranes performance is the material used for fabricating the membrane. This factor can actually determine the stability of the membrane under harsh conditions such as high temperature and pressure, chemically aggressive environments, and long periods of operation as well as the quality of the separation performance. Thus, it is critical to choose a material that suits best the operating conditions and the desired objective of the separation.

Inorganic membranes are fascinating due to their high chemical, thermal and mechanical stability and they have attracted a lot of attention in separation applications.

Graphene as a recently emerged novel inorganic material, has exhibited extraordinary separation performance and stability in gas separation and water purification applications. This material is easy in large-scale production and due to its chemical and mechanically robustness, it also is ideal to be applied under industrially relevant conditions.

The layered graphene membranes discussed in the last chapter exhibited excellent gas selectivity but with quite low permeability in some cases. In this chapter, it is aimed to increase the permeability of the membrane while maintaining the high selectivity which is essential in good separation performance.

As reported by Geim (1), graphene flakes are impermeable to all the gases even the ones as small as helium, thus the only permeation pathway for the gas molecules in pure layered graphene membranes is the interlayer spacing between the graphene flakes surface and edges. Therefore, the only way to improve the gas permeation rate in the membrane is to increase the space in between the graphene flakes surface and edges using spacer particles. These spacers need to be compatible with graphene

flakes and show reasonable stability and mechanical strength under the membrane pressing conditions, besides, the particles need to possess effective gas separation potential to ensure a high separation performance for the resulting membrane.

One of the other interesting inorganic materials used in membrane preparation is zeolite. Zeolite membranes also poses high chemical and thermal stability. In addition, due to their high adsorption capacity for carbon dioxide, being utilised for CO_2 capture from natural gas, biofuel, and syngas is one of the most favourable applications of this group of inorganic materials in chemical industries.

Thus, zeolite was utilised as the spacers in layered graphene membranes (Figure 5.1) to form asymmetric layered membranes with higher porosity and permeability.

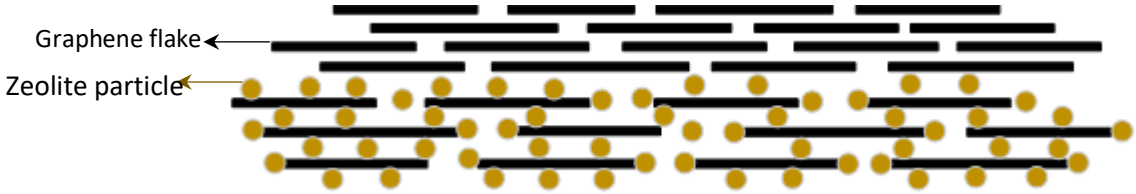

Figure 5.1 Schematic of asymmetric layered graphene membrane with zeolite particles used as spacers.

In this research, we introduced a facile way for combing these two inorganic materials to achieve high separation performance for the membrane. By utilising graphene as the selective layer for gas separation and zeolite layer as the porous support, the membrane can benefit from the separation properties of both graphene flakes and zeolite particles resulting in considerable enhancement in membrane separation performance.

5.2 Experimental Section

5.2.1 Materials and chemicals

Different types of graphene nanoplatelets were supplied by Sigma-Aldrich. The graphene flake sizes were 5, 15 and 25 µm with the surface area of 120-150 m^2/g and around 6-8 nm thickness.

Zeolite powder 13X and 4A were supplied by Sigma-Aldrich.

5.2.2 Composite membrane preparation

Composite membranes were made using one layer of graphene and zeolite mixed powder added to the pure graphene layer. In this method, first, graphene flakes were mixed with zeolite powder (20 – 80% wt%) by hand grinding or ball milling (100 rpm, 1 hr, ball mill grinder) and then a required amount was weighed and poured into the pressing module followed by the second layer of pure graphene nanoplatelets. Then the two layers (pure layer and mixed layer) were pressed together. The pressing pressure and time were kept constant at 8 MPa since it was the best pressure for the most optimum separation performance of the membrane as discussed in last chapter for pure graphene flakes.

The weight ratio of the mixed layer and pure layer was tested in different quantities to find the most optimum ratio for the membrane performance which will be discussed later. Moreover, the effect of graphene/zeolite weight ratio in the mixed powder was investigated to find the best weight ratio of the mixed layer which guarantees both high mechanical stability of the layer as well as good compatibility with the pure layer while improving the ultimate membrane performance in CO_2 capture.

For all the membranes, it is crucial to make sure that the surface of the membrane is smooth and crack-free since even smallest defects on the surface could affect the final performance and stability of the membrane in the future.

5.2.3 Characterization

The morphology of the graphene/zeolite mixed powder, the membrane cross-section and surface were characterized using SEM imaging (Neon) with the excitation voltage used was 5 kV.

5.2.4 Membrane performance evaluation

To evaluate the membrane gas separation performance at room temperature, similar setup and gases as described in chapter 3 were applied. The details of the experimental setups and calculations were described comprehensively in section 3.5.

As described in chapter 3, the experimental setup used for permeation tests at higher temperatures was quite different with the previously used for lower temperature measurement. In this setup, the membrane cell was covered with a flexible heather and insulated to insure a stable heating system. A digital thermometer with a metal sensor was inserted inside the membrane chamber to measure the precise temperature in the permeation cell.

5.3 Results and discussion

5.3.1 Composite layered membrane

To improve the graphene membrane performance, one idea is to add an adsorptive layer of zeolite (molecular sieve) to the pure graphene membrane to both increase the helium permeation and He/CO_2 selectivity. Zeolites are inorganic materials which can separate molecules based on not only their adsorption capacity at low temperatures but also their special porous structure. The separation based on adsorption difference is referred to as “Adsorption Selectivity”(2). Therefore, the important factor which can affect the membrane separation performance is the adsorption capability difference of each gas. In this case, carbon dioxide adsorption on zeolite is much higher than helium which is favourable for a higher permselectivity (3) . For example, for helium, there is some minor adsorption on zeolite which helps the helium

molecules to pass through the membrane easily. However, since there is a strong adsorption between carbon dioxide and zeolite, it is much harder for the gas molecules to desorb from the zeolite layer as easily as helium, therefore it is harder for carbon dioxide molecules to pass through the membrane which improves the selectivity of the membrane.

The initial purpose of adding an adsorptive layer to the structure of the membrane was to increase the He permeance as well as keeping the selectivity at a reasonably high value. For the highest thickness (around 0.75 mm) of pure membranes which was made of 0.15 g graphene, even though the selectivity was at its peak, but the helium permeance was low which deteriorated the overall separation performance of the membrane. Therefore, a portion of the pure membrane (0.04 g, 0.2 mm thick) was removed and the same amount of graphene/zeolite mixture was substituted.

Figure 5.2 illustrates a single graphene flake covered with zeolite particles which will affect the membrane structure and will be discussed later. Figures 5.3 illustrates the layered structure of the pure graphene layer with the graphene flakes assembled on top of each other. Figure 5.4 shows the structure of the mixed layer of the asymmetric membrane. As it can be observed in this image, the zeolite particles have been located between the graphene flakes.

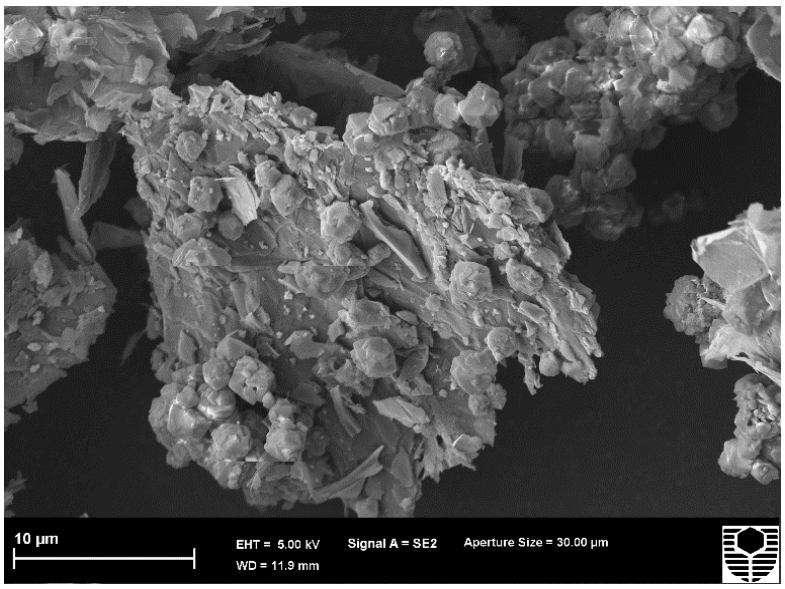

Figure 5.2 A graphene flake covered with zeolite particles

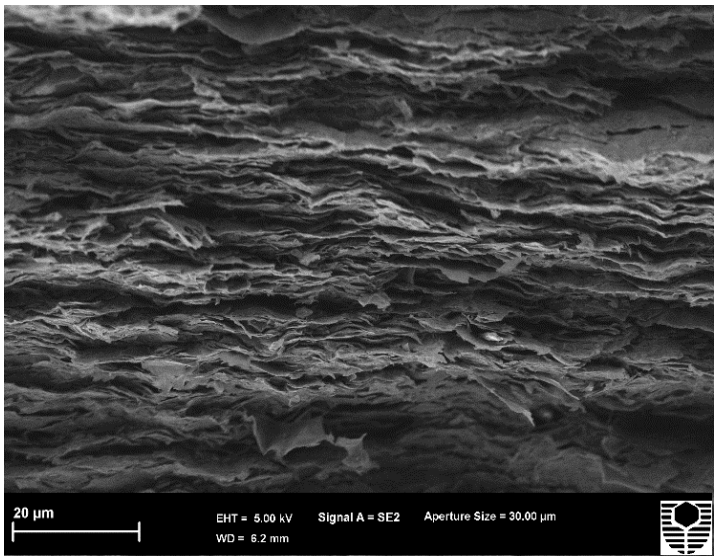

Figure 5.3 Pure graphene layer cross section. Graphene flake size is 5 µm and the membranes has been pressed under 8 MPa pressure for 2 minutes.

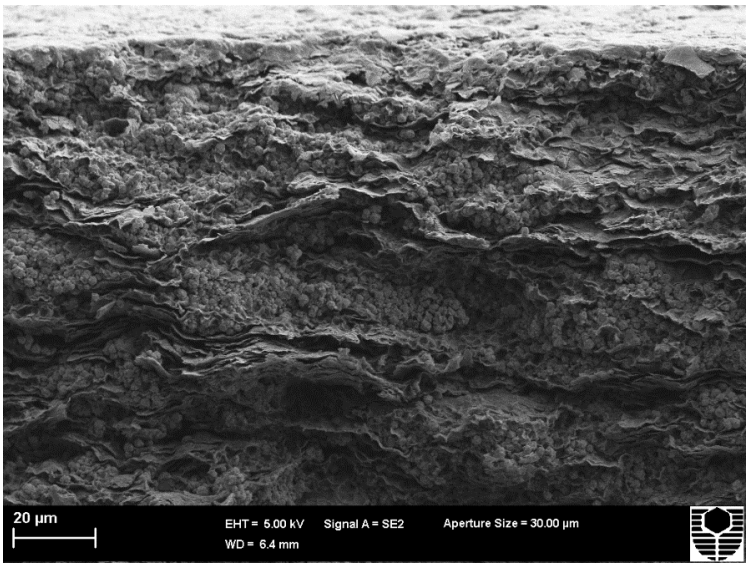

Figure 5.4 Mixed layer cross section. The mixed layer is made of 13X zeolite and 5 µm graphene and the membrane is pressed under 8 MPa for 2 minutes.

5.3.2 Separation performance

As mentioned before, to increase the separation performance of pure membranes, an adsorptive layer of zeolite was added to the membrane structure. To maintain the previous thickness, a certain amount of pure graphene nanoplatelets was replaced by the similar amount of graphene/zeolite mixture so that the overall weight and therefore thickness of the membrane was almost unchanged.

To find out the best choice of adsorptive layer for the composite layered membranes, a variety of mixtures were added to pure graphene layers. Also, the thickness of both layers was altered as well as the composition of the layers. The important factors affecting the separation performance were investigated and a series of membranes were fabricated using different mixed layers with four important factors changed to find the best pure/mixed composition. The following are the most important factors to be considered in the asymmetric layered membrane structure:

a) Zeolite type
b) Graphene flake size
c) Graphene/zeolite weight ratio in the mixed layer
d) Pure layer/mixed layer weight thickness portion in composite membrane

5.3.2.1 Zeolite/graphene mixture composition

a) Zeolite

Two types of zeolite (13X and 4A) were chosen to be used in the adsorptive layer. These two types were mixed in different weight ratios with 5 µm, 15 µm and 25 µm graphene flakes to make a range of binary mixtures of graphene/zeolite. To better identify the binary mixtures, they are called after graphene flake size/zeolite type/weight percentage of zeolite in the mixture e.g. 5µm/13X/20%.

The final asymmetric layered membrane including the pure graphene layer and the graphene/zeolite mixed layer was pressed under 8 MPa at room temperature and then, the membrane was sealed on the permeation cell for single gas permeation test to

study the gas separation performance. The effect of adding the adsorptive porous support was tested on three different sizes of pure layer graphene (5, 15 and 25 µm) and the pressing pressure and the thickness of the membranes were kept constant. As an example, the results of one type of composite membrane with the pure layer of 5 µm graphene are summarised in table 5.1.

As summarised in table 5.1, for higher weight percentages of zeolite (60%), the He permeance increased but the overall permselectivity of He/CO_2 dropped which could be because of the very high porosity in the support resulting in lower mechanical stability and forming defects in the membrane structure which reduces the separation performance.

In addition, the overall performance of the membrane which is both permeation and selectivity is much better when the mixed layer is made of 13X zeolite. However, since there is no such difference in helium adsorption between 13X and 4A zeolite the permeation rate of helium shows similar increment. Therefore, 13X-made composite membranes have higher He/CO_2 selectivity which makes them the favourable zeolite type. The different permeation rate of the gases through membranes made of 13X and 4A zeolite could be considered to be due to the difference in adsorption rates on the zeolite particles as reported in literature (4). The 13X zeolite adsorbs CO_2 much stronger than 4A which means it is harder for the gas molecules to pass to the other side of the membrane made of 13X zeolite resulting in smaller CO_2 permeation and higher selectivity. The reason of higher adsorption capacity of 13X zeolite than 4A zeolite should lie in the difference of their chemical nature at the surface as well as their different porosities providing stronger adsorption sites for CO_2 resulting in higher selectivity (5).

As illustrated in table 5.1, there is no such difference in helium permeation for the membranes made of different types of zeolite, while there is a considerable effect on the selectivities indicating that there is little adsorptive effect of zeolite layer on helium gas molecules than CO_2.

Mixed layer composition	He permeance ($molm^{-2}s^{-1}Pa^{-1}*10^{8}$)	Selectivity He/CO2
5µm/4A/60%	9.18	6.8
5µm/4A/40%	7.40	12.5
5µm/4A/20%	6.5	26.7
5µm/13X/60%	8.89	20
5µm/13X/40%	7.40	34
5µm/13X/20%	7.32	41
15µm/4A/60%	8.29	11
15µm/4A/40%	5.92	14
15µm/4A/20%	4.45	14.6
15µm/13X/60%	6.52	12.7
15µm/13X/40%	5.47	14.8
15µm/13X/20%	4.15	28
25µm/4A/60%	9.33	7.8
25µm/4A/40%	7.75	10.5
25µm/4A/20%	6.23	12.3
25µm/13X/60%	9.18	9.5
25µm/13X/40%	6.37	12.3
25µm/13X/20%	5.92	16

Table 5.1 Composite membrane performance at room temperature for different mixed support layers (the pure layer of all the composite membranes was 5 µm graphene and the membranes were pressed under 8 MPa pressure for 2 minutes).

It is also worth mentioning that for both composites, the lower the weight percentage of zeolite in the mixed layer, the higher the selectivity. However, the He permeance is higher for 60% mixed layer which could be overlooked since the difference in the selectivity in that composition is less than half of the selectivity in 20% composite membrane. Also, higher weight percentages of zeolite (more than 60%) in all three graphene sizes was tested and they showed really low stability with multiple defects on the surface of the membrane which made them inapplicable for the experimental section. Therefore, no results are available for mixed layers higher than 60%. Figure

5.10 illustrates the surface of a composite membrane made of 80% graphene/zeolite mixture.

b) Graphene

Graphene flake size is another important factor that can significantly affects the membrane performance. To investigate this effect, the mixed layer of the membrane was made with different flake sizes of graphene (5 µm, 15 µm and 25 µm). As indicated in Figure 5.5, the results show that the composite membrane containing 13X zeolite and 5 µm graphene had a better separation performance compared to the other composites in which 15 µm and 25 µm graphene was used in the mixed layer. The membrane performance was at its highest for the membranes with mixed layer of 20% and 40% of 13X zeolite in 5 µm graphene. The reason of better performance of the membrane when the mixed layer is made of 5 µm graphene, could be the higher compatibility of this particle size with zeolite which makes it a favourable composition to add to the membranes so that even though the He permeation increases considerably, the CO_2/He selectivity does not drop drastically. In fact, the smaller size of the graphene flakes could contribute to a more uniform and porous mixed structure which provides a more suitable environment for higher CO_2 adsorption.

SEM image of the two different mixtures of graphene/zeolite surface with 40% of 13X zeolite but with different graphene flake sizes are shown in Figure 5.6. As it is illustrated in Figure 5.6, the membranes made of the mixture of 5µm+13X showed a more uniform surface without any structural defects. However, as Figure 5.7 shows, the surface of the 15µm+13X mixed layer poses several structural defects on the surface which could be because of bigger flake size of graphene particles in the mixture, making the two components less compatible. This incompatibility results in detaching the zeolite particles from the structure producing defects which leads to lower stability and selectivity.

Finally, 5 µm graphene and 13X zeolite were chosen to be used in mixed layer for membrane performance improvement because of their high permeance and reasonable selectivity.

It is interesting, that this mixture addition improved the membrane gas separation performance regardless of the flake size of graphene sheets used in the selective (pure) layer.

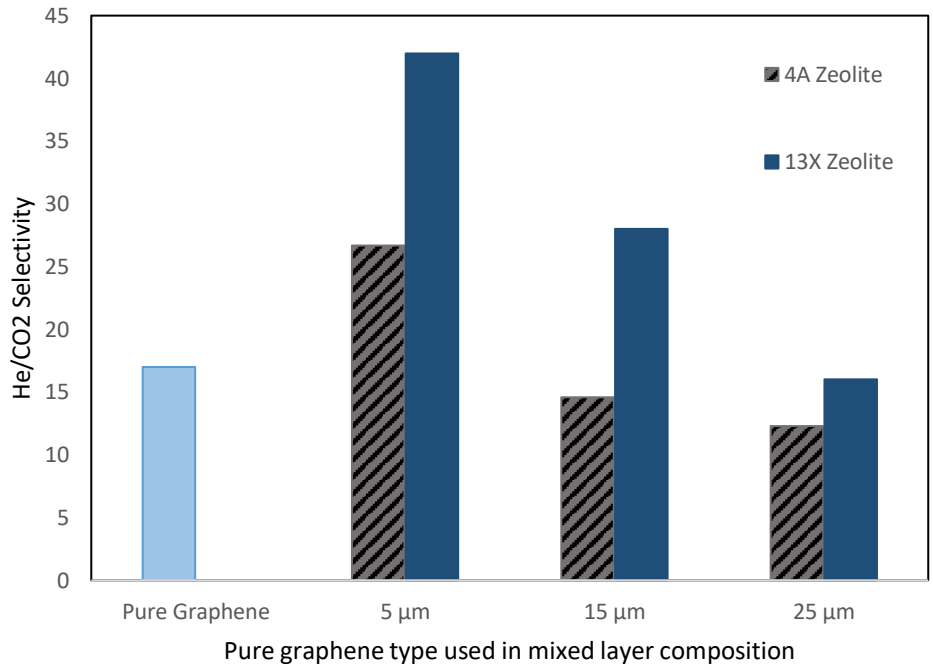

Figure 5.5 Membrane selectivity of composite membranes with different zeolite/graphene compositions in the mixed layer. All the membranes are pressed at 8 MPa for 2 minutes.

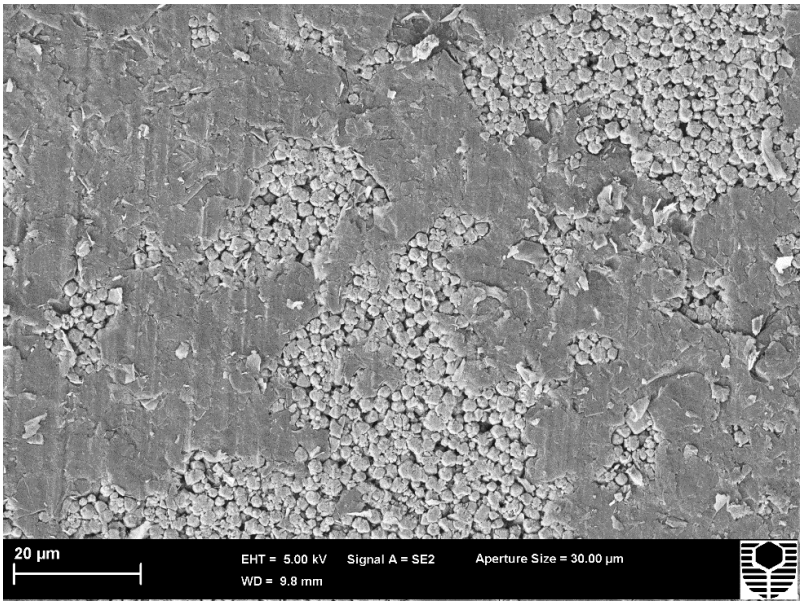

Figure 5.6 Zeolite/Graphene mixture using 5 µm graphene and 13X zeolite pressed at 8 MPa for 2 minutes.

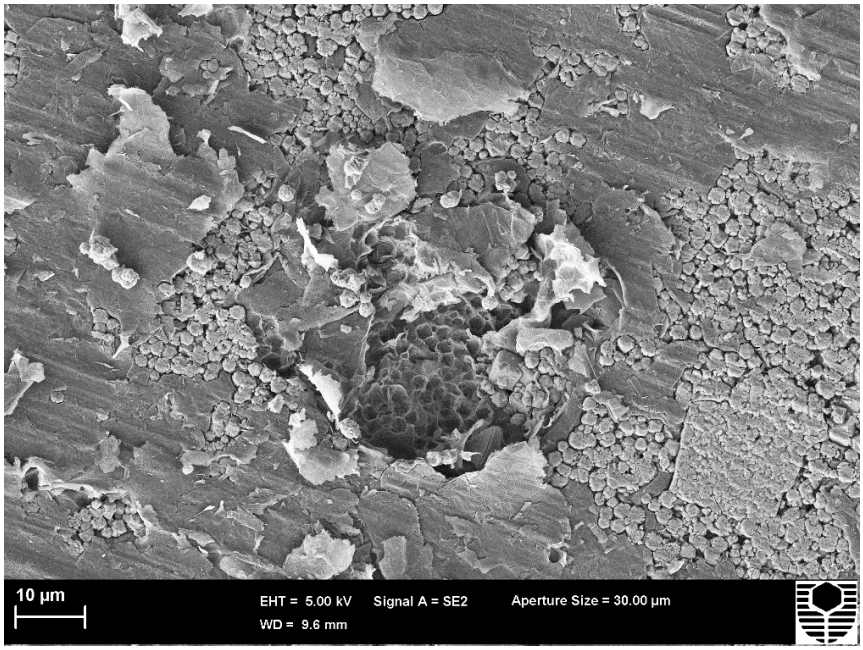

Figure 5.7 Zeolite/Graphene mixture using 25 µm graphene and 13X zeolite pressed at 8 MPa for 2 minutes.

5.3.2.2 Zeolite/graphene weight ratio in the mixture

At the beginning, pure zeolite (100%) was attempted to be added as the second layer to graphene. However, it showed very little stability during the membrane fabrication which resulted in broken membranes so that the membranes could not be tested. Therefore, certain amount of graphene was added to zeolite to increase the stability and prevent the mixed layer from structural defects. Different mixtures were tried with zeolite weight percentage of 20%-80%.

One way to find the best zeolite weight percentage in the graphene/zeolite mixture was to test a range of the ratios. Therefore, 4 different weight ratios were defined: 20%, 40%, 60% and 80%. In addition, the graphene flake size was also altered in the mixtures to find out the best performing adsorptive composition with high stability during the membrane fabrication and gas tests.

At this stage, it is necessary to find out the best graphene/zeolite weight ratio which provides the highest improvement on the membrane performance and also possess high mechanical stability. To achieve this purpose, the new mixed layer needed to

exhibit high helium permeation as well as good selectivity in comparison to the other mixed layers. Figure 5.10 shows a digital image of a composite membrane with the mixed layer made of 80% zeolite. As it is observable, the surface of the mixed layer is broken already and could not be used for gas permeation tests. 20% - 60% zeolite mixed layers exhibited more stability and were able to be used in gas tests. However, membranes made of the mixed layer containing more than 40% zeolite, did not show a drastic improvement in overall separation performance comparing to the pure membranes. Although they had a better permeation rate, the He/CO_2 selectivity was lower than the pristine graphene membranes which is not the objective of this research.

On the other hand, 20%-40% mixed layers made a significant improvement in membrane separation performance. Obviously, for the 20% membrane, the permeation flux was closer to the pure membrane with a higher selectivity. However, 40%-made membrane showed a much higher permeation rate as well as a reasonable selectivity. Depending on the separation purpose which could be either a higher permeation flux or a better selectivity, these adoptive layers could be selected in membrane structure.

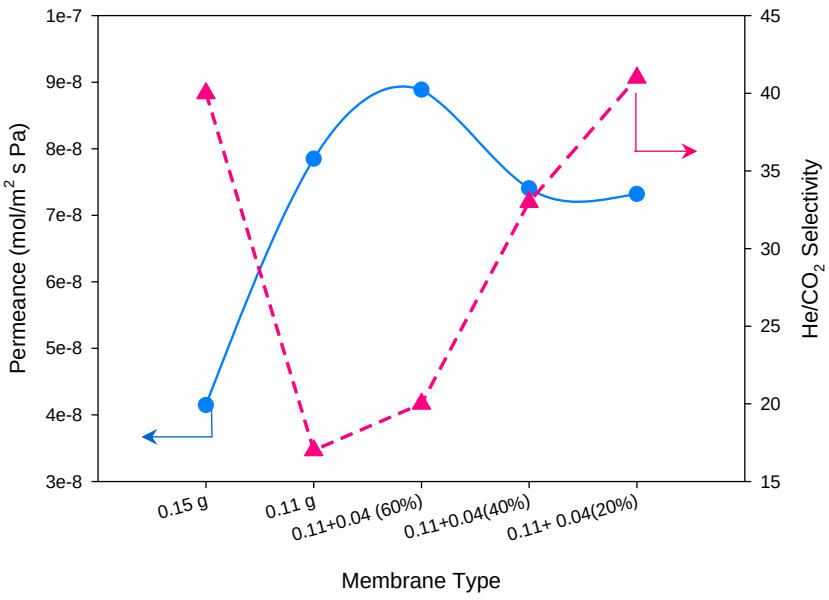

Figure 5.8 Gas separation performance of pure graphene and the corresponding asymmetric layered membrane. The graphene flake size used is 5 µm and the mixed layer 5 µm graphene and 13X zeolite. The membrane pressing pressure is 8 MPa and the duration is 2 minutes.

As showed in Figures 5.8 and 5.9, in general, substituting the 0.04 g adsorptive layer for the same amount of graphene in the thick pure membrane leads to higher helium permeation rate with small difference in He/CO_2 permselectivity.

On the other hand, comparing the performance of the individual thin pure membrane (0.55 mm thickness) with its corresponding asymmetric membrane (0.75 mm thickness) with different zeolite weight percentage (20%, 40%, and 60%), shows that the selectivity has been enhanced in all cases.

Although these results indicate that adding the adsorptive layer actually improves the separation performance of the graphene membranes, it should be noticed that there is a trade-off between the permeability and selectivity and the most optimum separation performance of the composite membranes is for 40% and 20% mixtures.

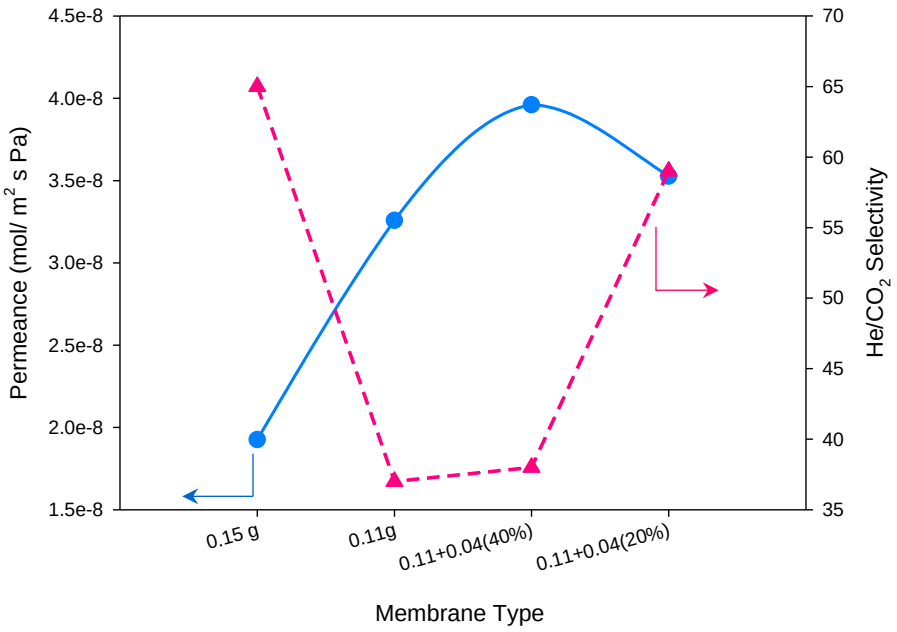

Figure 5.9 Gas separation performance of pure graphene and the corresponding asymmetric layered membrane. The graphene flake size used is 25 µm and the mixed layer 5 µm graphene and 13X zeolite. The membrane pressing pressure is 8 MPa and the duration is 2 minutes.

Figure 5.10 Defective surface of the composite membrane with the mixed layer of 80% zeolite pressed at 8 MPa for 2 minutes.

5.3.2.3 The effect of adding mixed layer to pure graphene membrane

The idea behind adding a zeolite/graphene layer to pure graphene is to increase the permeation rate of the membrane while maintaining the high selectivity which was proven to be a valid assumption based on the experimental results.

When the gas separation results of the best-performing 0.75 mm asymmetric membranes were compared to the results of their original pure membrane with the same thickness (with 0.15 g weight which is the same weight as the sum of the pure layer and adsorptive layer in the composite membranes), it was observed that the helium permeance increased to more than twice of its previous value and the He/CO_2 selectivity was maintained around 65. The increment in helium permeation is due to decreasing the thickness of the pure layer and adding a more porous zeolite/graphene layer instead to the membrane structure.

By combining zeolite powder with graphene flakes, the zeolite particles cover the graphene flakes (as illustrated in Figure 5.2) and when pressing the zeolite/graphene mixture into membranes, the zeolite particles occupy the space between the graphene nanoplatalets, leading to higher porosity and bigger space for gas permeation (Figure 5.1) . Therefore, by adding zeolite to the layered graphene nanoplatelets the interlayer spacing between the graphene flakes increases, reducing the molecular transport resistance and higher permeance. Besides, the highly porous zeolite/graphene mixture layer has substituted a part of the thickness of the pure graphene dense layer which

had low porosity and controlled the helium permeation. This substitution results in a reduction in the thickness of the size-selective layer leading to higher permeation rate.

To further study the separation effect of the adsorptive layer, the pure layer of the membrane (0.11 g weight and 0.55 mm thick) was tested but this time the mixed layer (0.2 mm thick) was excluded from the membrane structure. The results showed that the selectivity of the thin pure layer (0.55 mm thick) itself is smaller than the selectivity of the asymmetric layered membrane (0.75 mm) with the added porous support, however, the permeation rate of helium was almost the same. This indicates, that the mixed layer does not have any selectivity because of its structure and the reason of higher selectivity is another factor.

The reason of the high gas selectivity in asymmetric layered membranes which poses a smaller selective layer of the pure graphene layer is that the zeolite/graphene porous support which is added instead of a part of pure graphene layer, poses high adsorption capacities for polar gases like CO_2 which offsets the negative effect of the smaller pure graphene thickness on the selectivity by adsorbing CO_2 much stronger than the other gases which helps in maintaining the membrane good separation performance. It means that after passing through the pure layer, the permeants enter the mixed layer of the membrane and are adsorbed to the zeolite particles. This adsorption prevents CO_2 to permeate to the other side of the membrane and therefore, it reduces the permeation ability of the gas (6). In addition, the selectivity of the membrane can also be more improved by increasing the thickness of the adsorptive layer which will be discussed later.

For CO_2 which has high amount of adsorption on zeolite, when running the permeation test, no gas is detected on the permeate side immediately but after some time, carbon dioxide finally is observed and it keeps increasing until a steady state is achieved. This permeation rate change could be because of the initial adsorption of CO_2 on zeolite and once all the adsorptive pores are occupied by the gas molecules, the remaining carbon dioxide passes through the pores. However, this time the pores are smaller because the porous space is already occupied by CO_2 molecules decreasing the permeation rate through the membrane. Therefore, the CO_2 permeation rate in asymmetric layered membrane is smaller than the similar pure graphene membrane.

Based on the literatures, the adsorption of CO_2 on zeolite is much stronger than the adsorption of helium and nitrogen (4) due to presence of polar group of carbon dioxide which makes it easier to interact with the zeolite adsorption sites. This idea can also be confirmed by comparing the permeation rate of N_2 which is more than CO_2 even with a bigger kinetic diameter. Due to higher adsorption of CO_2 molecules on zeolite particles, they interact stronger with the adsorptive channels, surpassing its diffusion through the membrane. There is no such phenomenon for He or N_2 leading to high permeation rate for helium and high selectivity for He/CO_2 (7).

Interestingly, when comparing the results of pure graphene layers with and without their porous support, it is observed that in some membranes with porous support containing high amount of zeolite (more than 40%), the permeation rate of helium was even higher than pure layer rate itself even though actually there was a layer added to the pure layer and it was expected that the permeation in asymmetric layered to be lower than in pure membrane with smaller thickness. This exception could be explained by considering the method of the asymmetric membrane fabrication. In this method, once the mixed powder (adsorptive layer) and the pure graphene nanoplatelets (selective layer) were poured into the pressing sleeve, they were pressed together using the pressing machine. Therefore, there could not be a very precise line between the two layers which is because of some irregular graphene flake formation in the border of selective-adsorptive layers. This leads to a shorter pathway for gas penetration and therefore finally higher permeation rates for the gas molecules which do not possess high adsorption abilities on zeolite particles such as helium and nitrogen (8). The effect of this phenomenon can be less obvious in the membranes with mixed layer made of high graphene weight ratios. The reason is that the high weight ratio of graphene/zeolite makes the structure of the adsorptive layer close to pure graphene and therefore there is no such irregularity in the border of selective-adsorptive layers. Figure 5.11 illustrates this factor in the membrane structure:

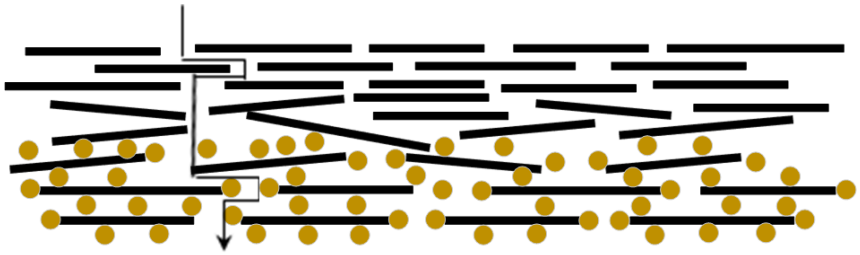

Figure 5.11 Schematic of irregular graphene flake formations in the asymmetric membrane structure.

It is worth mentioning that in membranes with mixed layers composed of more than 50% zeolite, the adsorptive layer was not able to decrease the CO_2 permeation either which was because of its highly porous (with very big pores) and irregular structure so that even the high adsorption of CO_2 was ineffective in blocking those molecules.

Therefore, by comparing the results of the asymmetric layered membranes, it can be concluded that in general, adding another layer with adsorptive properties can lead to a significant enhancement in membrane efficiency. The porous zeolite/graphene support assists the high membrane separation performance in two ways: 1) increasing the graphene interlayer spacing leading to higher permeation rates. 2) CO_2 adsorption leading to high He/CO_2 selectivity.

Figure 5.12 illustrates the effect of the porous support on the membrane performance. As is can be observed, the permeation rate of helium has been increase to twice while the He/CO_2 selectivity has an ignorable change.

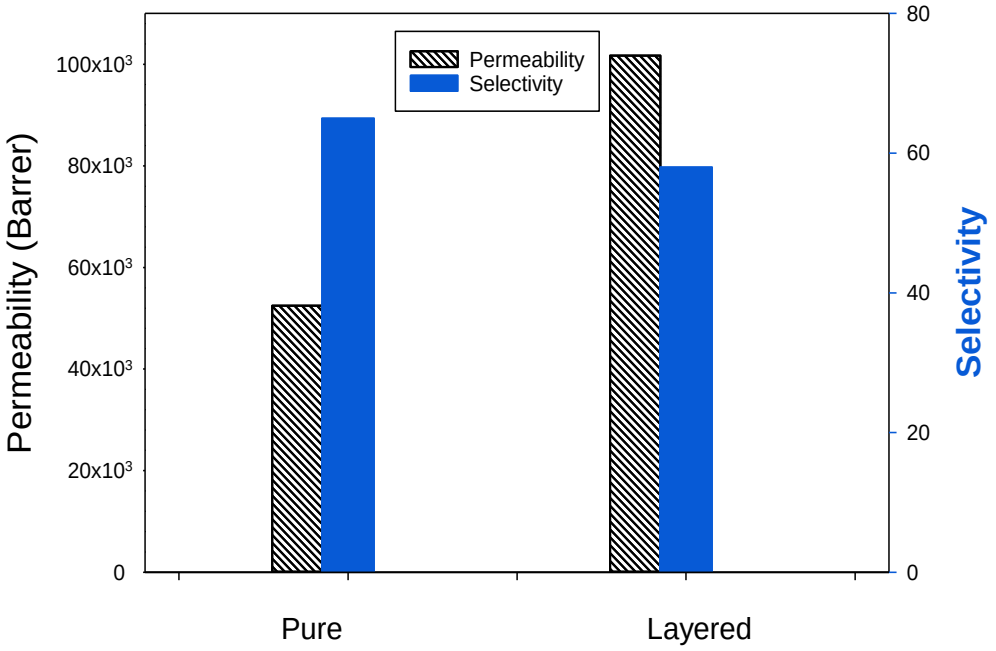

Figure 5.12 The effect of setting the porous mixed support in the pure graphene membrane structure.

5.3.2.4 The effect of pure graphene layer with different size

In this part, all three graphene flake sizes were tested as the pure layer of the composite membrane and their mixed layer were the same range of compositions to be able to observe the effect of the pure layer on membrane performance.

After doing all the tests in different composite membranes, as expected, it was observed that the composite membranes with the best separation performances are actually the ones with the pure layer made of graphene type which had showed the best separation in pure graphene membranes before. This means that similarly, composite membranes made of 25 µm graphene (pure layer) possess the highest He/CO_2 selectivity and the ones made of 5 µm graphene have the best helium permeation of all. The 15µm graphene layered membrane was excluded from the tests due to its very low permeation rate.

However, all of the membranes, even the worst performing ones in single-layered tests, after the adsorptive layer was added to their structure, they showed considerable improvements in gas separation efficiency.

Comparing the performance of the membranes in pure and composite state, it was observed that the membranes with the pure layer made of 5 µm graphene and the mixed layer of (13X+5µm) exhibited relatively higher improvement in selectivity than 25 µm graphene membrane (Figure 5.13). This could be also because of the compatibility between the particles of the two layers due to the similarity in their graphene types used (both 5 µm). In the other two graphene flake sizes, there is no such symmetry between the pure layer and the adsorptive mixture which is made of 13X zeolite and 5 µm graphene. Therefore, it could have caused some structural defects leading to smaller improvements.

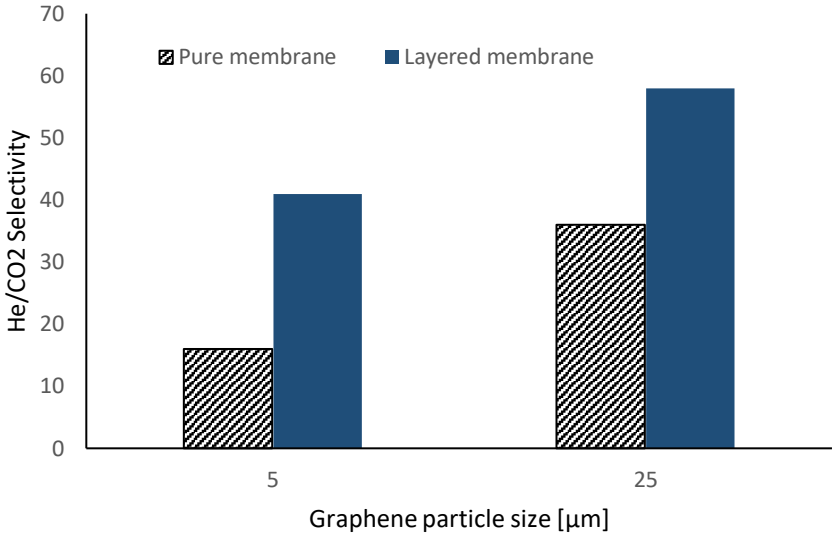

Figure 5.13 The effect of pure layer flake size on membrane performance improvement after addition of the adsorptive layers. The weight of the pure and asymmetric layered membranes is 0.11 g and 0.15 g respectively.

As illustrated in Figure 5.13, graphene particle size used in pure layer of the membranes, affect the amount of the improvement in the membrane performance after addition of the adsorptive layer. The composite membrane containing 5 µm graphene in its pure layer shows the highest selectivity improvement (from 17 to 41), while 25 µm membrane exhibits a lower rise in selectivity from pure to composite membrane (37 in pure state and 59 in asymmetric layered).

5.3.2.5 The effect of thickness

a) Mixed layer

To further investigate the effect of the adsorptive porous support on gas separation performance of the membranes, the thickness of the zeolite/graphene layer was altered. In this experiment, the thickness of the pure graphene layer was kept constant and the thickness of the mixed layer was altered between 0.01 g to more than the pure layer weight. As illustrated in Figure 5.14, by increasing the thickness of the zeolite/graphene mixed layer, the permeation rate of CO_2 and N_2 decreases while there is a small change in helium permenace. However, since the adsorption of CO_2 is much

stronger than He and N_2, the resulting selectivity is higher in value which means the separation performance of the membrane has been improved. Moreover, the change in He permeance (either increase or decrease) is negligible while the selectivity is improved significantly. Therefore, CO_2 adsorption on zeolite particles remarkably affects the permeability and selectivity of the membranes which can be observed by increasing the thickness of the porous support.

Having said that, in increasing the thickness of the adsorptive layer, one should consider the stability of the membrane. As mentioned before, high thicknesses of zeolite/graphene mixture especially with higher percentages of zeolite does no exhibit a very mechanically stable structure which could result in microstructural defects and poor separation performance. Therefore, in asymmetric layered membranes with thick adsorptive layer, the weight ratio of graphene in the mixture should be higher to ensure high mechanical stability during the experiments as well.

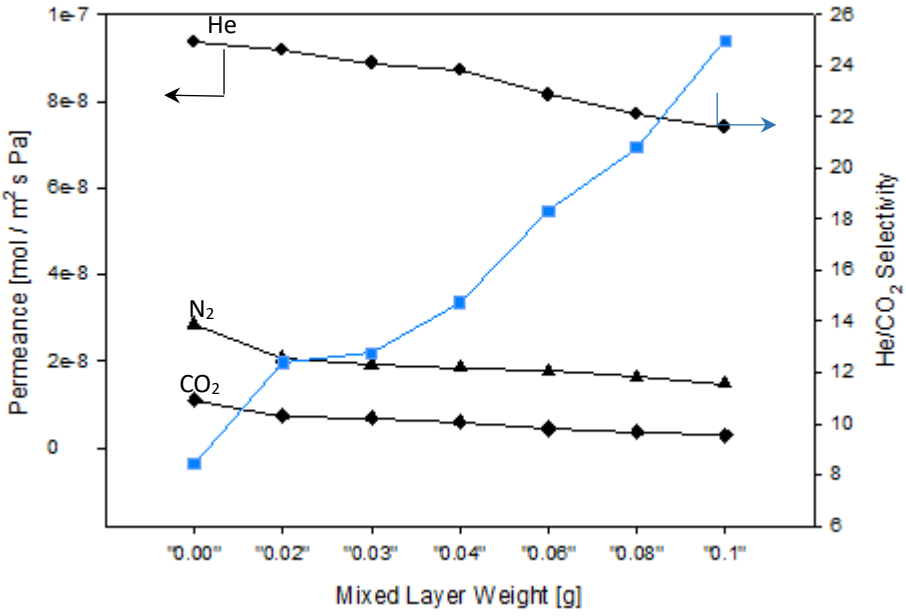

Figure 5.14 The effect of porous support (mixed layer) weight (thickness) on the membrane separation performance. The pure layer thickness was kept constant at around 0.35 mm using 0.07 g of 5 µm graphene and the mixed layer composition is 40% 5 µm graphene+13X zeolite. The membranes are pressed at 8 MPa pressure for 2 minutes.

b) Pure layer

Altering the thickness of the selective layer in composite membranes had the same effect on the membrane performance regardless of the graphene flake size, adsorptive later zeolite/graphene mixture ratio or component (Figure 5.15). In all of the mentioned membranes, by increasing the thickness of the pure layer (considering a fixed thickness of the mixed layer), the membrane selectivity increased while the He permeance decreased. Alerting the thickness of the pure layer, leaded to much sharper helium permeance decrease due to the change in thickness of the selective layer which is the most important factor in determining He permeation rate. The mixed layer thickness alteration had no such effect on He permeation rate since it is too porous for helium and instead it is much more effective for CO_2 because of adsorption.

Therefore, the effect of the selective layer thickness alteration on the membrane performance is almost the same as previous chapter for the pure graphene membrane.

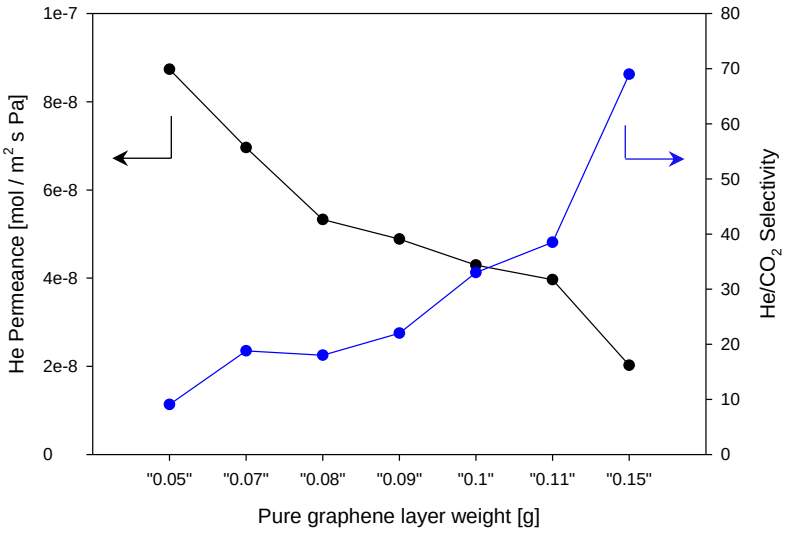

Figure 5.15 The effect of pure layer weight (thickness) on membrane separation performance. The graphene flakes size used in the pure layer is 25 µm, the mixed layer composition is 40%of 13X zeolite and 60% of 5 µm graphene with the constant thickness of 0.2 mm. The pressing pressure and time are 8 MPa and 2 minutes respectively.

5.3.2.6 Zeolite/graphene mixing method

Two methods were used for mixing graphene nanoplatelets and zeolite powder. The first method was to grind the graphene and zeolite powder using a hand grinder until it is uniform. The second method was to use ball milling device resulting a more uniform mixture as mentioned in chapter 3.

Unexpectedly, even though the spin speed of the ball mill was on moderate (100 rpm) for 1 hour, but the membranes made of ball-milled mixture showed a lower selectivity in the membrane performance. As illustrated in Figures 5.16 and 5.17, the SEM images shows the difference in the structure of the membrane surface made of hand-grinded and ball-milled mixtures. It can be observed that the surface of the membrane made of hand-grinded mixture, is more uniform and there is no crack or defect on the surface. However, for the ball-milled membrane, even though the surface of the membrane seemed smooth by naked eye, it showed a lot of defects under SEM microscope resulting in poor membrane performance. Therefore it was decided to utilise hand-grinding method in powder mixture preparation.

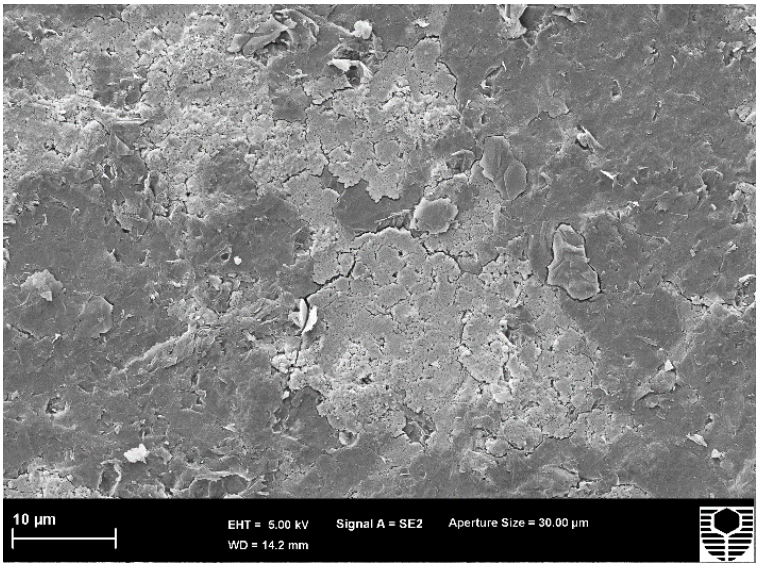

Figure 5.16 Membrane surface of the mixed layer-ball mill mixing of the mixture. The layer composition is 60% of 5 µm graphene and 40% of 13X zeolite and the pressing pressure and time is 8 MPa and 2 minutes respectively.

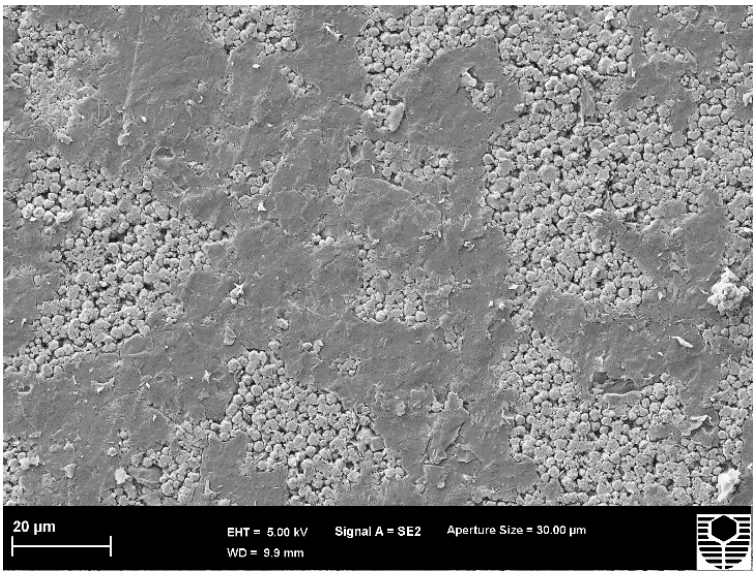

Figure 5.17 Membrane surface of the mixed layer- hand grinding mixing of the mixture. The layer composition is 60% 0f 5 µm graphene and 40% of 13X zeolite and the pressing pressure and time is 8 MPa and 2 minutes respectively.

5.4 Mass transport mechanism

To identify the mass transport mechanism of the gases through the membrane, single gas permeation test were carried out at 1bar pressure difference for 4 different membranes. To further probe the excellent gas sieving property of the fabricated membranes, three gases (He, CO_2, and N_2) were used in single gas permeation tests.

As Figure 5.18 shows, the separation performance of the membranes made of graphene and zeolite is higher than the graphite disc which have been reported in other literature (9). Comparing our best performing membrane and the graphite disc, there is an obvious improvement in selectivity. Permeability have been enhanced in all the composite membranes which is an important factor in gas separation applications.

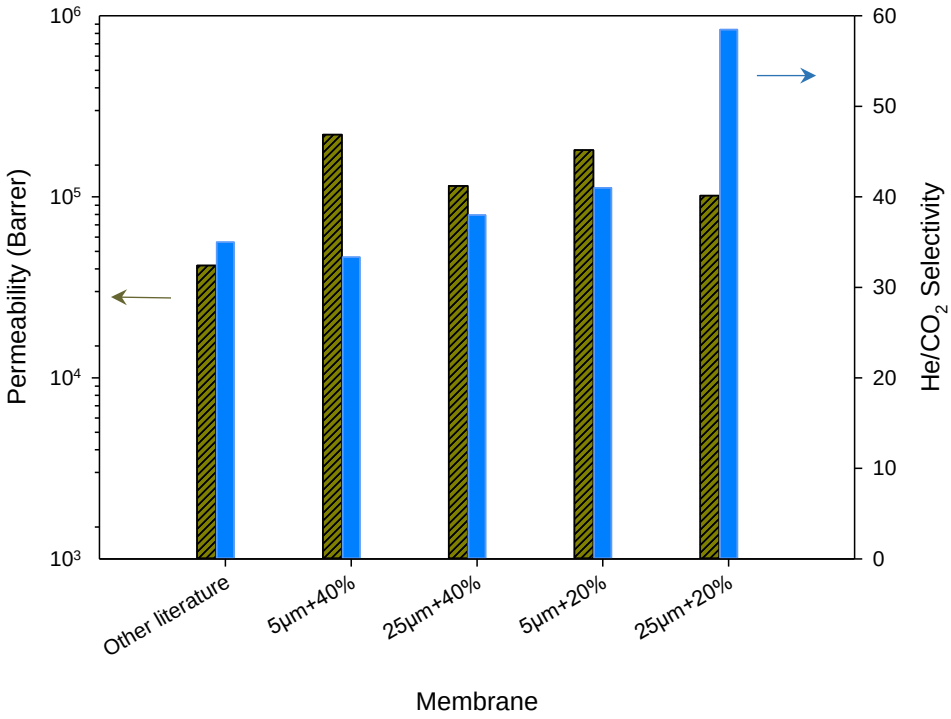

Figure 5.18 Permeability and selectivity of the fabricated membranes and a similar membrane reported in other literatures.

The molecular sieving mechanism of the membranes is illustrated in Figure 5.19 where it shows that the selectivity of the membranes is much higher than their theoretical Knudsen selectivity which was calculated using equation 2.12. The calculated Knudsen selectivity for He/CO_2 is 3.3 and this proves that molecular sieving is the dominant transport mechanism in the membranes.

Figure 5.20 illustrates the permeation rate of each probe gas at room temperature and 1 bar pressure difference as a function of the gases kinetic diameter. The permeation rate for nitrogen was slightly higher than carbon dioxide which is because of the stronger adsorption of CO_2 on graphene sheets and zeolite particles (10), affecting the gas transport through the membranes.

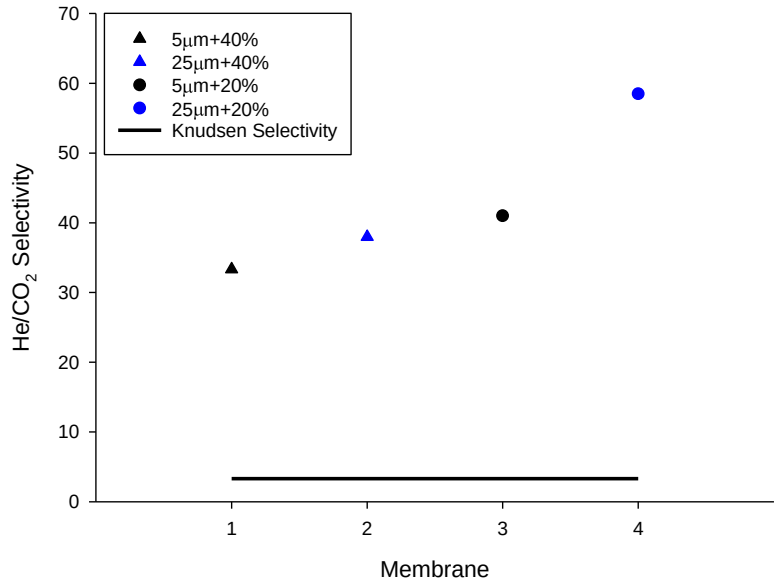

Figure 5.19 Theoretical Knudsen Selectivity and Experimental selectivity of four different composite membranes pressed at 8 MPa pressure for 2 minutes.

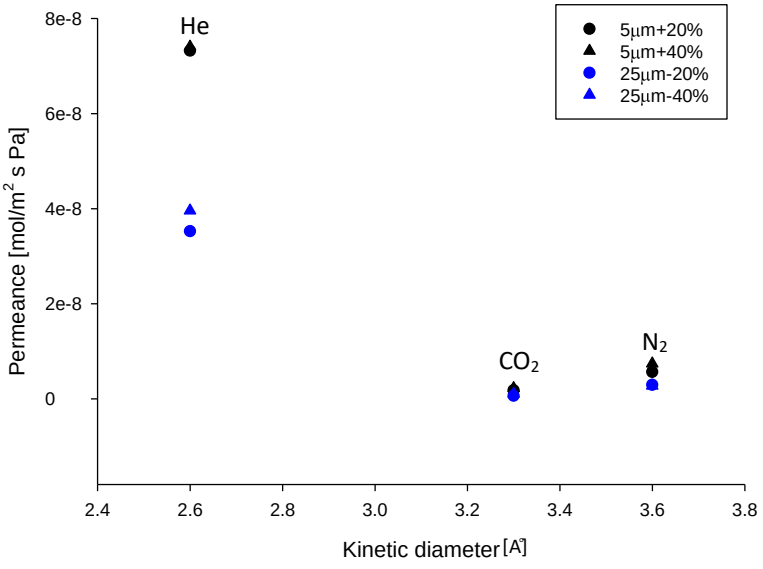

Figure 5.20 Single gas permeance of probe gases at room temperature as a function of gas kinetic diameter.

5.5 Effect of temperature on the membrane performance

To investigate the effect of temperature on the separation performance of the membrane, gas permeation tests were carried out at various temperatures from 24 to 60℃. The pressure difference was kept constant at 1 bar.

In membrane separation based on molecular sieving, two factors are usually considered. One is the molecules activated diffusion and the other one is preferable adsorption, which occur when the membrane pores are in the range of the molecules kinetic diameter (11, 12). Therefore, depending on the impact of the temperature on either of these two factors, the separation performance of the membrane could be affected.

As illustrated in Figure 5.21, by increasing the temperature in membrane cell, the permeation rate for both helium and carbon dioxide increases. However, there is a sharper increase in CO_2 permeance than for He and therefore, the He/CO_2 selectivity declines at higher temperatures. This means that temperature rise does not impose a positive effect on the membrane performance.

The reason for such a result is the adsorption properties of the membrane at higher temperatures. As reported in the literature, zeolite adsorption capacity decreases with temperature rise which means there is less obstacles for the gases to pass through the membrane resulting in higher permeability (3, 5). Thus, the effect of different adsorption capacities of gases which led to high selectivity at ambient temperature, plays a less considerable role at higher temperatures leading to lower selectivities (13).

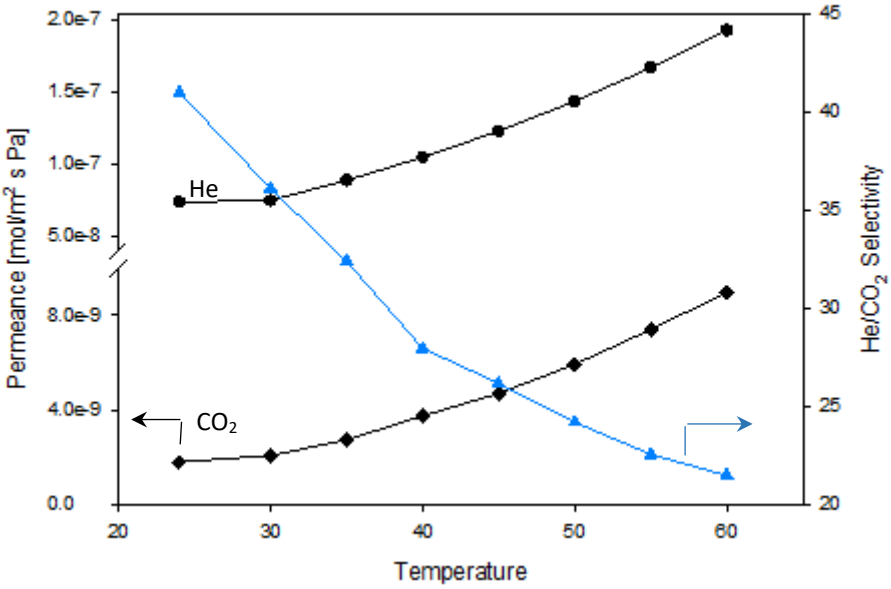

Figure 5.21 The effect of temperature on membrane separation performance. The membrane thickness is 0.75 mm made of 5 µm graphene in pure layer and 80% of 5 µm+20% of 13X zeolite in the mixed layer. The pressing pressure and time are 8 MPa and 2 minutes respectively.

5.6 Mathematical modelling for gas separation through the assembled graphene membranes

Gas permeation based on molecular sieving mechanism through the subnanometer channels of the graphene membranes can be described using the gas translation model. The model was firstly used for investigating the molecular sieving mechanism in zeolite pores and after that it was used for membranes with molecular sieving mechanism for gas separation (6, 14). The equation is described as follows:

$$p = \frac{\varphi}{L} D_c K \tag{5.1}$$

$$D_c = \frac{\alpha}{\mathrm{z}} \left(\frac{8RT}{\pi \mathrm{M}} \right)^{\frac{1}{2}} \exp\left(\frac{-E_d}{RT} \right) \tag{5.2}$$

Where p is the gas permeance, φ is the ratio of the membrane porosity ε to the tortuosity factor τ, L is the membrane thickness which is 0.75 mm here, D_c is the gas diffusivity in graphene laminates, K is the adsorption equilibrium constant which can

be estimated to (1/RT), α is the diffusion length, z is the diffusion coordination number, R is the gas constant, M is the gas molecular weight, and E_d is the activation energy of gas diffusion in the membrane. Thus, the final gas permeance (p) can be rewritten as follows:

$$p = \frac{\varphi}{L}\frac{\alpha}{z}\left(\frac{8}{\pi MRT}\right)^{\frac{1}{2}} \exp\left(\frac{-E_d}{RT}\right) \tag{5.3}$$

Taking logs from both sides results in the following equation:

$$\ln\left(pT^{\frac{1}{2}}\right) = \left(\frac{-E_d}{R}\right)\frac{1}{T} + \ln\left[\frac{\varphi}{L}\frac{\alpha}{z}\left(\frac{8}{\pi MR}\right)^{\frac{1}{2}}\right] \tag{5.4}$$

E_d can be calculated using the Arrhenius curves of the gas permeance vs 1/T as illustrated in Figure 5.22.

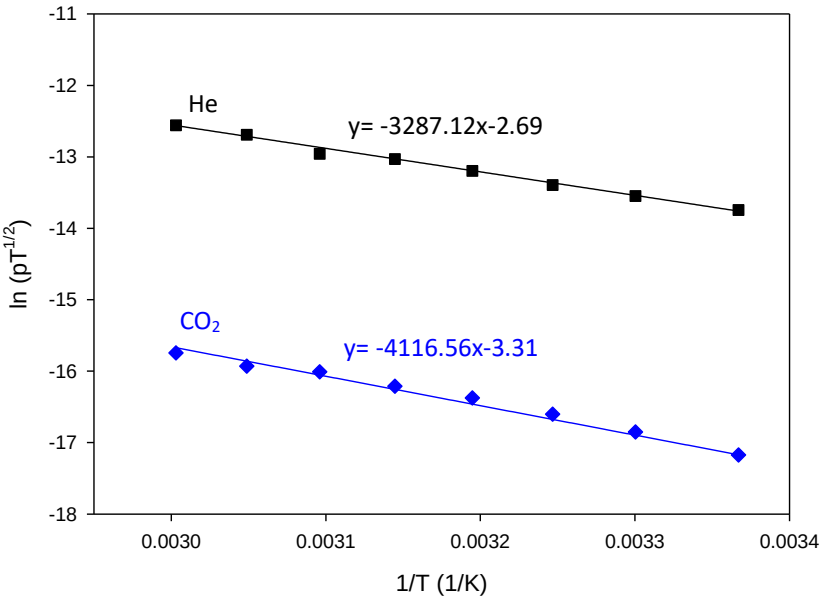

Figure 5.22 Logarithmic plot of the left side of equation 4.4 and 1/T

Using the above plot, the activation energy of the gases is calculated. The slope of the plots indicates the value of $\frac{-E_d}{R}$ and therefore E_d is estimated as:

$$E_d = -(Slope) * R \tag{5.5}$$

Therefore, the value of E_d equals to 27.329 and 34.225 kJ/mol for He and CO_2 respectively.

The activation energy for carbon dioxide in higher than E_d calculated for helium. This indicates that CO_2 permeation through the membrane is more temperature-sensitive than He. This is the reason that the increment rate of CO_2 permeance is higher than helium leading to a sharp decrease in He/CO_2 selectivity.

Therefore, the temperature dependence of equation 4.3 for helium permeance can be rewritten as the following:

$$p_{He} = 0.2768 \left(\frac{\varphi}{L}\frac{\alpha}{\mathrm{z}}\right)\left(\frac{1}{\mathrm{T}}\right)^{\frac{1}{2}} \exp\left(\frac{-3287.12}{T}\right) \tag{5.6}$$

And also, for carbon dioxide, the above equation will be as the following:

$$p_{CO2} = 0.0835\left(\frac{\varphi}{L}\frac{\alpha}{\mathrm{z}}\right)\left(\frac{1}{\mathrm{T}}\right)^{\frac{1}{2}} \exp\left(\frac{-4116.56}{T}\right) \tag{5.7}$$

Therefore, the theoretical selectivity can be calculated as follows:

$$S_{He,CO2} = \frac{p_{He}}{p_{CO2}} \tag{5.8}$$

Since the values of φ, α, L, z, π, R, and T are similar for both gases, therefore the above equation for selectivity calculation can be rewritten as the following:

$$S_{He,CO2} = \left(\frac{M_{CO2}}{M_{He}}\right)^{\frac{1}{2}} . \frac{\exp(\frac{-3287.12}{T})}{\exp\left(\frac{-4116.56}{T}\right)} \tag{5.9}$$

Therefore, by substituting the value of T at 297 K, the theoretical selectivity at room temperature can be calculated using the above equation and is equal to 46. The

experimental selectivity for the above membrane was calculated to be 41 which is close to the theoretical value. This further demonstrates that molecular sieving is the dominant separation mechanism in the developed graphene membranes.

5.7 Mixed gas permeation tests

Mixed gas permeation tests were carried out using the described setup in chapter 3 and the three probe gases. He and CO_2 were used as the feed gases in the mixture and N_2 as the sweep gas in the permeate side to send the permeated gases to the GC.

As expected, the results of the mixed gas permeation test on the asymmetric layered membrane showed a better separation performance than the pure membrane with the separation factors of 15 and 10 respectively. This is assumed to be because of the adsorptive porous support present in the structure of the membranes.

In pure membrane, when the gas mixture is sent through, there is a competition between the two gases to pass through graphene layers. When a second layer exists (in asymmetric membranes), the high adsorptive capability of zeolite particles adsorbs CO_2 molecules more strongly than helium resulting in stronger competition between He and CO_2 which prevents the carbon dioxide molecules to pass through while letting the smaller gases permeate easier. This results in higher separation factors for composite membranes. The following plot illustrates the mixed gas permeation results for one of the best performing membrane (0.75 mm thickness) fabricated using 25 µm graphene with excellent selectivity and reasonable helium permeance both in single and mixed gas permeation tests. The second membrane shows the corresponding asymmetric layered membrane with the adsorptive layer of 13X+5µm added to the membrane structure (0.9 mm thickness).

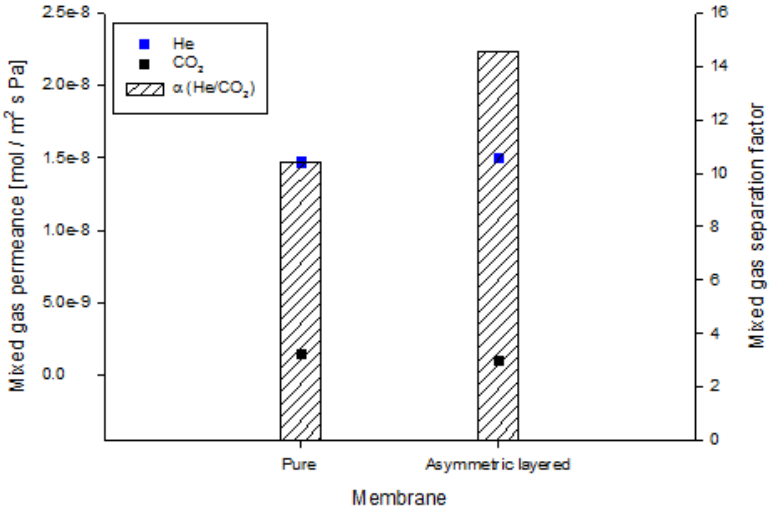

Figure 5.23 Mixed gas permeation rates and separation factor for pure and composite membranes at room temperature. Pure membrane is 0.75 mm from 25 µm graphene and the asymmetric membrane thickness is 0.95 mm made of 0.75 mm pure layer plus 0.2 mm mixed layer added to the membrane structure (60% of 5 µm graphene+40% of 13X zeolite composition).

binary gas permeation test, the helium permeation rate was almost similar to the single gas permeation test while there was a huge increase in CO_2 permeation rate. The reason of this increment in CO_2 permeation rate is due to the curved adsorption isotherm of this gas on zeolite and graphene. If we assume the 1st Fick Law to be valid for this situation, in lower partial pressures (like in the case of the binary gas permeation test), the concentration gradient as driving force is higher than the higher partial pressure (like in the case of single permeation tests) (9). Therefore, at the same operating pressure, the higher driving force for carbon dioxide in binary gas test due to its lower partial pressure leads to higher permeation rate for this gas than single gas permeation tests.

The results indicate that there is a good separation in binary gas mixtures and by changing the graphene flake size used in the membrane structure, based on the application the permeation rate and separation factor can be altered.

5.8 Conclusion

In this chapter, composite layered graphene and zeolite membrane was fabricated. A wide range of graphene/zeolite compositions as well as graphene flake sizes in pure layer were tested to find out the best membrane with the highest gas separation performance.

By changing the thickness of the mixed and pure layer, it was observed that the pure graphene layer is the selective part and the graphene/zeolite mixture is the porous support with preferable adsorption which slows down the carbon dioxide molecule transport but with less transfer resistance for He to pass through the support layer, leading to high separation performance. Overall, the membranes exhibited a considerable improvement after adding the zeolite adsorptive layer with higher permeability and selectivity comparing to the membranes reported by other literatures.

Single and mixed gas permeation tests for He, CO_2, and N_2 were carried out to study the separation mechanism of the fabricated membranes. Based on the membrane selectivity and comparing the results to Knudsen selectivity, it can be concluded that molecular sieving is the main transport mechanism of the gases through the membrane.

Performing gas permeation test at higher temperatures indicates that the permeation rate of gases increases with temperature rise. However, due to higher increment rate in CO_2 permeance than He, the selectivity drops by increasing the temperature.

References

1. Geim AK. Graphene: Status and Prospects. Science. 2009;324(5934):1530-4.
2. Kosinov N, Gascon J, Kapteijn F, Hensen EJM. Recent developments in zeolite membranes for gas separation. J Membrane Sci. 2016;499:65-79.
3. Zarghampoor MH, Mozaffarian M, Soleimani M, Takht Ravanchi M. Modeling of CO2 Adsorption on Activated Carbon and 13X Zeolite via Vacuum Swing Adsorption. IOP Conference Series: Materials Science and Engineering. 2017;206:012004.
4. Siriwardane RV, Shen M-S, Fisher EP, Poston JA. Adsorption of CO2 on Molecular Sieves and Activated Carbon. Energy & Fuels. 2001;15(2):279-84.
5. Hauchhum L, Mahanta P. Carbon dioxide adsorption on zeolites and activated carbon by pressure swing adsorption in a fixed bed. International Journal of Energy and Environmental Engineering. 2014;5(4):349-56.
6. Shen J, Liu G, Huang K, Chu Z, Jin W, Xu N. Subnanometer Two-Dimensional Graphene Oxide Channels for Ultrafast Gas Sieving. ACS Nano. 2016;10(3):3398-409.
7. Ding L, Wei Y, Li L, Zhang T, Wang H, Xue J, et al. MXene molecular sieving membranes for highly efficient gas separation. Nat Commun. 2018;9(1):155.
8. Aba NFD, Chong JY, Wang B, Mattevi C, Li K. Graphene oxide membranes on ceramic hollow fibers - Microstructural stability and nanofiltration performance. J Membrane Sci. 2015;484:87-94.
9. Schulz A, Steinbach F, Caro J. Pressed graphite crystals as gas separation membrane for steam reforming of ethanol. J Membrane Sci. 2014;469:284-91.
10. Liu Z, Grande CA, Li P, Yu J, Rodrigues AE. Adsorption and Desorption of Carbon Dioxide and Nitrogen on Zeolite 5A. Separation Science and Technology. 2011;46(3):434-51.
11. Rackley SA. Carbon Capture and Storage. Elsevier.
12. Zhu JC, Meng XX, Zhao JP, Jin Y, Yang NT, Zhang SG, et al. Facile hydrogen/nitrogen separation through graphene oxide membranes supported on YSZ ceramic hollow fibers. J Membrane Sci. 2017;535:143-50.
13. Kusakabe K, Kuroda T, Murata A, Morooka S. Formation of a Y-Type Zeolite Membrane on a Porous α-Alumina Tube for Gas Separation. Ind Eng Chem Res. 1997;36(3):649-55.
14. Xiao J, Wei J. Diffusion mechanism of hydrocarbons in zeolites—I. Theory. Chemical Engineering Science. 1992;47(5):1123-41.

Chapter 6 Conclusion and Recommendations

6.1 Conclusions

In this study, graphene-based membranes were fabricated using a facile method for efficient gas separation using molecular sieving mechanism. The thesis has focused on the impact of various factors on the membranes performance and how they affect the gas separation. Some of these factors were included in the preparation procedure of the membrane such as membrane pressing pressure and time. Besides, some of them were the properties of raw materials used in the membrane structure like powder particle size and graphene flake size.

After studying the above mentioned factors and their effect on the membrane performance, it was observed that if the surface area of the graphene nanoplatelets powder is similar, graphene membranes consisting of bigger flake sizes exhibit higher selectivity. However, when the initial powder surface area is different, the membranes made of smaller surface area material (bigger particles) show lower permeation rates which was not a favourable outcome for the membrane performance.

The pure graphene membranes exhibited excellent He/CO_2 selectivity based on molecular sieving mechanism. However, in some cases, the permeation rate of smaller gases (helium) was low. To further improve the gas permeance through the membrane, zeolite was added to the membrane structure as spacer in between the graphene layers to facilitate the molecular sieving mechanism for the gas separation while increasing the permeation rate of smaller gases. Therefore, a part of the pure membrane thickness was eliminated and instead a mixed layer of graphene and zeolite was added to the pure layer. Thus as two-layered asymmetric membrane was fabricated with the first layer (selective layer) being made of pure graphene and the second layer (porous support) being the graphene/zeolite mixture.

In this case, it was also important to find the most optimum mixture ratio and thickness of the first and second layer to ensure the highest selectivity and permeation rate possible with low structural defects which is critical in long-time membrane operations.

After investigating different membrane types, it was observed that one of the most important factors affecting the layered membrane performance is the compatibility between the zeolite and graphene particles which played an important role in membrane performance improvement.

The addition of the porous support to the pure membranes resulted in considerable enhancement in permeation rate (more than double) while keeping the high selectivity which was necessary for an effective gas separation. The reason of such improvement was considered as both the role of the zeolite particles in increasing the interlayer spacing of the graphene plates as well as their different adsorption capacity for various gases. For example, based on adsorption measurements, carbon dioxide was adsorbed on graphene and zeolite much stronger than the other two probe gases (He and N_2) which results in much lower CO_2 permeance and high selectivity. In addition, inert gases like helium does not exhibit high adsorption on zeolite or graphene. This means that the only layer affecting the helium permeation is the first pure layer which have been reduced in thickness leading to higher permeation rate for the target gas (helium).

The membrane performance was studied at higher temperatures and it was observed that by increasing the temperature, the separation performance of the membrane decreases. In addition, using mathematical modelling of the gas transport through the membranes, the theoretical selectivity was calculated which was very close to the experimental value. This further demonstrated that molecular sieving was the main transport mechanism for the membranes.

Finally, mixed gas permeation tests were also carried out and the results showed good separation performance of the He/CO_2 binary gas mixture. As expected, the asymmetric layered membranes exhibited better performance than pure graphene membranes which was due to their porous adsorptive support present in the membrane structure.

6.2 Recommendations and future works

Based on the results of this study, the following recommendations are made for further research in this area:

1. For more investigation of graphene nanoplatelets and their functional groups on their edges and surface affecting the membrane performance, graphene derivatives such as reduced graphene oxide or graphene oxide can also be used in the membrane structure.

2. To further improve the asymmetric layered membrane performance, a very thin layer of graphene oxide can be coated on the pure graphene layer surface. To ensure high adhesion between the two layers, a cross-linking method should be considered on the surface of the graphene layer before GO coating.

3. Using a support with high porosity and mechanical stability (such as aluminium support) and attaching them to the thin membranes to increase their stability and protect them from breaking during the experiments would make them more practical for higher pressure permeation tests.

4. Fabricating 3-4 layered asymmetric membranes with gradual changes in their structure.

5. It is also recommended to use cross-flow gas permeation setup instead of dead-end one to ensure continues gas flow to the feed side of the membranes and that there is no accumulation on the membrane surface. When using the dead-end setup, to prevent accumulation of the molecules with low permeation rates on the membrane feed side it was necessary to purge the system regularly which made the experimental procedure slow (especially in mixed gas permeation tests using the GC).

'Every reasonable effort has been made to acknowledge the owners of copyright material. I would be pleased to hear from any copyright owner who has been omitted or incorrectly acknowledged.'

Appendix I

Chapter 4

The following tables are the experimental data used in chapter 4 in different figures:

Data used in Figure 4.4

Pressing time (min)	He Permeance (10^{-8}mol $m^{-2}s^{-1}Pa^{-1}$)	Selectivity He/CO_2
0.5	11.00	15.67
1	7.80	16.2
2	7.25	17
5	6.20	10.2345
10	5.50	8.456

Data used in Figure 4.5

Pressing pressure (MPa)	He Permeance (10^{-8}mol $m^{-2}s^{-1}Pa^{-1}$)	Selectivity He/CO_2
20	4.20	14.5
18	4.87	14
15	5.37	13
12	6.46	12.4
10	6.80	12.1
8	7.25	17
6	11.86	13
4	16.48	9

Data used in Figure 4.6

Graphene flake size (μm)	Membrane weight (g)	He Permeance (10^{-8}mol $m^{-2}s^{-1}Pa^{-1}$)	Selectivity He/CO_2
5.00	0.11	7.25	17
	0.15	4.63	40
15.00	0.11	0.88	20
	0.15	0.74	50
25.00	0.11	3.47	37
	0.15	2.02	65

Data used in Figure 4.9

Membrane weight (g)	He Permeance (10^{-8}mol $m^{-2}s^{-1}Pa^{-1}$)	Selectivity He/CO_2
0.15	2.02	65
0.14	2.56	50
0.125	2.90	40
0.11	3.47	37
0.1	3.85	26
0.09	4.74	16
0.08	6.37	14

Adsorption tests used in Figure 4.10					
5 µm graphene		15 µm graphene		25 µm graphene	
Absolute pressure (kPa)	Quantity adsorbed [cm3 /g STP]	Absolute pressure (kPa)	Quantity adsorbed [cm3 /g STP]	Absolute pressure (kPa)	Quantity adsorbed [cm3 /g STP]
1.334214596	1.514718049	1.468657662	0.600378474	1.345202184	1.3257314
4.679829134	3.702888774	4.584313895	1.790457474	5.061457282	3.513247681
9.281022951	5.538189105	8.229109805	2.751328045	9.187453558	5.048534749
11.53530891	6.238588634	11.52627136	3.424000767	11.47047861	5.732791007
15.17091775	7.191584881	15.23527913	4.065275568	15.13480621	6.653721209
18.66350853	7.976254873	18.74744533	4.569424826	18.677814	7.417490966
22.21359988	8.672995732	22.24886107	5.016416645	22.18976354	8.091610737
25.69361846	9.290102912	25.74843167	5.411568368	25.69960551	8.6906946
29.21971276	9.857863648	29.25065708	5.774033741	29.20734398	9.23825472
32.72440785	10.37630378	32.75727869	6.089414609	32.71831297	9.732943281
36.23201815	10.85645658	36.25538049	6.401394476	36.22709098	10.20593496
39.7395837	11.31093837	39.76412596	6.678358501	39.74353031	10.63855925
40.00300611	11.40821405	40.02450092	6.761348856	40.00840117	10.72979582
43.23646897	11.76248178	43.26626796	6.951194994	43.24656335	11.0704287
48.52342554	12.32886327	48.56455986	7.295089624	48.46729407	11.61007813
50.15374838	12.56145199	50.18910925	7.433192338	50.15286548	11.81416812
53.71286	12.89202682	53.72413023	7.629887529	53.68600266	12.14543938
57.10201891	13.22122507	57.13408008	7.827297487	57.10511517	12.46580795
60.63269047	13.56845203	60.65744023	8.034848133	60.624724	12.78800687
64.12913226	13.88995773	64.14980927	8.231705092	64.1168652	13.09052806
67.60219135	14.2174438	67.6358922	8.423728527	67.60066967	13.3897791
71.11107922	14.51324721	71.12065689	8.610896031	71.09581355	13.67933704
74.57680249	14.83019477	74.61544679	8.793173732	74.58048872	13.96473911
78.08672787	15.14711542	78.10696547	8.968831164	78.07695491	14.24007813
81.58231524	15.41831017	81.59062347	9.150798597	81.56458394	14.50445374
85.04200059	15.71885402	85.08721987	9.330267082	85.05181424	14.76720543
88.55099018	16.02866741	88.56830646	9.510814061	88.54453726	15.02698442
92.04028736	16.32036516	92.06235587	9.694998456	92.03440406	15.27981811
95.5243441	16.60934284	95.55166933	9.881399993	95.52263525	15.52881565
99.01625337	16.8950598	99.02394317	10.07005859	99.01483747	15.7711639
102.5061853	17.17559569	102.5135903	10.26190111	102.5010913	16.01337746
105.9922275	17.45821417	105.9992094	10.45752506	105.9904048	16.25812575
109.4841368	17.73296524	109.4877742	10.65574752	109.4842914	16.49055461
112.9672821	18.0086602	112.9709846	10.86227202	112.9615697	16.7289972
116.4602086	18.28568171	116.4662872	11.06761719	116.4635775	16.96241594
119.95	18.55624643	119.9468449	11.27807126	119.946259	17.19409551

Chapter 5

The following tables are the experimental data used in chapter 5 in different figures:

Single gas permeation test for the asymmetric layered membranes. (in all the following membrane, the weight of the pure layer and mixed layer is 0.11 g and 0.04 g respectively)

Membrane Composition						Permeance (10^{-8}mol $m^{-2}s^{-1}Pa^{-1}$)		
Pure layer (µm)	Adsorptive layer composition							
	Graphene size (µm)			Zeolite type				
	5	15	25	4A	13X	He	CO_2	N_2
5	80%	-	-	-	20%	7.32	0.179	0.56
	60%	-	-	-	40%	7.4	0.22	0.74
	20%	-	-	-	60%	8.89	0.445	1.185
	-	80%	-	-	20%	4.15	0.148	0.44
	-	60%	-	-	40%	5.47	0.37	1.19
	-	20%	-	-	60%	6.52	0.513	1.41
	-	-	80%	-	20%	5.92	0.37	1.2
	-	-	60%	-	40%	6.37	0.518	1.48
	-	-	40%	-	60%	9.18	0.966	2.22
	80%	-	-	20%	-	6.5	0.243	0.69
	60%	-	-	40%	-	7.4	0.592	0.97
	20%	-	-	60%	-	9.18	1.35	1.86
	-	80%	-	20%	-	4.45	0.304	0.67
	-	60%	-	40%	-	5.92	0.422	1.19
	-	20%	-	60%	-	8.29	0.753	1.7
	-	-	80%	20%	-	6.23	0.506	1.26
	-	-	60%	40%	-	7.75	0.738	1.78
	-	-	40%	60%	-	9.33	1.196	2.37
25	80%	-	-	-	20%	3.52	0.06	0.293
	60%	-	-	-	40%	3.96	0.104	0.277
	20%	-	-	-	60%	4.8	0.062	0.56
	-	60%	-	-	40%	3.03	0.106	
	-	-	80%	-	20%	2.97	0.108	0.3
	-	-	60%	-	40%	3.55	0.13	0.518
	-	-	40%	-	60%	4	0.148	0.67

The effect of mixed layer thickness on the membrane performance (Figure 5.14).

Mixed layer weight (g)	Permeance (10^{-8}mol $m^{-1}s^{-1}Pa^{-1}$)		
	He	CO_2	N_2
0	9.36	1.11	2.85
0.02	9.18	0.74	2.07
0.03	8.89	0.70	1.93
0.04	8.74	0.59	1.85
0.06	8.15	0.44	1.78
0.08	7.70	0.37	1.63
0.1	7.40	0.30	1.48

The effect of pure layer thickness on the membrane performance (Figure 5.15).

Pure layer weight (g)	Permeance (10^{-8}mol $m^{-1}s^{-1}Pa^{-1}$)	
	He	CO_2
0.05	8.74	0.963
0.07	6.96	0.37
0.08	5.33	0.296
0.09	4.89	0.22
0.1	4.29	0.131
0.11	3.96	0.104
0.15	2.22	0.032

Gas permeance temperature dependence (Figure 5.21).

Membrane Type	Composition		Temp. (°C)	Permeance (10^{-8}mol $m^{-1}s^{-1}Pa^{-1}$)	
	graphene flake size (μm)	Bottom layer zeolite weight ratio		He	CO_2
Asymmetric graphene +zeolite	5	20% (13X)	24	7.38	0.179
			30	7.51	0.208
			35	8.9	0.275
			40	10.5	0.375
			45	12.3	0.47
			50	14.4	0.593
			55	16.7	0.739
			60	19.3	0.897

Appendix II

Manuscript **'Experimental and theoretical exploration of gas permeation mechanism through 2D graphene (not graphene oxide) membranes' -** Journal of Membrane Science – accepted for publication Jan 2020.

Fatemeh A. Nezhad, Ning Han, Zhangfeng Shen, Yun Jin, Yangang Wang, Naitao Yang, Shaomin Liu

Name	**Conception and design**	**Acquisition of data & method**	**Data conditioning & manipulation**	**Analysis & statistical method**	**Interpretation & discussion**	**Final approval**
Fatemeh A.Nezhad	☒	☒	☒	☐	☒	☐
I acknowledge that these represent my contribution to the above research output.						
Ning Han	☐	☐	☐	☒	☒	☐
I acknowledge that these represent my contribution to the above research output.						
Zhangfeng Shen	☒	☐	☐	☒	☒	☐
I acknowledge that these represent my contribution to the above research output.						

Yun Jin	☒	☐	☐	☒	☒	☐
I acknowledge that these represent my contribution to the above research output.						
Yangang Wang	☐	☐	☐	☒	☒	☐
I acknowledge that these represent my contribution to the above research output.						
Naitao Yang	☐	☐	☐	☒	☒	☐
I acknowledge that these represent my contribution to the above research output.						
Shaomin Liu	☒	☐	☐	☒	☒	☒
I acknowledge that these represent my contribution to the above research output.						